



NTNU – Trondheim
Norwegian University of
Science and Technology

Diatoms Investigated by Atomic Force Microscopy

Torstein Svendsgaard

Master of Science in Mechanical Engineering

Submission date: June 2015

Supervisor: Christian Thaulow, IPM

Norwegian University of Science and Technology
Department of Engineering Design and Materials

**MASTER THESIS SPRING 2015
FOR
STUD.TECHN. TORSTEIN V SVENDSGAARD**

Morphology and properties of biosilica from diatoms

Morfologi og egenskaper av biosilika fra diatomer.

Diatom is the name of a large group of unicellular algae, which gets their name from the structure of the cell wall. The diatoms make an exoskeleton of silica which consists of two separated valves connected by one or several girdle bands. The diameter of the diatom *Coscinodiscus* sp., the diatom to be focused in this work, is about 200-400 μm , which makes it one of the largest diatom species.

Nanomechanical testing has been performed to reveal the elasticity modulus and the fracture strength of biosilica. Test specimens were machined with Focused Ion Beam from the frustule of *Coscinodiscus* sp., and subsequently tested with a nanoindenter device. The testing included both full thickness three point bending beams and cantilever beams machined from the inner wall of the frustule. The tests indicate a low E modulus, about 35 GPa and a very high stress at fracture, in the range of 3400MPa for the cantilever beam and 2500MPa for the three point bending test. In contrast, fused silica is reported to have E modulus of 70GPa and fracture strength of about 100MPa.

How has the diatom biosilica got such extraordinary mechanical properties? How far have we come in the understanding of the details in the bio mineralization process, where patterning is performed simultaneously as the mineralization? Which mechanisms control the morphology at the nano-scale?

More than 40 years ago, it was discovered that the frustules contain different organic components, indicating that biosilica is a composite material, and later the existence of biosilica spheres were confirmed by AFM investigation of live diatoms under natural conditions [Crawford, 2001]. Cleaved cross-sections, revealed the nanostructure to be composed of a conglomerate of densely packed silica spheres, about 40 nm in diameter.

We have been searching for evidences of the spherical surfaces in our experiments and have found some indications of spherical shapes on the fracture surfaces, but it is generally hard to find clear evidences of the spheres.

"We are ignorant of the state of organic matter inside the purported STV's (Silica Transport Vesicles), even whether any of the silica-binding proteins are in them. Such organic macromolecules could be trapped within the silica spheres during STV formation, or between them when they sinter inside the SDV, or both. There is a clear need for a definitive study of the contents of the STV's." R Gordon ["The glass Menagerie, 2008]

We speculate that the organic material forms an organic matrix that can act as a kind of grease that maybe lubricates rotation of the spheres. This might explain the low modulus of elasticity combined with the high strength. The lack of clear evidences of spheres in our examinations might be due to the cleansing treatment, which removes the organic material. This will stimulate direct contact between the spheres and make the bulk material appear rather monolithic.

The aim of the Thesis is to examine live and cleaned diatoms and determine the morphology, and if possible to determine the mechanical properties.

The following tasks shall be performed

1. Present a literature review on the morphology of diatoms
2. Present AFM, and how it can be applied to determine morphology and mechanical properties of diatoms.
3. Finalize the setup of the existing AFM in Nanomechanical lab in order to make it available for the investigations
4. Determine the morphology and mechanical properties of *Coscinodiscus* of live diatoms, and eventually compare with cleaned species.

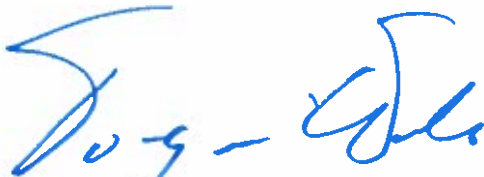
Formal requirements:

Three weeks after start of the thesis work, an A3 sheet illustrating the work is to be handed in. A template for this presentation is available on the IPM's web site under the menu "Masteroppgave" (<http://www.ntnu.no/ipm/masteroppgave>). This sheet should be updated one week before the master's thesis is submitted.

Risk assessment of experimental activities shall always be performed. Experimental work defined in the problem description shall be planed and risk assessed up-front and within 3 weeks after receiving the problem text. Any specific experimental activities which are not properly covered by the general risk assessment shall be particularly assessed before performing the experimental work. Risk assessments should be signed by the supervisor and copies shall be included in the appendix of the thesis.

The thesis should include the signed problem text, and be written as a research report with summary both in English and Norwegian, conclusion, literature references, table of contents, etc. During preparation of the text, the candidate should make efforts to create a well arranged and well written report. To ease the evaluation of the thesis, it is important to cross-reference text, tables and figures. For evaluation of the work a thorough discussion of results is appreciated.

The thesis shall be submitted electronically via DAIM, NTNU's system for Digital Archiving and Submission of Master's theses.



Torgeir Welo
Head of Division



Christian Thaulow
Professor/Supervisor

Preface

This master's thesis is written as a requirement to obtain the degree *Master of Science* at the Norwegian University of Science and Technology(NTNU). The work was performed in the 10th semester at NTNU, from the 14th of January to the 10th of June 2015. It serves as final documentation of specialization done at the Department of Engineering Design and Materials, with Prof. Dr. Christian Thaulow as supervisor.

Through the work with this thesis I have been working with both equipment and materials that were new to me. Preparing and installing an atomic force microscopy have been challenging, but also a fine way to learn to know the equipment. Working with biological material have also proven to be a challenge, with samples that are fragile and difficult to handle, but all the more rewarding when successful results are obtained.

I would like to thank Prof. Dr. Christian Thaulow, through his positive attitude and encouraging conversations he has provided guidance when needed. Thanks to Prof. Dr. Afrooz Barnoush for his guidance regarding the AFM installation. Also a big thanks to the research group, especially PhD candidate Anette Brocks Hagen for bring me up to speed on the AFM and helping me out with the installation at Nanomechanical lab. A thanks to fellow students at room 212 Perleporten for discussions of both academic and non-academic topics, making my days interesting. At last, thanks to Magnus B. Følstad(Staff engineer at Department of Materials Science and Engineering) for help with the Agilent AFM system and Matilde S. Chauton(Postdoc. at the Department of Biotechnology) for suppling diatom samples and assisting in the cleaning process.

Norwegian University Of Science and Technology

Abstract

Faculty of Engineering Science and Technology
Department of Engineering Design and Materials

Master's Thesis

Diatoms Investigated by Atomic Force Microscopy

by Torstein V. SVENDSGAARD

Diatoms are microscopic algae which have a complex outer cell wall (frustule) made up by silicon dioxide and organic proteins, collectively called biosilica. The mechanical properties of the diatom frustule have been a popular area of research in recent years. The biosilica seems to be outperforming human produced fused silica in terms of strength. The morphology and mechanical properties of the diatom *Coscinodiscus sp.*, examined by atomic force microscopy, is reported in this thesis.

The frustule is made up by three layers, where it has been found a decrease in pore size from the inner to the outer layer. The mean pore diameter was determined to be $832 \pm 133 \text{ nm}$, $447 \pm 73 \text{ nm}$ and $72 \pm 12 \text{ nm}$ for the inner (foramen), mid (cribrum) and outer (cribellum) layer, respectively. Cleaved frustules have also been investigated, where a layered structure of the biosilica was observed.

The mechanical properties of the diatom frustule have been examined by a novel AFM method, Peak Force Quantitative Nanomechanical Mapping, where the elastic modulus of the sample is mapped. Young's modulus was determined to be $27 \pm 4.2 \text{ GPa}$ and $25 \pm 3.2 \text{ GPa}$ for the foramen and cribellum layer, respectively. A slight decrease in elastic modulus was found towards the edge of the frustule on the inner layer. An interesting characteristic was found, namely a decrease in Young's modulus of the material surrounding the larger pores in the inner layer.

The reported results indicate that the biosilica is a layered composite material, where local variations in material properties are observed.

Norges Teknisk-Naturvitenskapelige Universitet

Sammendrag

Institutt for Produktutvikling og Materialer

Fakultet for ingeniørvitenskap og teknologi

Masteroppgave

Diatoms Investigated by Atomic Force Microscopy

av Torstein V. SVENDSGAARD

Kiselalger er mikroskopiske alger som har en kompleks cellevegg (frustule) bestående av silisiumdioksid og organiske proteiner, kalt biosilica. Mekanisk testing av celleveggen har gitt indikasjoner på at biosilica har egenskaper som skiller seg ut fra vanlig silisiumdioksid, som er meget sprøtt. Morfologi og mekaniske egenskaper av kiselalgen *Coscinodiscus sp.*, er undersøkt med atomkraftmikroskopi og rapportert i denne Master oppgaven.

Frustulen består av tre porøse lag, hvor det har blitt påvist en reduksjon i porestørrelse fra det indre til det ytre lag. Midlere pore diameter ble funnet å være $832 \pm 133\text{nm}$, $447 \pm 73\text{nm}$ og $72 \pm 12\text{nm}$ for det indre (foramen), midterst (cribrum) og ytre (cribellum) laget henholdsvis. Delte frustuler har også blitt undersøkt, hvor en lagdelt struktur av biosilica ble observert.

De mekaniske egenskapene til diatom frustuler har blitt undersøkt ved bruk av en ny AFM metode, Peak Force Quantitative Nanomechanical Mapping, hvor elastisk modulus av prøven kartlegges. Young's modulus ble bestemt til å være $27 \pm 4.2\text{GPa}$ og $25 \pm 3.2\text{GPa}$ for foramen og cribellum henholdsvis, og en liten reduksjon i modulus ble observert mot kanten av frustulen. En interessant egenskap ble funnet, nemlig en reduksjon i elastisitetsmodul av materialet som omgir porene i det indre lag (foramen).

De rapporterte resultatene indikerer at biosilica er et lagdelt komposittmateriale, hvor lokale variasjoner i materialegenskaper er observert.

Contents

Preface	iii
Abstract	v
Sammendrag	vi
List of Figures	xi
Abbreviations	xiii
Symbols	xv
1 Introduction	1
2 Background and Theory	3
2.1 Diatom	3
2.1.1 Frustule	5
2.1.2 Morphology	8
2.1.3 Mechanical Testing by Atomic Force Microscopy	10
2.2 Scanning Probe Microscopy	12
2.2.1 Tip-Sampel Interaction	13
2.2.2 Atomic Force Microscopy	15
2.2.3 Components	17
2.2.4 Operational Modes	20
2.2.5 Peak Force Quantitative Nanomechanical Mapping	25
3 Methods	29
3.1 AFM setup at Nanomechanical lab	29
3.1.1 Hysitron TI 950 TriboIndenter	30
3.1.2 Agilent 5420 AFM - Installation	30
3.1.3 Agilent 5420 AFM - Calibration	34
3.2 Procedure for AFM imaging and AFM-to-optic Calibration	35
3.2.1 Planning and Starting an AFM Session	35
3.2.2 AFM-to-optic Calibration	36

3.3	AFM Imaging of Diatoms	37
3.3.1	Sample Preparation	38
3.3.2	Selection of Operational mode and Probe	39
3.3.3	Imaging Procedure	40
3.3.4	Quantitative Nanomechanical Mapping	41
3.4	Analysis Tool	44
3.5	Literature Review Methodology	46
4	Results	47
4.1	Morphology of <i>Coscinodiscus sp.</i> Determined by AFM	47
4.1.1	Foramen	48
4.1.2	Cribrum	49
4.1.3	Cribellum	50
4.1.4	Cleaved Frustules	51
4.2	Peak Force Quantitative Nanomechanical Mapping	52
4.2.1	Foramen	53
4.2.2	Cribellum	53
4.3	Summary of Results	55
5	Discussion	57
5.1	Morphology of <i>Coscinodiscus sp.</i> Determined by AFM	57
5.1.1	Foramen	58
5.1.2	Cribrum	59
5.1.3	Cribellum	59
5.1.4	Cleaved Frustules	60
5.2	Peak Force Quantitative Nanomechanical Mapping	61
5.2.1	Foramen	62
5.2.2	Cribellum	63
6	Conclusion and Further Work	65
6.1	Conclusion	65
6.2	Further Work	66
A	Email correspondance	69
A.1	Hysitron email correspondance	69
A.2	Agilent email correspondance	79
B	Agilent 5420 AFM operating procedure	85
B.1	Procedure for AFM imaging and calibration	85
B.1.1	AFM-to-optic calibration	85
B.1.2	Imaging using the Agilent 5420 AFM	86
B.1.3	Ending an AFM scan	86
B.2	Performance of Agilent 5420 AFM	86

C	Extended Results	89
C.1	Morphology of <i>Coscinodiscus sp.</i> Determined by AFM	89
C.2	Peak Force Quantitative Nanomechanical Mapping	95
D	Cleaning Procedure	99
E	Formal Requierments	101
	Bibliography	105

List of Figures

2.1	Diatom Frustule	4
2.2	Binary Fission Reproduction	6
2.3	Block Structure of Silica	7
2.4	Diatom Morphology	8
2.5	Nanomechanical Mapping	11
2.6	Force Response Curve	13
2.7	AFM Principle	16
2.8	AFM Probe	17
2.9	Deflection Detector	18
2.10	Tip-Sample Interaction Model	23
2.11	Peak Force QNM	26
3.1	Agilent 5420 AFM	31
3.2	Mounting Bracket	32
3.3	AFM Installation Process	33
3.4	Calibration Samples	34
3.5	Optic-to-AFM calibration	37
3.6	Veeco Multimode V	38
3.7	Probe Selection Chart	42
3.8	Overview QNM Samples	43
3.9	Pore Size Tool	44
3.10	Particle Analysis	45
3.11	Foramen Pore Stiffness Method	46
4.1	Foramen Layer	48
4.2	Cribrum Layer	49
4.3	Cribellum Layer	50
4.4	Cleaved Cribellum and Cribrum	52
4.5	Cleaved Foramen	52
4.6	Foramen QNM	54
4.7	Foramen Pore QNM	55
4.8	Cribellum QNM	55
A.1	Basic AFM principle	70
A.2	Attached Images Agilent	80
A.3	Attached Image Agilent	82

A.4 Attached Image Agilent	83
C.1 Foramen Pore Size	90
C.2 Cribellum Pore Size	92
C.3 Cribrum Pore Size	92
C.4 Cribrum Pore Size	97
C.5 Cribrum Pore Size	98

Abbreviations

AAC	A coustic A lternating C urrent
AFM	A tomic F orce M icroscop
AM	A mplitude M odulation
FEA	F inite E lement A nalysis
FIB	F ocused I on B eam
FM	F requency M odulation
LCPA	L ong C hained P olyamines
PFQNM	P eak F orce Q uantitative N anomechanical M apping
SEM	S canning E lectron M icroscop
SPM	S canning P robe M icroscop

Symbols

E_r	Reduced Young's Modulus	Pa
E_s	Sample Young's Modulus	Pa
E_{tip}	Tip Young's Modulus	Pa
ν_s	Sample Poisson's ratio	-
ν_{tip}	Tip Poisson's ratio	-
α	Deflection Sensitivity	m/V

Chapter 1

Introduction

To reduce the environmental impact that humans have on this Earth and to push the limits of human engineered structures lighter, yet strong, materials are required in the future. To create the next generation of engineering materials, scientists have looked toward nature. Inspiration is found in one of nature's largest ecological group of organism, the diatoms, in particular the micrometer-sized cell wall enclosing the living diatom. The nanostructured cell wall is made out of hydrated silicon dioxide(biosilica) and can withstand large forces and deformation. This is quite contrary of what one might think, since fused silica produce by humans are a brittle ceramic, with low fracture toughness. In order to understand how the biosilica is structured and determine its mechanical properties a thorough investigation by atomic force microscopy(AFM) is presented in this thesis.

Determining the cell wall's morphology and mechanical properties by AFM is the main focus area in this thesis. The term morphology is her referring to the study of form and shape, this means determining the surface structure of the cell wall as well as the nanostructure of the biosilica. As this will be the first comprehensive AFM study performed at NTNU on diatoms, it will be emphasized on demonstrating the capabilities of atomic force microscopy and exploit the properties this method provide with regard to image resolution and

accuracy. Also, determining the mechanical properties of the biosilica by using a novel AFM method will be presented.

Since the topic of diatoms are not widely known for most people, the first chapter will start by introducing what diatoms are. There will be special emphasis on aspects relevant for the experimental work, such as the morphology, formation and chemical composition of the cell wall. An introduction of atomic force microscopy is given in the same chapter explaining the theory and operational modes of this microscopy method. The following chapters will present methodology, results and discussion with regard to the experimental work. Installing an AFM in the nanomechanical lab has also been performed and is presented along with other experimental methods in [chapter 3](#). In the end a conclusion is given based on the results presented earlier and a suggestion for further work.

Chapter 2

Background and Theory

This chapter presents the necessary background and theory to understand much of the experimental work in this thesis. The chapter is divided into two parts; the first part assumes that the reader knows little or nothing about diatoms, and presents what diatoms are and relevant literature on the morphology and mechanical properties of diatoms. The second part present the principle of atomic force microscopy with its basic components and different modes of operation.

2.1 Diatom

The diatoms are single celled algae, a group of eukaryotic microorganisms, that are present in almost every water habitat on earth[43]. It is estimated to be 10^5 diatom species, which makes it one of the larges and most significant groups of organisms on Earth[46]. Most diatoms live by photosynthesis and take up nutrition available in the surrounding water. Due to the large abundance, they are responsible for 40 to 45% of the carbon fixation in the oceans, making them more significant the all the world's tropical rainforest with regard to carbon storage[37].

The diatom cell is an ordinary eukaryotic algae, which means that it contains the same organelles as other algae(nucleus, mitochondria, plastids, etc)[46]. What

differentiate the diatoms from other algae is the silicified cell wall enclosing the living cell, with the major constituent material being silicon dioxide. The cell wall is made up by two valves that are overlapping and held together by a thinner structure, namely girdle bands. Collectively are the three siliceous parts of the diatom cell wall called *frustule*, see [Figure 2.1](#) for examples of frustules from a variety of diatom species. A interesting feature of the frustule is the nano-structured pattern that is unique for each individual diatom. The pattern is porous, with a variation of the pores through the thickness of the valve. In addition to the siliceous parts of the frustule, there is some organic material surrounding the frustule and in-between the different layers of the of the frustule binding it all together. The frustule's purpose is for mechanical protection of the nucleus and filtering of water.

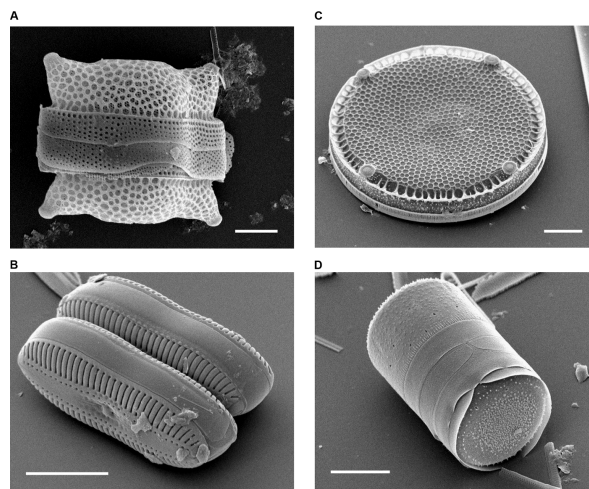


Figure 2.1: Illustrations of various diatom species, as listed: **(A)** *Bidulphia reticulata* (size bar = 10 micrometres), **(B)** *Diploneis sp.* (size bar = 10 micrometres), **(C)** *Eupodiscus radiatus* (size bar = 20 micrometres), **(D)** *Melosira varians* (size bar = 10 micrometres). Reprinted with description from Bradbury [6]

The diatoms was first discovered in 1703 by an unknown British scientist[7]. From then and until present time a large effort have been put into discovering and classifying different diatom species. The classification was debated and much uncertainty on how to differentiate between species, genus and family was one of the origin of the debate. A large collection on the classification

was published by Round et al. [46] and a brief summary of this classification is given below. The diatoms (Bacillariophyta) are divided into three classes; centric, pennate without raphe and pennate with raphe. The centric diatoms have pattern that is radial symmetric as in [Figure 2.1\(C,D\)](#), while the pennate diatoms are bilaterally symmetrical as in [Figure 2.1\(B\)](#). Where the raphe is a longitudinal groove, believed to enhance a gliding movement. The classes are further divided into subclasses, order, family and genus based on taxonomy.

In the later 20th century and into present time the research on diatoms have continued. The focus have now shifted towards understanding the silica cell wall surrounding the diatom nucleus. Scientists have been fascinated by the nano-sized patterned silica shell, and much effort have been put into understanding how the diatoms builds the cell wall and if humans can learn how to make similar structures. The silica cell wall will be discussed in great detail in below sections.

2.1.1 Frustule

The frustule of a diatom is comprised by two valves that are overlapping and held together by girdle bands. The larger overlapping valve is called *epivalve* and the smaller valve is called *hypovalve*. The two sets of valves is associated with its own set of girdle bands, namely *epicingulum* and *hypocingulum*, which holds the frustule together. A collective term for the two sets of valve and girdle band are *hypotheca* and *epitheca*.

Diatoms reproduce by binary fission, meaning that the daughter cells receives one valve and girdle band from the parent cell, while the other valve of the daughter cell is produced during cell division, illustrated in [Figure 2.2](#). This means that the set of valves and girdle bands always differs in age. When a cell divides the hypotheca becomes the epitheca of one daughter cell and the old epitheca becomes the new epitheca of the other daughter cell. Such cell division should lead to a decline in cell size, but it have been observed that the

cell size is restored in a population by auxospore; a cell which expanded before cell division. The above information is taken from Round et al. [46].

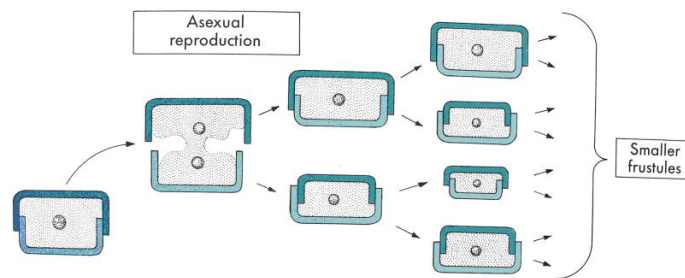


Figure 2.2: Illustration of diatom reproduction and decline in cell size.
Reprinted from <http://www.bio.vu.nl/thb/deb/quest2007.html> [23]

The new hypotheca forms during cell division in a specialized vesicle, named silica deposition vesicle(SDV)[13]. There have been a great amount of research going into understanding how the diatoms forms the silica frustule and which role SDV has in silica formation. A review performed by Gordon et al. [16] sums up the silica formation in five steps:

1. Nucleation of silica spheres of 30 to 50 nm diameter, inside a transport vesicle[15]
2. Transportation of these vesicles to the rim of a membrane bag, termed silicalemma(SL), where the silica spheres are released
3. Precipitation of silica spheres onto a growing valve [20, 51]
4. Pore formation[50, 52]
5. Thickening and pattern formation in a third dimension[15, 20, 33, 54]

The chemistry of the diatom frustule have been studied by researchers in order to understand the biomineralization process and frustule formation. Only in more recent times have the secret behind the chemistry of the frustule formation been partially revealed. It is suggested that organic matter have an important

role in the nucleation of silica spheres and species specific pattern formation[30, 31, 47, 56].

The chemical composition of the biosilica have been identified by analyzing the content of diatom frustules dissolved in hydrofluoric acid[30, 31, 47, 56]. It have been shown that phosphoproteins(silaffins and silacidins) and long-chain polyamines(LCPA) are the main organic constituent in the biosilica. *In vivo* studies have demonstrated that silaffins promotes the formation of silica spheres and silacidins controls the size of the spheres, when added to a silicic acid, as illustrated in Figure 2.3[30, 56]. Another study showed that mixing phosphoproteins with long-chain polyamines creates a block-like structure made up by silica spheres[31]. Scheffel et al. [47] have more recently identified another six insoluble proteins that are a part of the diatom frustule. These proteins, called cingulins, forms micronized rings which act as a scaffold for the silica nanostructure. *In vivo* studies have confirmed that microrings of cingulins added to a silicic acid enhance precipitation of nonporpuse silica at preferred sites[47].

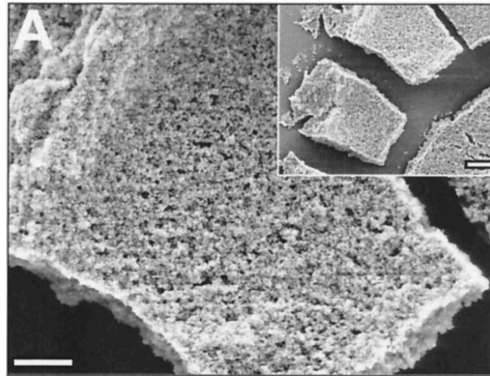


Figure 2.3: Block-like structure made up by silica spheres created *in vivo*. Scale bars, 500nm, 1 μ m(Inset). Reprinted from Kröger et al. [31]

It have been hypothesized that cingulin microrings act as an organic template for the formation of silica within the SDV. Silica precipitates attach to the microrings and forms a densely packed silica structure around the ring, but leaving the middle of the ring open. The block-like structure produced by phosphoproteins and LCPA could fill in between the the microrings, completing the frustule. It should be pointed out that the cingulins microrings was only

found in the girdle bands and not in the valve. However, 42 new proteins was identified by Scheffel et al. [47] and the functions of which are unknown. This indicates that there is still much to discover regarding the role of organic material in biosilica and frustule formation.

2.1.2 Morphology

The diatoms subjected to investigation in this work is a species within the *Coscinodiscus* genus, which belongs to the centric group of diatoms. It is a large genus and can be found in many aqueous environments, including lakes. In a light microscope the frustule of the *Coscinodiscus sp.* looks like a thin coin or barrel-shaped, depending on the specific species[46]. There have been performed numerous investigations of the genus using more sophisticated equipment, such as AFM and SEM, to reveal the nanostructure of the valves[34–36]. Three layers are identified in the *Coscinodiscus sp*; foramen, cribrum and cribellum, listed in order from the innermost(closest to the cell nucleus) and towards the outermost layer.

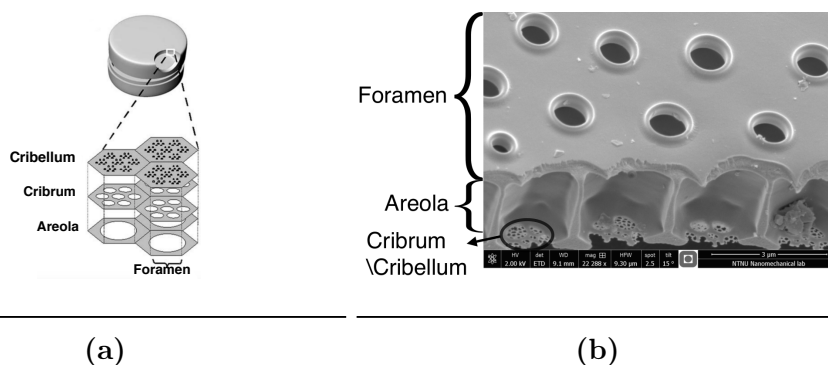


Figure 2.4: (a) Schematic illustration of the layered diatom frustule, reprinted from Losic et al. [35]. (b) SEM image of a cleaved *Coscinodiscus sp.* frustule. The larger holes are the foramen layer, which is connected by the areolae structure to the cribrum and cribellum pores

The cribellum layer has a hillock topography with domes and clusters of pores, arranged with 5-7 pores per cluster and 20 clusters per dome. The cribrum show a similar structure with a dome-like topography and an arrangement of 20 pores per dome. Areola, a hexagonal hole pattern of thin wall elements connects the

cribrum to the foramen layer. The foramen consists of larger pores, overlapping the honeycomb structure of the areolae. The pore diameter was reported to be decreasing in size from the inner to the outer layer, with a pore diameter of 1153 ± 131 nm, 45 ± 9 nm and 192 ± 35 nm for the foramen, cribrum and cribellum layer respectively [35]. Losic et al. [34, 35] identified the layers to be made up by silica nodules during AFM investigations, which they concluded originates from deposition of silica in form of spheres in the SDV. The nodule size ranged from 20 to 70 nm in diameter.

Morphology of Biosilica Investigated by AFM

A variety of different diatom species have been investigated by atomic force microscopy (AFM) [10, 35, 43]. AFM produces high resolution topography images of the scanned surface which can be used to determine pore size and surface roughness of the frustule as well as identify the smallest building blocks of the biosilica.

Crawford et al. [10] used AFM to scrape away the organic matter (mucilage) on the surface of the frustule of the diatom *Pinnularia viridis*. A smooth surface was revealed. Detergent cleaned frustules were cleaved in two to reveal its cross section. A granular appearance was found, due to the presence of silica spheres. The average silica particle diameter was determined to be 44.8 ± 0.7 nm. Cleaved samples of the diatom *H. amphioxys* were also investigated by AFM and silica spheres with average diameter of 37.1 ± 1.4 to 38.1 ± 0.5 nm were found on the valve and girdle band respectively. As mentioned earlier Losic et al. [35] have identified a granular structure on the diatom *Coscinodiscus sp.*, the size of the silica particles was determined to be 20 to 70 nm. The particle size was smaller on the inner layers compared to the other layers of the frustule.

The observations in the AFM by Crawford et al. [10] confirm that the frustule formation can be in the form of aggregation of silica particles. This is not the first time silica spheres have been observed. Chiappino and Volcani [9], the pioneer researchers on diatoms, observed "knolls" at the central nodule of a

growing valve. The central nodule is where the first silica is deposited during cell division, and can be identified on mature cells as the pore-less region in center of the valve. The knolls later disappeared as the valve matured. It was believed that the knolls were silica, deposited in form of spheres and they vanish when the valve matures due to a compacting of the silica spheres in form of an additional filler.

Other microorganisms, such as the deep sea sponge, are also made mostly out of biosilica. Silica nanospheres have been observed in these organisms, similar to that observed in diatoms[41, 57]. It has also been demonstrated that the sponges have a structure of at least six levels of hierarchy. The main structural component is made up of alternating layers of silica and organic material, resulting in a tough and elastic structure.

2.1.3 Mechanical Testing by Atomic Force Microscopy

Almqvist et al. [1] used AFM to image and test mechanical properties of the diatom species *Navicula pelliculosa* at ambient conditions, as illustrated in Figure 2.5. Whole frustules were imaged and tested using Nanoscope III Multimode (Digital Instruments, U.S.A.) AFM. Almqvist et al. [1] report measurements of Young's modulus on different spots around the frustule and a clear trend was found; the outer regions (edge of the frustule) had generally a lower modulus than the central regions of the frustule. The outer region had a Young's modulus ranging from 15 to 110 GPa and the central region a modulus ranging from 30 to 300 GPa[1]. Vickers hardness was also tested using AFM and the same trend was seen for the hardness as for the Young's modulus; softer at the outer regions and harder at the inner/central regions. Almqvist et al. [1] pointed out that there are some uncertainties in the used AFM method, which can question the quantitiveness of the reported values. However, the trend of a softer material at the edge of the frustule compared to the central part would not be affected by the lacking quantitiveness.

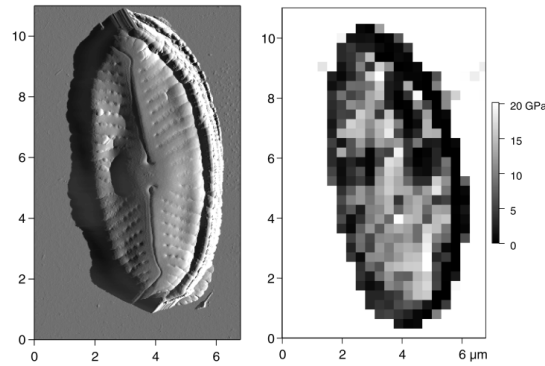


Figure 2.5: Topography image(left) and elasticity map(right) of the diatom *Navicula pelliculosa*. Reprinted from Almqvist et al. [1]

Losic et al. [36] performed nanoindentations on the frustule of *Coscinodiscus sp.* diatoms by using AFM with a diamond probe. Precise indentation forces and depths was measured and corresponding Young's modulus and hardness could be found by using a calibrated probe. Indentations was performed on all three layers; cribellum, cribrum and foramen. Young's modulus for the respective layers was determined to be $3.4 \pm 1.35 \text{ GPa}$, $1.7 \pm 0.84 \text{ GPa}$ and $15.61 \pm 5.13 \text{ GPa}$. The variation in these measurements is mainly attributed to difference in pore size and porosity of the layers. It does not necessarily correlates to the mechanical properties of the biosilica.

Pletikapić et al. [45] have performed a quantitative nanomechanical mapping of the weakly silicified frustule of the diatom *Cylindrotheca closterium* by using a Bioscope Catalyst (Bruker, USA) AFM. They demonstrated that Young's modulus varies between different regions of the frustule, corresponding to changes in degree of silicification. Young's modulus is reported to vary from 21.3 to 200MPa, from the least silicified to most silicified region. These reported values of Young's modulus are several order of magnitude lower than what others have reported[1, 36].

Mechanical properties of diatoms have been tested by other means than AFM[5, 19, 42]. Studies preformed by Hamm et al. [19] found that the frustule can withstand high compression forces and deform elastically without breaking. By finite element analysis(FEA) Hamm et al. [19] showed that the highest stress

values within the frustule were 680MPa at a maximum while having a low Young's modulus at 22.4GPa. Bjørnøy [5] performed nanoindentation hardness testing and bending test of cantilevers milled out of the frustule by Focused ion beam(FIB). A Young's modulus of 4 ± 1.5 GPa and a fracture strength of 316MPa to 365MPa was reported. Morland [42] simulated a cantilever and 3 point bending test performed by Vebner [55] and Prof. Christian Thaulow, by finite element analysis to obtain material properties. A young's modulus of 32.8 and 36.7GPa, and a Mises stress of 3415MPa and 2690MPa was reported for the two tests, respectively.

2.2 Scanning Probe Microscopy

Atomic force microscopy(AFM) is a probe-based microscope and belongs under the umbrella of scanning probe microscopy(SPM). The first probe microscope was developed by Binnig et al. [3] at the IBM Zurich Research Laboratory in Switzerland. This was called a scanning tunneling microscope(STM) and *Binnig* and *Roher* received the Nobel Prize in Physics for the invention in 1986.

The principle behind STM is fairly straight forward[2]; A tip is brought into close proximity(0.3-1nm) of the surface to be imaged. A voltage difference between the tip and sample allows electrons to "tunnel" between the two pieces and a tunneling current can be measured. The sample is scanned horizontally under the fixed tip in x- and y-direction, and the tunneling current is measured and recored at a defined number of points. The tunneling current exhibit an exponential increase with decreasing tip-sample separation. Hight changes of the surface can be calculated by using a known mathematically expression for all measurements of the tunneling current. A three dimensional topography image can be created by relating the hight measurements to their relative x- and y-coordinates.

Binnig et al. [4] further developed the STM to the system we today know as atomic force microscopy (AFM) which can image all surfaces, conductive or non-conductive, down to the atomic level. AFM is in principle similar to STM with one important exception; AFM measures the force between the tip and sample while STM measures the tunneling current.

2.2.1 Tip-Sampel Interaction

Interactions between the AFM tip and sample surface is comprised of two types of interactions; *attractive* and *repulsive* interactions. Van der Waals interaction, electrostatic force and meniscus force makes up the attractive part [8, 49]. Repulsion by electron-electron Coulomb interaction and Pauli-exclusion interaction constitutes the repulsive part [49]. Figure 2.6 illustrates the attractive and repulsive forces acting on an AFM tip as a function of tip-sample separation.

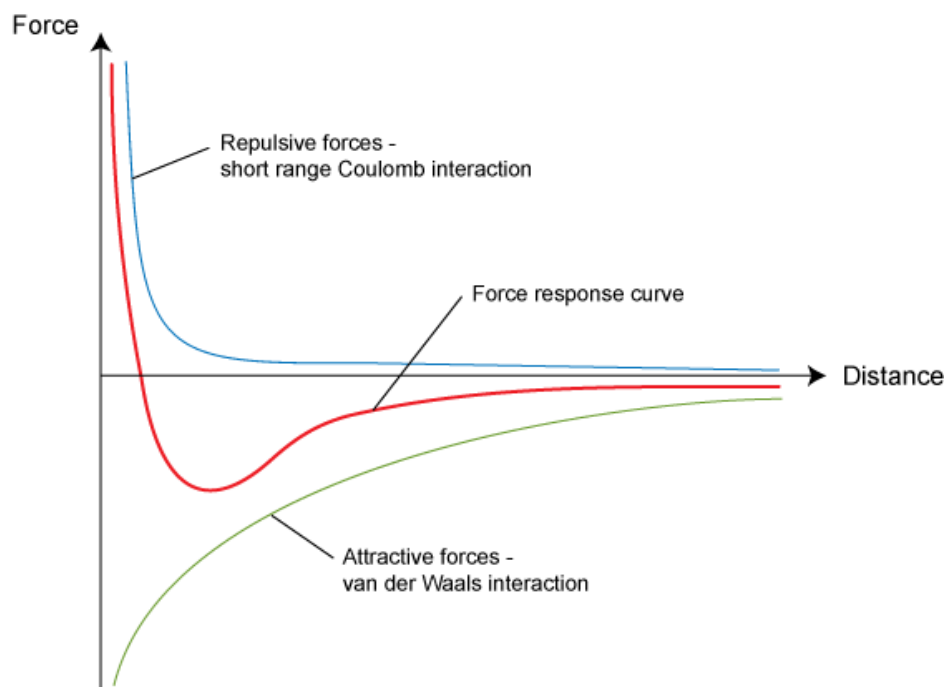


Figure 2.6: Graph is illustrating how attractive and repulsive forces act, and how the sum of those interaction creates a force-distance curve. Figure reprinted from <http://www.doitpoms.ac.uk/tlplib/afm/> [24].

Attractive Interactions

Van der Waals interactions are forces between atoms or molecules other than those due to bond formation or electrostatic interaction of ions[39]. There are three forces contributing to the Van der Waals force; Keesom(orientation), Debye(induction) and London(dispersion) force[8, 28]. The Keesom force is caused by attraction between two permanent dipoles, and is averaged over different orientation of the dipoles[8]. The Debye force is caused by a permanent dipole inducing a dipole in a neighboring molecule, thereby being a dipole-induced dipole force[8]. The London force is caused by fluctuation in the electron density in an electron cloud, so that fluctuating dipole moments occurs[8]. The latter is the most important contribution to the Van der Waals force as it acts between all molecules or atoms, where the Keesom and Debye force requires the presence of a permanent dipole. The three contributions to the Van der Waals potential scales by r^{-6} , as in Equation 2.1, where r is the distance between two interacting atoms.

$$w_L(r) = -\frac{C_k + C_D + C_L}{r^6} \quad (2.1)$$

The coefficients C_K , C_D and C_L is contributions from the Keesom, Debye and London force, respectively, and varies for different materials. The above expression is only valid for two interacting atoms. Hamaker [18] derived the interaction caused by the London force between a sphere and flat surface to be proportional to r^{-3} .

A conductive or charged sample and tip with a potential difference can cause an electrostatic force. This is a relatively long range force compared to the Van der Waals force, and can be one order of magnitude larger than the Van der Waals force at equal tip-sample separation[49].

Most samples will have a thin water layer on top of the sample surface due to absorbed water vapor from the surrounding environment. When a tip is brought into close proximity of a surface, this water layer can create a bridge of water(meniscus) between the tip and sample. The bridge will cause an attractive force between the tip and sample, also known as a capillary force[49].

Repulsive Interaction

A repulsive force is caused by close to overlapping electron clouds, in the form of Coulomb force or Pauli exclusion[8]. The repulsive force increases exponentially with decreasing distance between of the interacting atoms, which can be modeled by the Lennard-Jones potential as in Equation 2.2[32].

$$w_{LJ} = -4\epsilon \left(\frac{\sigma^6}{z^6} - \frac{\sigma^{12}}{z^{12}} \right) \quad (2.2)$$

Where ϵ is the depth of the potential well, σ is the finite distance at which the force is zero, z is the distance between interacting atoms[32]. The z^{-6} term is related to the Van der Waals force and the z^{-12} term is related to the repulsive force.

When a tip is brought into contact with a sample surface it imposes an elastic deformation on the sample. The repulsive force is for this case dependent on tip radius, imposed deformation and material properties. Such interactions can be modeled by contact mechanics, which will be discussed in a later section.

2.2.2 Atomic Force Microscopy

Atomic force microscopy (AFM) uses a scanning technique to obtain a topography image of the sample surface. AFM images contains accurate information of the sample surface and makes it possible to construct 3D images and surface profiles of the sample. Topography images are the most usual output from an AFM scan, but mapping of other outputs such as friction, adhesion, and modulus is possible, depending on the AFM system used. AFM images have a square shape and the scan size, specified by the user, sets the length of the squares sides. A typically AFM system have scan size range from $100\mu\text{m}$ to less than 10nm . Atomic resolution is possible under ideal conditions. AFM have the advantage of high resolution in both horizontal and vertical direction, compared to other microscopy methods such as scanning electron microscopes (SEM). This

makes AFM suitable for obtaining surface profiles and properties such as surface roughness, area and inclination.

The basic operational principle of an AFM is similar to the earlier explained STM, the main difference is that the tip-sample interaction is the source of the image in AFM. When using AFM an image is obtained by horizontally scanning a sharp tip mounted on the end of a small cantilever over the sample surface. A detector measures the deflection of the cantilever due to the force exerted on the tip by the sample, and records the corresponding x- and y-coordinates. The scan is performed in a raster manner, scanning one line at the time and performing a predefined number of samples per line, as illustrated in Figure 2.7a. A raster scan can be performed in two directions, either from left to right or from right to left in the fast scanning direction, which is referred to as the *trace* and *retrace*. It is common to use a resolution of 256 to 512 samples per line and line per scan, creating an image consisting of 256×256 to 512×512 pixels. Each pixel of the image is given color corresponding to the measured height at each sample. A color coded image is in this way created, which contains information of the surface topography in three dimensions.

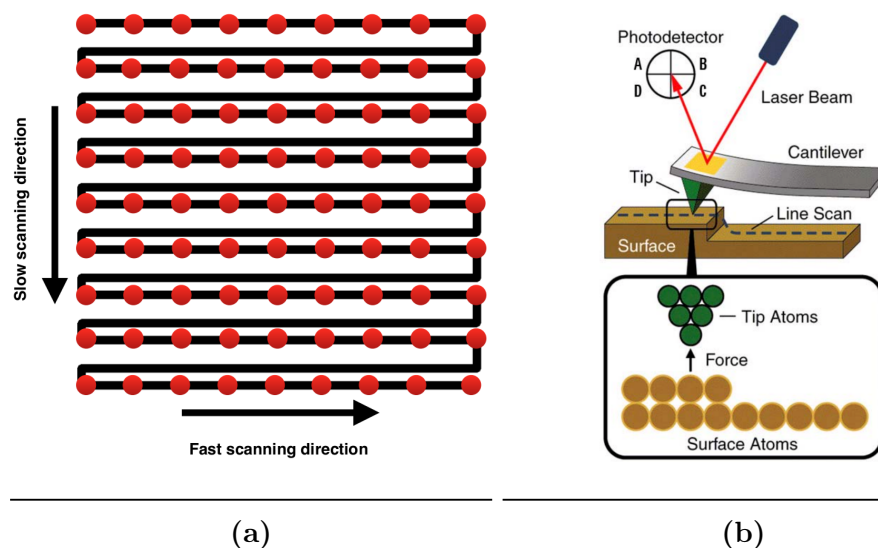


Figure 2.7: (a) Illustrates a raster scan pattern, where the red dots symbolizes the individual samples, and the black line connecting the red dots illustrates the scanning direction together with the arrows. (b) Illustrates a generic AFM setup with necessary components, reprinted from <http://www.keysight.com/> [26]

2.2.3 Components

This section will go through the basic components of an AFM and how they work. Only essential components for understanding the principle of AFM is explained. The descriptions will be based on an AFM system delivered by Agilent, but it is relevant for all AFM systems.

Probe

The probe interacts with the sample to image the surface[2]. It consists of a base, with a cantilever and a tip on the end of the cantilever, illustrated in Figure 2.8. It is mounted in a holder fixing the base during imaging. The cantilever is sticking out and is therefore free to swing and bend. The probe is usually made out of silicon or silicon nitride and can have a reflective layer of aluminum on the backside of the base.

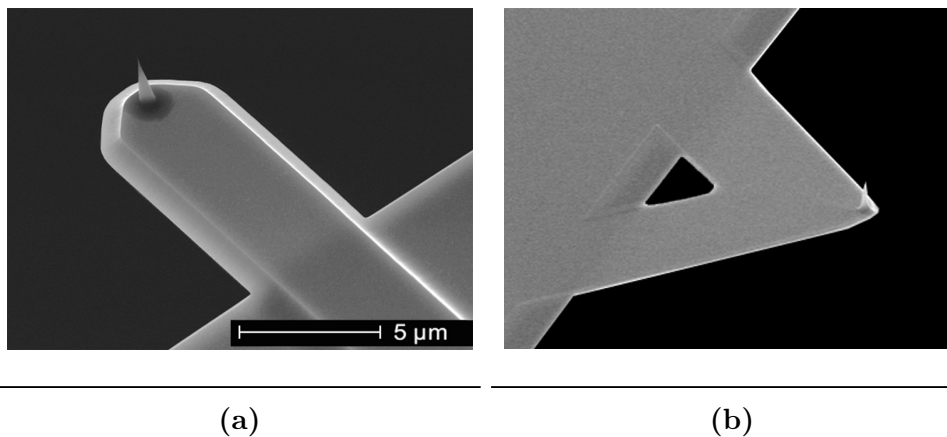


Figure 2.8: AFM probe with (a) a rectangular and (b) triangular cantilever and sharp tip at the end. Reprinted from <http://www.nanoandmore.com/> [27] and <http://nanoprobes.com/> [22]

A large selection of probes are available on the market, some of which are adapted to specific applications, while others are made for general purposes. The difference lies in the cantilever geometry, providing different mechanical behavior of the cantilever. The behavior is quantified by the natural frequency and stiffness of the cantilever. The tip can be pyramidal or tetrahedral in shape and is made out of the same material as the cantilever. A small tip radius,

typically 1 to 10nm, is necessary to obtain high resolution images. The tip will become rounded due to wear with normal usage, which makes it necessary to change the probe. Special tips coated with industrial diamond or diamond-like carbon exist for imaging of very hard surfaces and nanoindentation.

Deflection Detector

There are several ways of measuring the deflection of the cantilever, such as electron tunneling, optical interferometry, laser beam deflection and capacitance method, visualized in Figure 2.9a. Electron tunneling and capacitance method is rarely used due to inaccuracy in the measurements and limited working distance[2]. The optical interferometry method is suitable for very small cantilevers, but it is not common in commercial AFM systems[14]. The most common method is the laser beam deflection method, where a laser beam is focused on the back of the cantilever, which reflects the laser onto a photodetector. The photodetector is divided into four quadrants and initially the reflected laser is adjusted to be focused in the center of the four quadrants. The photodetector measures the change in light intensity of the upper and lower half in Volts(V), caused by the vertical deflection of the cantilever. The left and right half of the photodetector can measure the lateral bending of the cantilever to obtain frictional measurements.

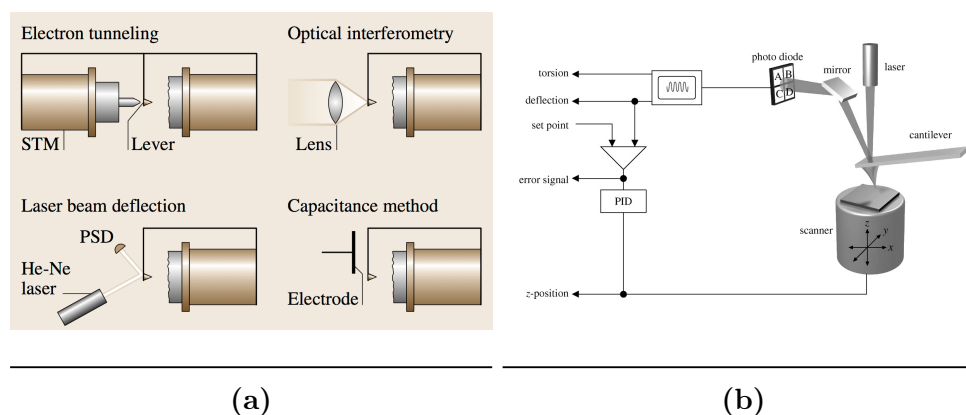


Figure 2.9: (a) Visualizing different deflection detectors, where the most common is the laser beam deflection method, reprinted from Bhushan [2]. (b) Generic AFM setup with feedback system, reprinted from <http://imgkid.com/normal-force-definition.shtml> [21].

Scanner

The scanner moves the tip and sample relative to each other so that an image can be obtained. It is usually mounted underneath the sample, so that it moves the sample around while the probe remains fixed[2]. It is also possible to mount the scanner on the probe, so that the probe moves around and the sample remains fixed. The scanner can move in all three principal direction independently, as illustrated in [Figure 2.9b](#).

The scanner is made up by tube(s) of piezoelectric material, often referred to as a piezo actuator. The piezoelectric material will contract or expand in one direction when a current is applied to the material. The direction of the electric field governs the movement, one direction will cause the material to expand and the revers direction will cause the material to retract.

Piezoelectric materials exhibit a non-ideal behavior, such as non-linearity and hysteresis, which have to be accounted for to obtain an accurate image[17]. Non-linearities are manifested by a non-linear correlation between actual extension or retraction of the piezo actuator and applied voltage. Hysteresis is a behavior in which the extension of the piezo element does not match the retraction caused by an equal and opposite electric field[38]. These non-ideal behaviors is counteracted by routinely performing calibrations of the scanner. Effects such as bow, cross coupling, aging and creep are other characteristic unwanted behavior of piezoelectric material, which are also contracted by calibration and scanner design[38].

Feedback System

The most common mode of AFM operation, constant force, requires a feedback system. The feedback system purpose is to keep the interaction between the tip and sample constant by controlling the tip-sample distance[2]. This is achieved by using the measured deflection(static mode) or phase and amplitude(dynamic mode) in a feedback system. The feedback system compares the actual measurements with a predefined set point, and calculates the error. The error signal is

sent back through a controller, usually a proportional-integral-derivative(PID) controller, to the piezo-electric actuator(scanner). The actuator will adjust the tip-sample separation so that the measured deflection or amplitude and phase will be equal to the set point.

2.2.4 Operational Modes

There are two modes of operation normally used in AFM; static(contact) and dynamic(non-contact) mode[2, 40]. It should be noted that AFM manufacturers often operates with their own mode names, such as MAC mode, AC mode, Peak Force QNM and ScanAsyst. All these modes are in principle equal to either static or dynamic mode.

Static Mode of Operation

In static mode the tip is brought into contact with the sample surface and the cantilever bends due to the repulsive force acting on the tip[2]. This is done by approaching the probe towards the sample surface with the piezo actuator in the scanner. The cantilever starts to bend due to contact forces and the piezo actuator stops the lowering process when a user-defined set point is reached. The set point can be defined in Volts or Newtons. If it is defined in Newtons, the probe is lowered until the force acting on the tip is equal to the defined force calculated by Equation 2.3[40].

$$F = kz \tag{2.3}$$

Where F is the force measured in Newton, k is the spring constant of the cantilever measured in Newton/meters and z is the deflection of the cantilever in meters. For a cantilever with constant cross section the spring constant is $k = \frac{3EI}{l^3}$. Where E is Young's modulus, l is the length and I is the moment of inertia of the cantilever. Typical spring constants for AFM probes used in static mode are varying from 0.001 to 100N/m[40]. The tip is scanned over

the surface while remaining in contact. Within the static mode there are two possible methods to obtain an image; constant height or constant force.

In the constant height mode the piezo actuator remains fixed in the vertical direction during the scan[2]. When the cantilever is scanned over the surface it will deflect due to changes in topography of the sample. The deflection is measured and recorded throughout the scan and an image containing information of the surface in three dimensions is obtained. This method has a limited working range and is used on samples with small variations in topography.

In constant force mode the force between the tip and sample is held constant by adjusting the height of the sample relative to the tip with the piezo actuator in the scanner[2]. This is achieved by sending the error signal (measured deflection minus set point deflection) back, through a PID controller, to the scanner. The scanner continuously adjusts the tip-sample height to maintain a constant deflection, which translates to a constant force between the tip and sample. In this case the extension or retraction of the piezo actuator is recorded and used directly to create a topography image of the sample.

In static mode of operation the AFM will be most accurate when the tip is pushed against the sample with enough force. This can damage both the sample and tip if the force is high enough. This problem can be avoided by using the dynamic mode of operation, which minimizes the tip-sample interaction.

Dynamic Mode

In dynamic mode of operation the probe is oscillated at or close to its resonance frequency. When scanning the sample, small changes in frequency, phase and amplitude can be measured due to a change in tip-sample force. In the literature there are many modes of operation that go under the umbrella of dynamic mode, such as frequency-modulation, amplitude modulation, self-excitation, constant-excitation, non-contact mode, intermittent-contact mode, tapping mode and constant-amplitude-mode[2]. The most relevant modes of operation will be explained in the following paragraphs.

In order to illustrate and explain how the dynamic mode works, the cantilever can be modeled by a mass-spring system. This will illustrate the main principles and some of the mathematics which forms the basis of dynamic AFM. The mass balance of the cantilever system excited by a sinusoidal external force can be expressed as in [Equation 2.4](#).

$$m\ddot{z} + \lambda\dot{z} + kz = C_0 \cos(\omega t) \quad (2.4)$$

Where λ is the damping coefficient and m is the mass of the system and k is the spring constant. The solution to this differential equation is given by $z = C_0 \cos(\omega - \varphi)$. The amplitude and phase have the known form as in [Equation 2.5](#) and [Equation 2.6](#)[29].

$$A_{max}(\omega) = \frac{C_0/m}{\sqrt{(\omega_0^2 - \omega^2)^2 + (2\gamma\omega)^2}} \quad (2.5)$$

$$\varphi = \arctan \frac{2\gamma\omega}{\omega_0^2 - \omega^2} \quad (2.6)$$

where $\omega_0^2 = k/m$ is the natural frequency and $\gamma = \lambda/2m$.

A distance dependent force, $F(x)$, can be added to [Equation 2.4](#) to include the tip-sample interaction. A coupled spring system, where the tip-sample interaction is modeled as a spring can then approximate the dynamic AFM system as in [Figure 2.10](#). Assuming that the force will be harmonic a Taylor expansion around the zero deflection of the cantilever will to first order represent the force by $F(x) \approx F(z_0) + \frac{\partial F}{\partial z} z$. The gradient($\frac{\partial F}{\partial z}$) can be defined to be k_{ts} . Through manipulation of [Equation 2.4](#) and defining $k_{eff} = k - k_{ts}$ a similar expression as above is obtained in [Equation 2.7](#). For details of this example see [\[53\]](#).

$$m\ddot{z} + \lambda\dot{z} + k_{eff}z = C_0 \cos(\omega t) \quad (2.7)$$

A shift in the resonant frequency can be observed due to the tip-sample inter-

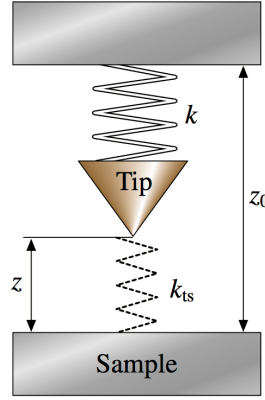


Figure 2.10: Simplified model of tip and forces in dynamic AFM, modeled as a coupled spring system. Reprinted from Bhushan [2]

action. The new resonance frequency can be calculated under the assumption of small k_{ts} , expressed in Equation 2.8.

$$\omega_0 + \Delta\omega = \sqrt{\frac{k_{eff}}{m}} \approx \sqrt{\frac{k}{m}} \left(1 - \frac{k_{ts}}{2k}\right) = \omega_0 \left(1 - \frac{k_{ts}}{2k}\right) \quad (2.8)$$

The shift of the resonance frequency is therefore proportional to the force gradient, as in Equation 2.9.

$$\Delta\omega \approx -\frac{1}{2k} \cdot \left. \frac{\partial F}{\partial z} \right|_{z=z_0} \quad (2.9)$$

This simplified example illustrates that the resonance frequency of the cantilever shifts proportional to the force gradient, due to long range interaction forces. From Equation 2.5 and Equation 2.6 it can be observed that both the amplitude and phase are dependent on the resonance frequency. This phenomenon is utilized in dynamic mode AFM, where a shift in amplitude and phase can be measured and related to the topographic change of the sample.

Operating an AFM in dynamic mode can be performed in several different ways. Amplitude modulation (AM) is one of the most frequently used operational mode of dynamic AFM [2]. The cantilever is then excited to a frequency at or close to its resonance frequency and the tip is lowered towards the sample surface. The amplitude and phase of the oscillating cantilever will shift as the

tip interacts with the sample through Van der Waals forces. When the measured amplitude is reduced to a predefined fraction of the original amplitude, the tip has reached the starting position for the scan. Topographic changes will cause the distance between the tip and sample to vary during scanning and a reduction or increase in amplitude away from the set point can be measured due to this change. The amplitude error signal (measured amplitude minus set point amplitude) is used in the feedback system to adjust the tip sample separation so that the set point amplitude is regained. The z-movement of the piezo translator can be used directly to create a topographic image of the surface. Tapping mode or intermittent contact mode of operation is closely related to the AM mode. The difference is that the tip-sample separation is smaller than in AM mode, so the tip will come in contact with the surface at its lowest point during each oscillation. A change in topography will cause a drastically change in amplitude, which is easily detected. The amplitude error signal is used in the feedback system, similar to AM mode, to adjust the piezo actuator position. Tapping mode is often considered to be a combination of static and dynamic mode since it has both dynamic and static elements.

Another dynamic mode of operating is the frequency modulation (FM). In FM mode the cantilever is always excited at its current resonance frequency and at a constant amplitude[2]. This is achieved by using the frequency as a feedback signal and shifting it by 90 degree, so that the cantilever is excited at a frequency shifted 90 degrees compared to measured frequency. The measured amplitude is also used as a feedback channel to maintain a constant amplitude and the frequency shift is used to obtain topography information of the sample.

The different mode of operation have have certain drawback and advantages over each other, which is illustrated in [Table 2.1](#).

Table 2.1: Advantages and disadvantages of different operating modes of AFM, adapted from <http://www.doitpoms.ac.uk/tlplib/afm/> [25]

Mode	Advantage	Disadvantages
Static	<ul style="list-style-type: none"> • High scan speeds • Easier to scan samples with high roughness 	<ul style="list-style-type: none"> • Lateral (shear) forces may distort features in the image • Capillary forces can disturb the image in ambient condition • High contact force can cause tip to damage sample, or vice versa, resulting in reduced resolution
Dynamic	<ul style="list-style-type: none"> • Lateral forces almost eliminated • Higher lateral resolution on most samples • Lower forces so less damage to soft samples or tips 	<ul style="list-style-type: none"> • Slower scan speed than in contact mode

2.2.5 Peak Force Quantitative Nanomechanical Mapping

AFM can be used to obtain mechanical properties such as elastic modulus, energy dissipation and adhesion of the sample. The following section will explain the basic principle of Peak Force Quantitative Nanomechanical Mapping (PFQNM) developed by Veeco Inc [44]. PFQNM is a specialized tapping mode, where the maximum force on the tip is controlled rather than the amplitude which is normal for most tapping modes. The core of PFQNM is the force curve, where the tip-sample force vs. separation is plotted and analyzed to obtain mechanical properties. See [Figure 2.11c](#) for an example of a force curve. From each pixel of an PFQNM image a force curve is obtained and analyzed on the fly, which produces a high resolution map of mechanical properties.

A interpretation, adapted from Pittenger et al. [44], of the force curve in [Figure 2.11a](#) is presented to give an understanding of the process. **(A)** When the tip is far from the sample it feels no forces. **(B)** As it approaches the surface the force increases until the stiffness of the cantilever is overcome and it "jumps to contact". **(C)** The tip stays in contact until the Z modulation reaches its bottom position where the peak force occurs. **(D)** The probe withdraws and reaches its minimum force where the tip is pulled of the sample surface. **(E)** The force on

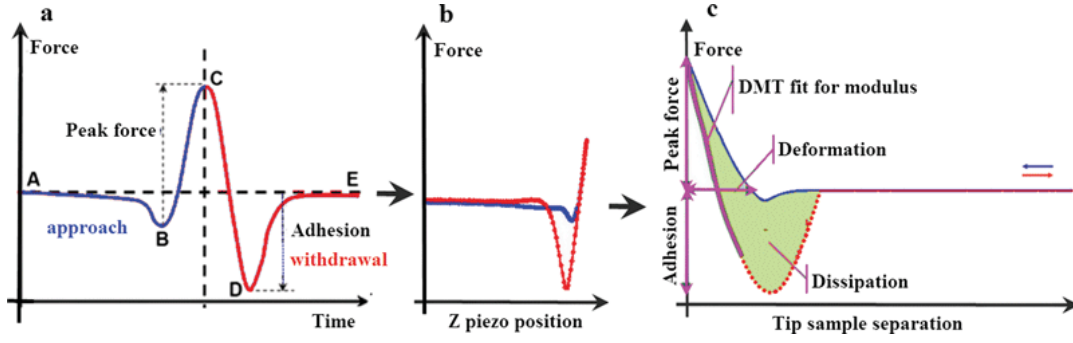


Figure 2.11: (a) Force vs. time plot for one oscillation. (b) traditional force vs. Z piezo position curve. (c) Force vs. tip-sample separation. Reprinted from Pittenger et al. [44].

the tip decreases as it moves away from the sample until maximum tip-sample separation.

The Z-position of the piezo and deflection of the cantilever is measured as a function of time, so the time variable can be eliminated as in Figure 2.11b. The force vs. tip-sample separation curve is obtained by subtracting the deflection of the cantilever from the Z-position of the piezo. This curve can be used for fitting purposes of different models as illustrated in Figure 2.11c.

The reduced modulus is calculated using the retractive part of the force curve and fitting it to the DMT model given by Equation 2.10 for each pixel[11, 44]. The DMT model is similar to the Hertz contact model, but it also includes the effect of Van der Waals forces acting along the perimeter of the contact area.

$$F - F_{adh} = \frac{4}{3}E_r\sqrt{R(d - d_0)^3} \quad (2.10)$$

E_r is the reduced modulus, $F - F_{adh}$ is the force on the cantilever relative to the adhesion force, R is the tip radius and $d - d_0$ is the deformation of the sample. Young's modulus can further be calculated if the Poisson's ratio of the sample is known, through Equation 2.11

$$E_r = \left[\frac{1 - \nu_s^2}{E_s} + \frac{1 - \nu_{tip}^2}{E_{tip}} \right]^{-1} \quad (2.11)$$

Where E_s, E_{tip} and ν_s, ν_{tip} are the Young's modulus and Poisson's ratio of the sample and tip, respectively. The tip is assumed to be infinite stiff and thus reducing the expression to [Equation 2.12](#).

$$E_r = \left[\frac{1 - \nu_s^2}{E_s} \right]^{-1} \quad (2.12)$$

To obtain quantitative measurement of Young's modulus, the unknowns variables in [Equation 2.10](#) and [Equation 2.12](#) are determined by calibrating the AFM system. There are two methods to do this, the relative and absolute method of calibration.

The relative method relies on using a reference sample with known Young's modulus. First, the deflection sensitivity is obtained by a weak indent in a hard reference sample. This will obtain the constant α in Hook's law as in [Equation 2.13](#). Where F is the force in Newtons k is the spring constant in N/m , V is the deflection of the cantilever measured in volt and α is the deflection sensitivity in m/V . The deflection sensitivity converts the measured deflection from units of volts to meters, ensuring that the force is in Newtons.

$$F = k\alpha V \quad (2.13)$$

The nominal spring constant of the cantilever is provided by the manufacturer and can be entered manually in the software. Next, a less stiff reference sample with known modulus is scanned and an initial tip radius is assumed. This will produce measurements of Young's modulus, which can be used as a starting point for finding the tip radius. By iterating through different tip radii and matching the measured modulus to the known modulus of the reference sample, a tip radius is obtained. The sample can now be scanned with a calibrated tip. However, the tip radius determined is a function of the deformation, and the measurements of Young's modulus is only correct when it is measured with the same deformation as during calibration. The force must therefore be adjusted to ensure a deformation of the sample equal to the deformation measured during

tip calibration. This is why it is called the relative method, the parameters are only calibrated relative to each other.

The absolute method uses a build-in function in the software to obtain an accurate spring constant, by finding its resonance frequency. The tip radius is obtained by scanning a tip-calibration sample, and running the image through the software. Absolute measurements of the spring constant and tip radius are determined by this method.

PeakForce QNM is considered a quantitative method by the producers of the system[44]. To get reproducible results the calibration have to be performed accurately. Reports on the performance of PeakForce QNM ability to measure quantitative material properties have shown a good correspondence between the AFM measured properties and the known bulk properties[12, 58].

Chapter 3

Methods

This section consists of three parts; the first part describe the work carried out in order to install an AFM in the Nanomechanical lab at NTNU. The second part describes how the experiments have been performed and analyzed. The last part describes how information presented in the literature review was gathered.

3.1 AFM setup at Nanomechanical lab

Nanomechanical lab at NTNU was opened in 2006 and is a part of NTNU's focus on nanotechnology. The core of nanomechanical lab's equipment is an ESEM Quanta 650(FEI, USA) and a TI 950 TriboIndenter®(Hysitron Inc.,USA). The TriboIndenter is used to characterize mechanical properties of various materials. The characterization can be performed at ambient condition, in liquid or with a electrical potential applied to the material. An Agilent 5420 AFM was purchased in 2012 by Nanomechanical lab, which was planned to be installed inside the TriboIndenter chamber. There have been efforts to prepare the AFM for installation by others, but the task has never been completed. Much work in this thesis has been put into planning and installing the Agilent AFM. The following section will document how this work has been performed and give a brief introduction to some of the equipment used.

3.1.1 Hysitron TI 950 TriboIndenter

The Hysitron TI 950 TriboIndenter® has three main components; optical camera system, transducer assembly and stage, marked in [Figure 3.3d](#). All this is mounted inside a vibration and acoustic isolated chamber and connected to a software package delivered by Hysitron Inc. The optical camera is used to locate specific areas of interest on the sample and have a magnification range from 20x to 200x zoom. Positioning of the sample is done by the stage which can move in all three principal directions. The transducer assembly is the "heart" of the Hysitron equipment where a variety of nanoindentation probes can be mounted and accurate indentation forces and deformations are measured. A maximum force of 10mN can be applied and minimum force and displacement of 30nN and 0.2nm can be measured.

The system is used to perform high precision indentation, scratch and wear testing. It is also possible to perform in-situ imaging, by scanning probe microscopy (SPM). Numerous upgrades and extra equipment is available such as Modulus Mapping, dynamic material testing and electrical contact resistance testing.

3.1.2 Agilent 5420 AFM - Installation

The Agilent 5420 AFM is a high precision atomic force microscope, which at its best can give atomic resolution. All necessary equipment and software for imaging and analyzing samples was delivered in the package. This particular model was chosen for two main reasons; its ability to operate in both liquid and at ambient condition, and the scanner mounting position. In most AFMs the sample is mounted on top of the scanner, so that the sample moves underneath the tip. AFMs delivered by Agilent have the probe mounted onto the scanner, so that the probe moves over the sample. Since our sample will be mounted on the Hysitron stage, it is necessary to have a probe that can be scanned over the sample to make a successful integration between the two system. The Agilent

AFM and TI950 TriboIndenter will be operated using their designated software packages, meaning that the user will have to switch between the Agilent and Hysitron software. The idea is that the user will be doing indents (or other tests) with the TriboIndenter and then move the stage so that the indents are located underneath the AFM probe, by using the Hysitron software. The user can then switch to the Agilent software and approach the probe to image the area of interest. The Agilent 5420 AFM should, at ideal conditions, give higher resolution images than the SPM function built into the TriboIndenter.

The Agilent 5420 AFM is delivered from the producer as an independent product for use in material research. It is in no way prepared to be installed inside other equipment, such as the TI950 TriboIndenter. To mount the AFM in the Hysitron chamber it is therefore necessary to do several modifications of both the Agilent 5420 AFM and the TI 950 TriboIndenter. When the author received the project it was already started on this work. The AFM system had been dismantled from its base and all wire-connections was screwed free, as illustrated in [Figure 3.1](#). Note that scanner is removable and can later be installed in the scanner support imaged [Figure 3.1b](#).

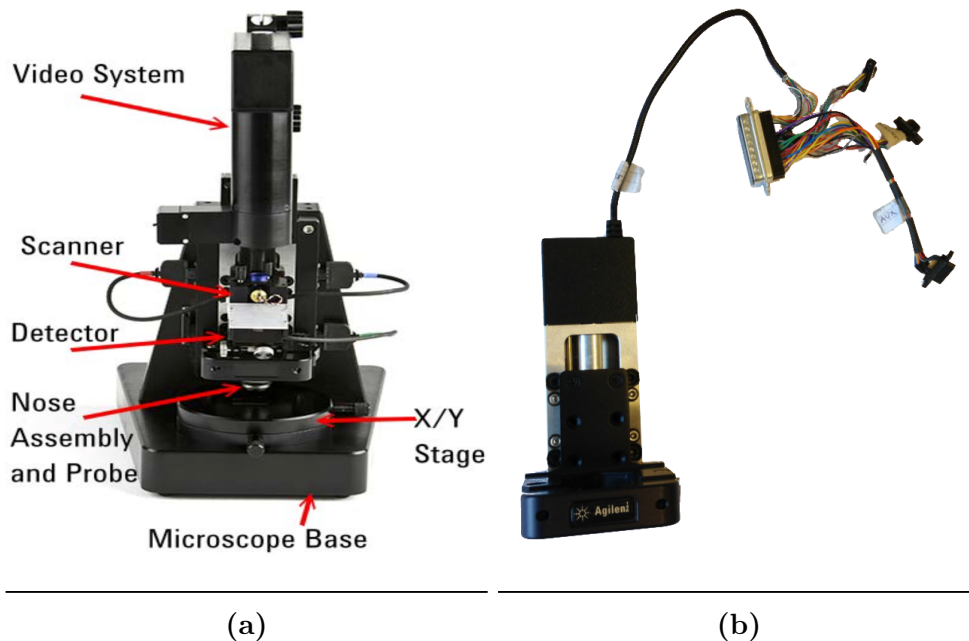


Figure 3.1: (a) Agilent 5420 AFM as delivered from manufacturer, reprinted from [38]. (b) Dismantled scanner support, to be mounted in TI950 TriboIndenter

The AFM in the dismantled condition was the starting point for the work in this thesis and several adaptations had to be made in order to install it inside the Hysitron chamber and make it operational. A mounting bracket was delivered by Hysitron, which have room for the AFM in addition to the transducer and optical microscope. The AFM is mounted onto this plate by using a dovetail-rail system from Edmund Optics Inc. It was necessary to design and produce an adapter plate between the dovetail and the AFM scanner support to avoid drilling new holes in the dovetail-rail system. The parts are illustrated in [Figure 3.2](#).

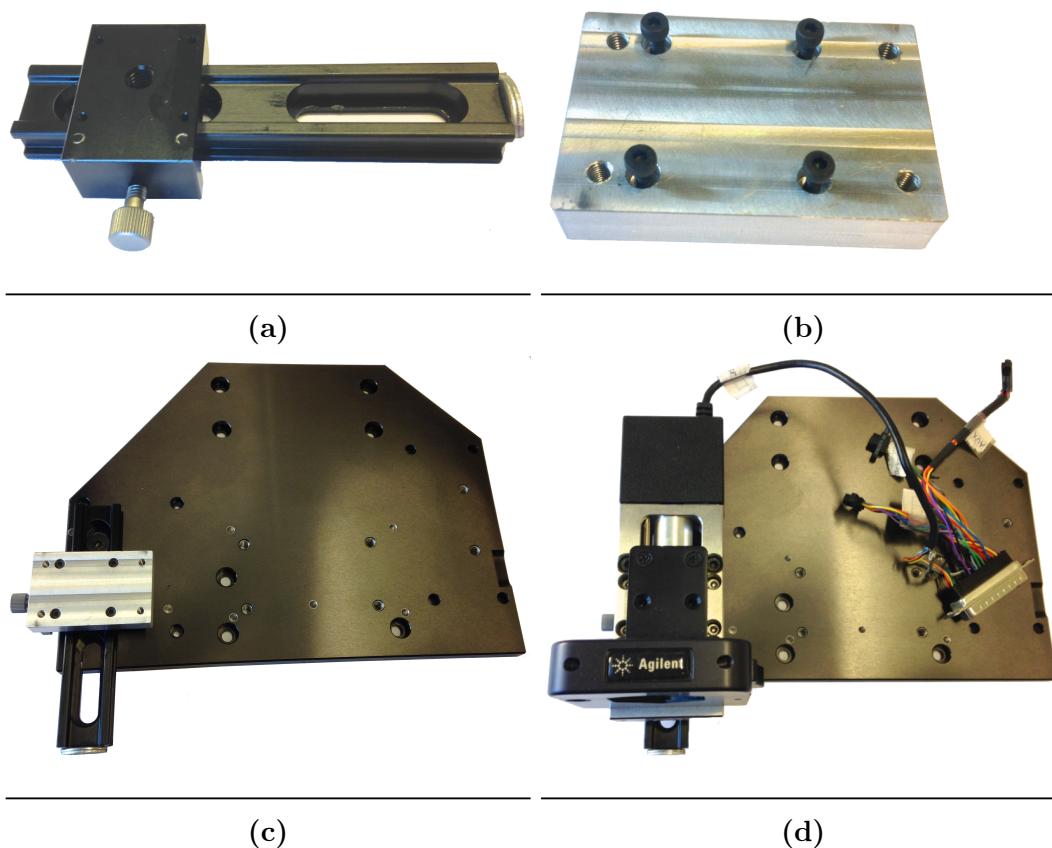


Figure 3.2: (a)Dovetail-rail system and (b)adapter plate for mounting AFM on dovetail-rail system. (c)Mounting bracket from Hysitron with dovetail-rail system and (d) scanner support mounted.

The next step of the installation was to replace the bracket installed in the Hysitron TriboIndenter with the new and larger bracket. This work involves dismantling the optics and transducer assembly, and is not a standard operation described in the manual from Hysitron. With assistance from a Hysitron service

engineer, the acoustic enclosure top was removed to access the granite frame on which the bracket is mounted, as in [Figure 3.3b](#). The transducer assembly and optic was first dismantled from the bracket, then the bracket was dismantled from the granite frame. The new bracket was mounted onto the frame, and the optic and transducer assembly was mounted onto the new bracket. [Figure 3.3c](#) and [Figure 3.3d](#) illustrates how the chamber looks before and after the AFM installation. The scanner support was mounted as in [Figure 3.2d](#), where the scanner can be inserted into the support on a later occasion. Two cables to the AFM was also pulled inside the TriboIndenter through a slit in the acoustic enclosure, which goes back to the AFM controller. To plan and perform the installation of the new bracket in a safe manner, a continuous dialogue was held with Hysitron and Agilent, see [Appendix A](#) for email correspondence.

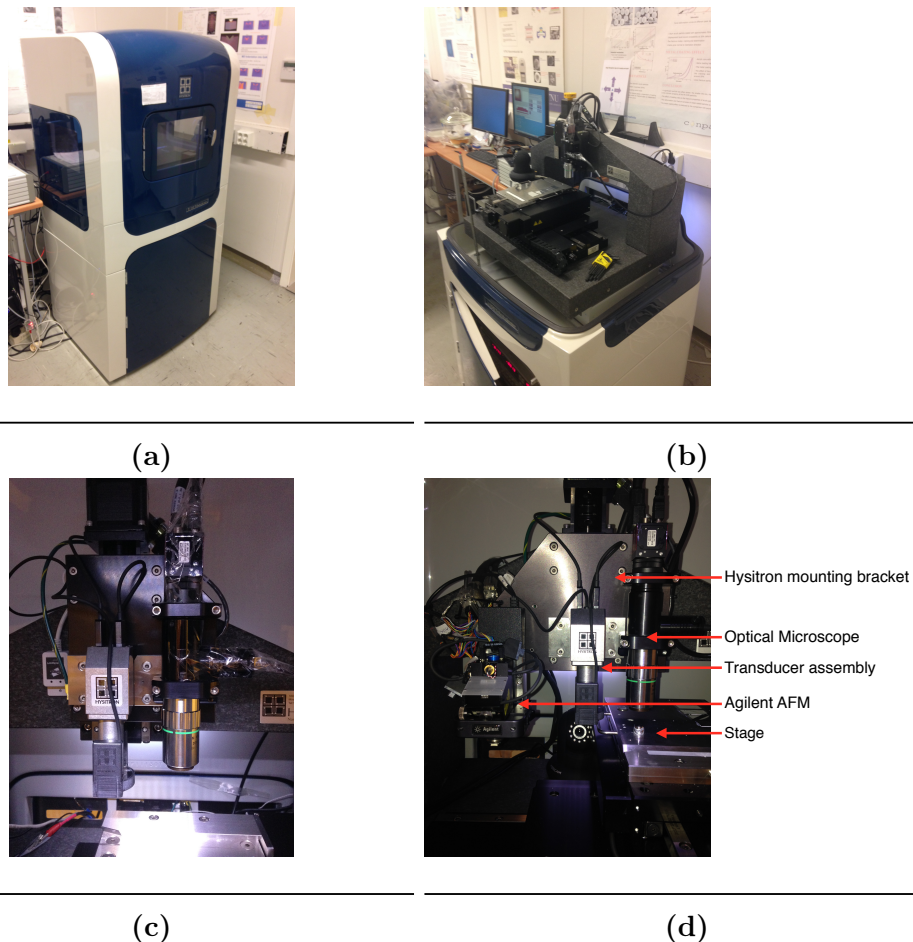


Figure 3.3: (a) Hysitron TI 950 Triboindenter with acoustic enclosure, and (b) without the enclosure exposing the granite frame. (c) The original setup and (d) the new setup with AFM.

3.1.3 Agilent 5420 AFM - Calibration

After installing the Agilent 5420 AFM it was necessary to perform a calibration of the scanner and an optic-to-AFM calibration. Calibration of the AFM has to be performed regularly, about twice a year, to ensure that the AFM will produce accurate images. The piezo actuator in the AFM exhibit a non-ideal behavior and the calibration tries to counteract this unwanted behavior, as described in [chapter 2](#).

Calibration is performed by scanning a sample with known characteristic dimensions, in our case a chessboard-like sample was used, as imaged in [Figure 3.4](#). The square features on the calibration sample are $5 \times 5 \mu\text{m}$ and has a height differ-

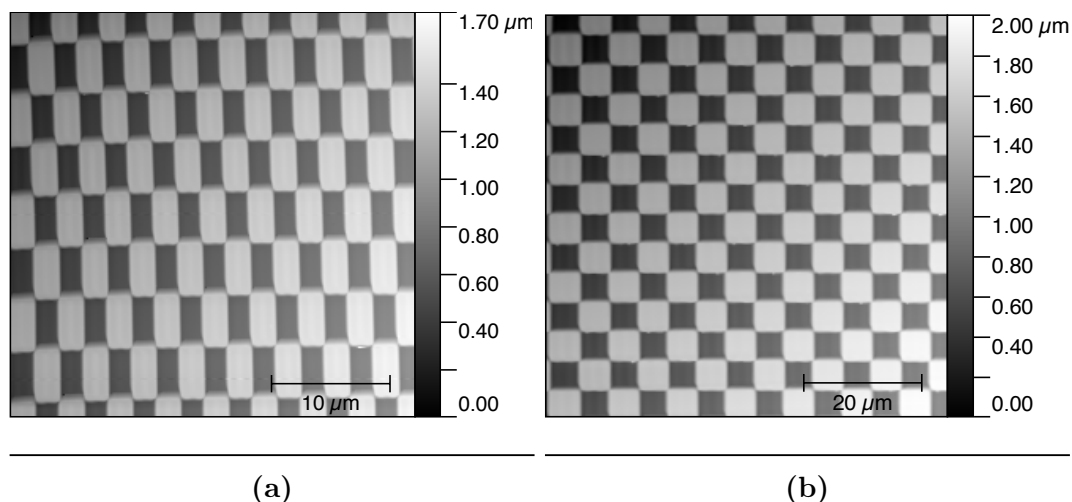


Figure 3.4: Calibration sample (a) before and (b) after calibration

ence of $2 \mu\text{m}$ between the highest and lowest feature. The calibration procedure goes through several steps to counteract different phenomenon related to the behavior of the piezo actuator. First, correction of non-linearities in x-direction was performed. This corrects the difference in measured length of the features in x-direction, which should be $5 \mu\text{m}$ in both ends of the scanner range. Second, the hysteresis in x-direction is corrected, which is manifested by an offset of the trace and retrace of the scan. Third, the x-sensitivity is corrected to get an accurate measurement of total length in x-direction. This done by measuring the length between ten features, which should be $50 \mu\text{m}$. If the measured

length deviates from the actual length, a correction has to be made to the x-sensitivity data. Similar calibration was also performed in y- and z-direction. The calibration was performed in accordance to the *Agilent 5420 AFM USER MANUAL - Scanner Maintenance and Calibration*, and details can be found there in Chapter 8 for the curious reader[38].

3.2 Procedure for AFM imaging and AFM-to-optic Calibration

In order to transfer knowledge of how to use the Agilent 5420 AFM integrated with the Hysitron TI950 TriboIndenter, a brief procedure of operation is given. This procedure assumes some basic knowledge of AFM. A procedure for manually calibrating the the AFM-to-optic is also presented.

3.2.1 Planning and Starting an AFM Session

The user has to decide which mode of operation they want to use before starting up the system. The two modes available are contact and Acoustic AC(tapping) mode. There are several factors that the user must take into account when choosing mode of operation, a short summary of these are found in [Table 2.1](#).

When an operating mode is chosen, the user must install a probe corresponding to the chosen mode. Currently there are only two probes to choose between, contact and AAC. It is possible to order other probes with different cantilever characteristics such as stiffness and resonance frequency in the future if that is needed. The scanner can now be mounted into the scanner support, by simply pushing a knob on the right side of the support to open it. Three wires have to be connected to the scanner and detector; red cable from scanner goes to cable marked *Scan HV*, blue cable from scanner goes to cable marked *Scan LV* and green cable from detector goes to cable marked *detector*. The system can now be powered on, this is done by powering up the controller and MAC III box.

The laser has to be aligned so that it reflects off the cantilever, and the photodetector has to be adjusted so that the reflected laser spot is in the center of the detector's four quadrants. Detailed description of this is found in the *Agilent 5420 AFM USER MANUAL - Preparing for imaging*[38]. The AFM is now ready to be engaged and scan the sample surface, see [Appendix B](#) for a step-by-step procedure on how to do this successfully.

3.2.2 AFM-to-optic Calibration

Every time the AFM probe is changed an AFM-to-optic calibration has to be performed to determine the distance from the center of the optical camera in the Hysitron equipment to the AFM tip. This calibration is done manually and involves switch between the Hysitron and Agilent software. Care has to be taken so that neither the AFM or Hysitron equipment is damaged during the calibration. An aluminum sample is used for this calibration which has a series of indents decreasing in size. The larger indents are some hundred micrometers in size, and visible for the human eye. At the end of the series of indents there has been made a *H-pattern* of small indents with the TriboIndenter. See [Figure 3.5](#) for images taken during tip-to-optic calibration.

During calibration, the x- and y-coordinates of the stage is recorded first when the H-pattern is in center of the optical camera image. Thereafter the stage is moved so that the AFM is imaging the H-pattern and a second set of coordinates can be recorded. The distance from the optical camera to the AFM tip is found by subtracting the two coordinate sets. The larger indents are used as visual references and guiding the user towards the H-pattern. A step-by-step procedure for calibrating and imaging can be found in [Appendix B](#)

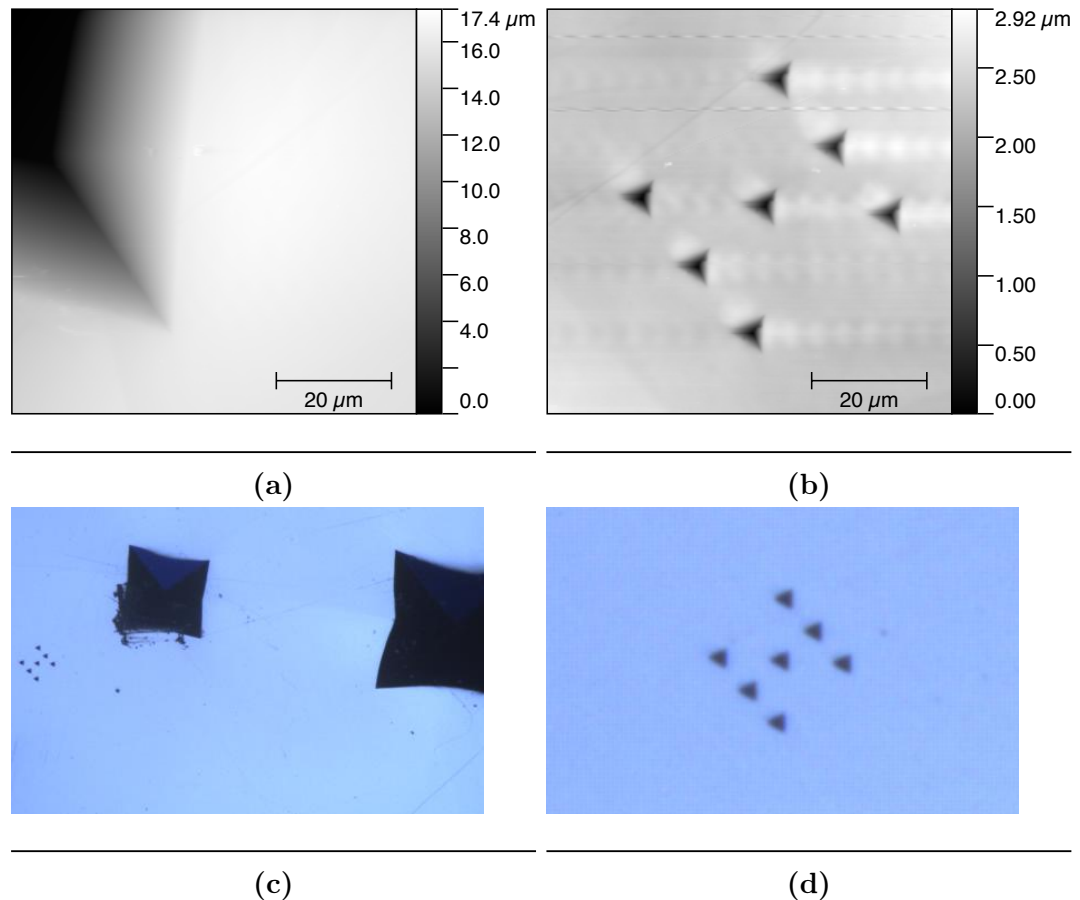


Figure 3.5: AFM and optical images taken during optic-to-AFM calibration. (a) Edge of large indent image by AFM, (b) H-pattern imaged by AFM. (c) Large indents and H-pattern imaged by the optical microscope, and (d) magnified optical microscope image of H-pattern

3.3 AFM Imaging of Diatoms

The *Coscinodiscus sp.* diatom have been investigated by AFM in order to determine the morphology of the frustule. Through these studies it has been focused on exploiting the good features that AFM provides compared to other microscopy techniques. The different layers have been imaged to decide surface characteristics and cleaved frustules have been imaged to find the structure of the biosilica. A novel AFM method (PFQNM) has also been used to map the mechanical properties of the frustule. Due to time-consuming preparation of the Agilent AFM most of the AFM scans have been performed at NTNU Nanolab using a Multimode V AFM (Veeco Corp., USA), imaged in [Figure 3.6](#). The Multimode V have the same operational principles as described in [chapter 2](#),

and is the only AFM that have the ability to map mechanical properties by Peak Force QNM.

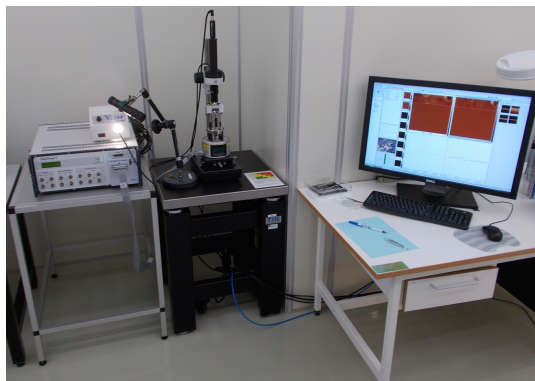


Figure 3.6: Veeco Multimode V AFM at NTNU Nanolab

3.3.1 Sample Preparation

Diatom samples from a trawl haul in the trondheimfjord was made available for investigation by the biological department at NTNU. These samples was cleaned with a mild detergent, sodium dodecyl sulfate (SDS) mixed with ethylenediaminetetraacetic acid (EDTA), to remove organic material surrounding the frustules. The cleaning process is performed by suspending a small amount of frozen diatom mass in MQ-water and centrifuging several times. Thereafter the samples are resuspended in detergent and centrifuged to rinse the samples. This is repeated until the green color of the samples turn into blank/white color, indicating that excess organic material is removed. The samples is then rinsed in MQ-water again, dried and suspended in ethanol for storage. A detailed description of this procedure can be found in [Appendix D](#). Samples cleaned with a more aggressive detergent, sulfuric acid, was also available from the work of earlier master's students.

It was attempted to make a culture of living diatoms in cooperation with the biological department at NTNU. A small amount of living diatoms was set in diatom medium at 18°C with lights on for 16 hours to culture for two weeks.

Unfortunately no culture could be found after this period. For reasons unknown, it is believed that small amount of living diatoms that we started with was already dead.

Cleaned diatoms was stored on test tubes in ethanol. Samples was drawn from the test tubes using a pipette and dispensed onto a thin magnetic substrate which can be placed in the AFM. Double sided tape was used to adhere the samples to the substrate. The frustules have most likely been divided during cleaning or dispensation and only single valves could be observed on the substrate. Other methods for securing the sample was also considered, such as coating the substrate with polylysine. This is a widely used method for securing biological samples to the underlying substrate, unfortunately it was not available at NTNU.

3.3.2 Selection of Operational mode and Probe

To examine diatoms using AFM it was first necessary to test out different operating modes to find which mode that would produce the highest image quality. Tapping mode, contact mode and ScanAsyst PFQNM was tested out on the same diatom sample. Tapping and contact mode is described in [chapter 2](#). ScanAsyst PFQNM is a specialized branch of tapping mode where the software makes continuous adjustments of gains in the feedback system and the set point, in order to enhance the image quality. In combination with a calibrated tip the ScanAsyst PFQNM mode will also give mechanical properties of the sample. This mode was developed by Veeco Inc. and is therefore only available by using the Multimode V (Veeco Inc., USA).

By comparing the image quality and ease of use of different modes, ScanAsyst PFQNM was chosen as the favorable operating mode. The main reason for this choice was that ScanAsyst PFQNM was the mode that produced images with the the least amount of noise. Diatom samples lying against a substrate is not inherently stable, as the convex or concave surface of the diatom frustules

can cause the diatom to move or vibrate due to interactions with the AFM tip. This would be manifested by noise in the AFM image. The ScanAsyst PFQNM will automatically lower the interaction force and scanning rate if the software detects instabilities in the system. A probe specialized for this mode is delivered by Bruker Inc. It is a triangular probe with stiffness of 0.4N/m and nominal tip radius of 2nm which is capable of producing images with high magnification.

3.3.3 Imaging Procedure

Prepared substrates was placed on top of the scanner in the AFM and the particular diatom to be imaged had to be located in the AFM. This was done by manually adjusting the substrate position with a twizer to roughly place the diatom underneath the probe. A fine adjustment of the probe position was performed by using dedicated adjustment screws on the AFM and checking the alignment through the optical microscope. The probe was then lowered towards the sample and the imaging procedure starts automatically. Scanning parameters such as scan rate, size and resolution can be adjusted when the probe is engaged. Typical scanning parameters that was chosen was a scan rate of 1Hz, size from 20 μ m to 250nm and resolution of 256 to 512 samples per line.

Imaging diatoms demands a lot of trail and error to find suitable samples. It was often observed that the imaged diatom was unstable and moved during imaging. If this was observed the set point was manually increased, which results in a increased tip-sample interaction. The point of this was to press the valve into the substrate so that it would adhered better to the tape. If this method was not successful, another diatom sample was found and imaged.

Cleaved diatom valves was also investigated by AFM. Cleaving the diatom valves and positioning them proved to be a challenge. Crawford et al. [10] mounted frustules on optical fibers and cleaved the frustule with a specialized cleaving tool. This method could not be used, since such a cleaving tool was

not available at NTNU. A simpler method was attempted; diatoms on a magnet substrate was cleaved by using a sharp needle under a stereomicroscope (Nikon Instruments Europe, Amsterdam). The needle was used to manipulate the diatom into the wanted position with the cleaved surface in a close to horizontal position. The sharp end of the valve towards the substrate had a tendency to sink into the double sided tape, which has a glue-like texture, during the handling and thereby fixing the diatom in a close to vertical position. The cleaved surface was imaged by positioning the probe close to the area of interest and choosing a small scan size to minimize the tip-sample interaction. Some of the cleaved valves proved to be unstable, resulting in an image with noise or no image at all. It was attempted to stabilize the sample by performing an indent on the fractured surface, with the intention to press the valve into the tape so that it would be fixed better to substrate. This was done by using the *ramp* function in the Multimode software, which allows the user to prescribe a vertical movement of the tip with nanometer precision. If this method was not successful another diatom sample was found and imaged.

3.3.4 Quantitative Nanomechanical Mapping

Quantitative Nanomechanical Mapping (QNM) of diatoms have been performed to obtain mechanical properties such as Young's modulus of the biosilica. To make this method quantitative it is crucial to select a suitable probe and perform calibration of the probe before imaging. Selection of the probe is based on the recommendation found in the QNM user manual from Bruker Inc. as illustrated in [Figure 3.7](#). An initial guess of the sample Young's modulus is needed in order to use this chart. From experiments performed at NTNU and published material from Hamm et al. [19] and Almqvist et al. [1] it is reasonable to assume a Young's modulus in the range from 7 to 30 GPa. There are two probes suitable for imaging such samples; TAP525A and DNISP-HS. DNISP-HS is an expensive diamond probe, and it is not available at NTNU Nanolab. TAP525A is a silicon

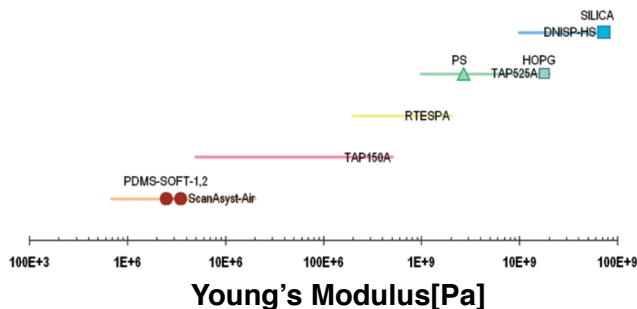


Figure 3.7: Probe selection chart from Bruker Inc.[44]

nitride probe, with a nominal cantilever stiffness of 200N/m. TAP525A was chosen as the preferred cantilever due to sufficient stiffness and availability.

Calibration was performed on a calibration sample of fused silica and sapphire, with Young's Modulus of 72.9GPa and 450GPa respectively. The relative method of calibration was used, as described in [chapter 2](#). The absolute method was considered, but this method is not suitable for stiff cantilevers ($k > 1\text{N/m}$) and was therefore not used[44]. First, several weak indents were performed on a stiff surface (sapphire) to update the deflection sensitivity. Five indents were performed at different locations on the sapphire sample. An average deflection sensitivity was calculated and entered into the software. The user manual suggests that one indent is enough to ensure reliable sensitivity calibration, but a contaminated sample surface can cause biased calibration and thus several indentations were performed to counteract this bias.

The next step in the calibration process is to find the tip radius. This is done by scanning a sample with known Young's modulus, in our case fused silica was used. A scan size of $1\mu\text{m}$ was chosen and a sufficiently high force to cause deformation in the range of 4nm to 6nm of the sample was used. The exact deformation was recorded, which will be used during imaging. The tip radius is found by iterating through different radii until the measured Young's modulus

equals the known modulus of the reference sample. The probe is calibrated when these steps has been performed.

A substrate with diatom frustules mounted was than installed in the AFM for quantitative nanomechanical mapping. The QNM procedure is similar to normal imaging by AFM with a few exceptions. Controlling the deformation of the sample is crucial for obtaining accurate results. The calibration performed is only valid for a sample deformation equal to the deformation recorded during calibration. A small scanning area was used to set the deformation, typically $1\mu\text{m}$. The force between the tip and sample was adjusted through the software until a deformation equal to the deformation during calibration was measured.

Both the foramen and cribellum/cribrum layer was imaged using PFQNM. A large scan of the whole frustule was first attempted, this induced movement and instabilities in the system. It was therefore performed three smaller scans from the center and radial outwards towards the rim of the frustule as marked in [Figure 3.8](#). A scan size of $5\mu\text{m}$ was used for the mid and edge region, and $10\mu\text{m}$ was used for the central nodule(CN) to cover the whole pore-less area. The middle layer(cribrum) is concealed by the outer(cribellum) and inner(foramen) layer, so the mapping has only been performed on the two latter.

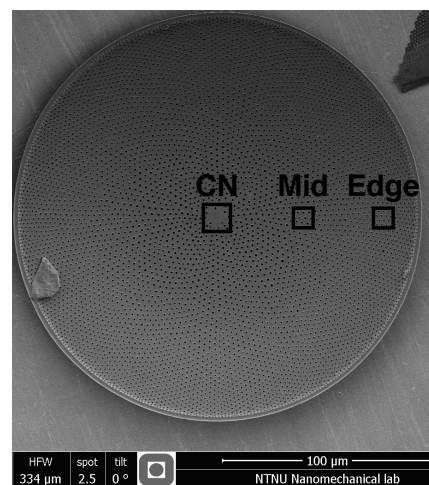


Figure 3.8: The three regions investigated by Peak Force QNM, marked with CN(central nodule), mid and edge

3.4 Analysis Tool

A dedicated software for analyzing SPM images have been use to acquire information from the AFM images, namely Gwyddion. This software is free and have a whole range of built in functions. In this work it have been used to determine the pore size, create 3D-images and calculate Young's modulus of the different layers.

The pore size was found by masking the the relevant pores from which the masked area and corresponding disc radius is calculated within the software. Pores was masked by using a built in masking tool, *mark by segmentation*, which marks the lowest areas on the image. The masks was checked manually and corrections were applied, either by extending the mask or erasing the mask, as needed. [Figure 3.9](#) illustrates one example of how this tool was used. An alternative method for measuring pore size was considered, but it proved to be less accurate than the masking method. The alternative method was to cross measure the diameter of a pore using a ruler tool and performing two measurements normal to each other.

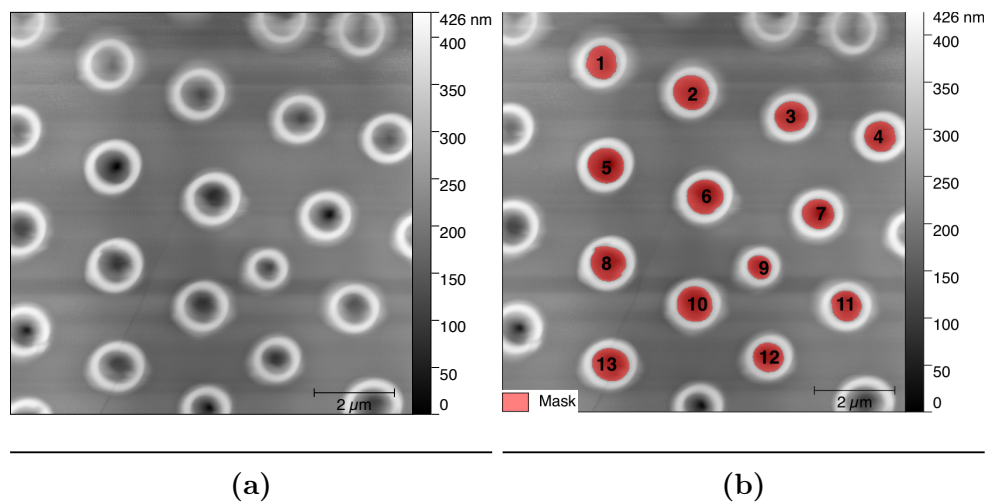


Figure 3.9: (a)Image of foramen and (b)masked image used to calculate pore diameter

Gwyddion was also used to determine the size of a granular structure observed on one of the layers as in [Figure 3.10](#). The size of the granular structure was

determined from the surface profile by roughly measuring the length between each peak as marked in [Figure 3.10\(b\)](#).

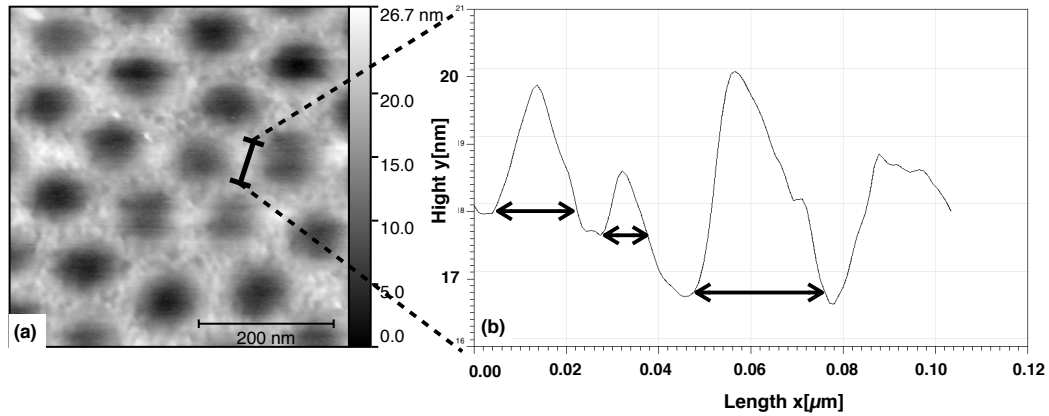


Figure 3.10: (a) AFM scan with black line marking surface profile. (b) Surface profile with arrows marking granular structure.

Young's modulus was determined for each PFQNM scan by using an average function in Gwyddion. This takes all the measurements in one scan, which are 65536 in a scan with 256-by-256 samples, and calculates the average modulus. Young's modulus, layer and location of the measurement was noted in a spreadsheet. This was performed for multiple samples and tip calibration and in the end an average modulus could be calculated for each region which includes the uncertainty introduced by different tip calibration and local variation in the samples.

The masking tool was also used to find Young's modulus of local regions on the frustule. More specifically, it was used to find the modulus of the lip surrounding the foramen pores, as illustrated in [Figure 3.11](#). The modulus of the "lips" and the constituent material was determined in order to get a comparative result. An alternative method was considered; namely creating modulus profiles across the pores and determining the peak modulus. This would result in fewer measurements than the masking method and was therefore considered to be a less suitable method for obtaining these results.

Gwyddion was also used to create 2D- and 3D-images for presenting the frustule structure and morphology and calculate the surface roughness, R_a , of the

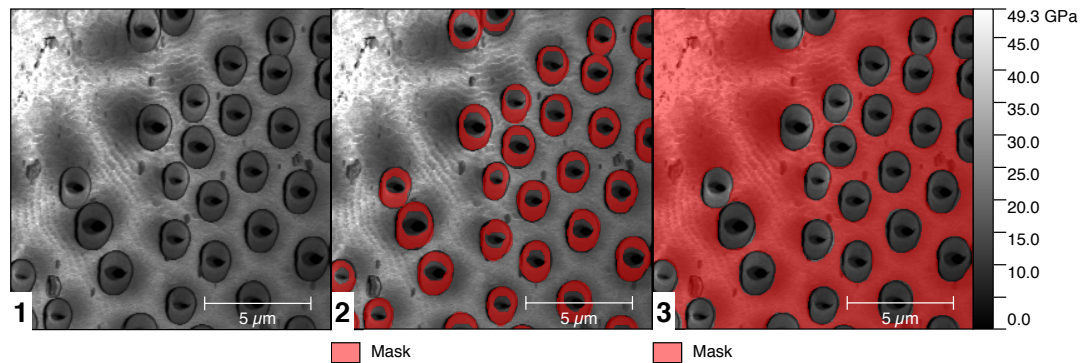


Figure 3.11: Illustration of how the masking tool is used to determining Young's modulus of local regions. **(1)**Unmasked image, **(2)**masking of pores and **(3)**masked constituent material

imaged surfaces. The raw image from the AFM was then used and no filters were applied in order preserve the accuracy of the image.

3.5 Literature Review Methodology

A review of literature on both diatoms and AFM, relevant for this thesis, have been presented in [chapter 2](#). The source of this information are articles available through Google Scholar and Engineering Village. Key words in the search is included, but not limited to: *Diatom*, *biosilica*, *Coscinodiscus*, *biological materials*, *sea sponge*, *diatom mechanical properties*, *AFM*, *SPM*, *peak force quantitative nanomechanical mapping*, *dynamic AFM* and *static AFM*.

Chapter 4

Results

The following chapter will present the results obtained in the experimental work. It consists of two parts; first, the morphology of the *Coscinodiscus sp.* diatom frustule have been determined by using atomic force microscopy. Characteristic pore size and surface structure of the three layers are reported in addition to the nanostructure of a cleaved frustule. Second, quantitative nanomechanical mapping of Young's modulus is reported of the three layers.

4.1 Morphology of *Coscinodiscus sp.* Determined by AFM

The diatom frustule have been investigated thoroughly by AFM in order to determine its morphology. Investigating living diatoms was the initial objective, but this was abandoned when no live samples was available. Diatoms cleaned by two methods, SDS and H_2SO_4 , was available. The SDS cleaned frustules had a thick layer of *mucilage*(organic material) surrounding the frustule, which made it difficult to image by AFM. The AFM images was therefore taken on samples cleaned by H_2SO_4 .

4.1.1 Foramen

The foramen layer is a thick porous internal plate in the frustule. The mean pore diameter was determined to be $832 \pm 133\text{nm}$, measured on 6 diatoms with 82 measurements. Extended results can be found in [Appendix C Figure C.1](#) and [Table C.1](#). The pores are ordered in a straight line radially from the central part towards the edge, illustrated in [Figure 4.1\(b\)](#). The pores have a raised edge, which are referred to as "lip", as in [Figure 4.1\(c\)](#) and [\(d\)](#).

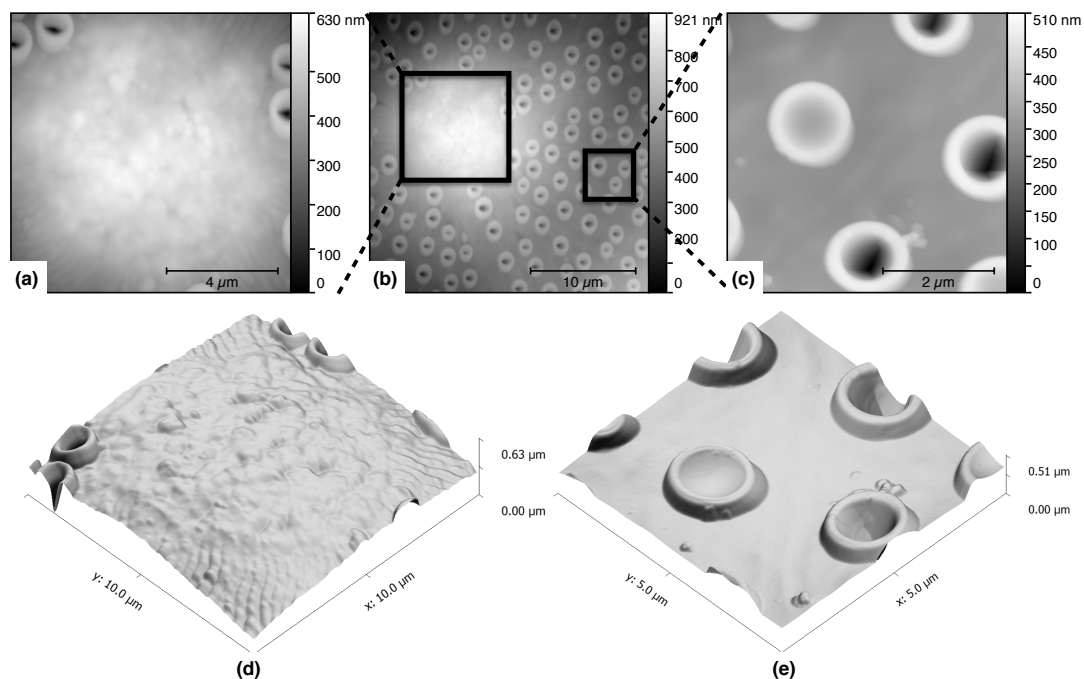


Figure 4.1: (b) Large scan size of foramen with pores visible. The rectangles marks the area imaged in (a,c). Higher magnification image show the 2D and 3D profile at (a,d) the central nodule and (c,e) towards the edge of the layer. A granular structure is observed at the central nodule and a porous structure with "lips" around the pores are observed anywhere else.

The central nodule have no pores and is slightly elevated compared to the surrounding structure, seen in [Figure 4.1\(a\)](#) and [\(d\)](#). The surface structure of the central nodule is granular, with particle nodules visible as in [Figure 4.1\(d\)](#). Measuring the particle size was difficult due to the natural curvature of the surface, instead the surface roughness was calculated at the central nodule. The roughness, R_a , was found to be $47 \pm 7.5\text{nm}$. To get a comparative result,

the surface roughness was calculated between the pores of the region imaged in [Figure 4.1\(c,e\)](#). This surface roughness was calculated to be $4.9 \pm 1.6\text{nm}$.

4.1.2 Cribrum

Cribrum, the middle layer, was imaged through the outer layer. Determining the real surface structure of the cribrum layer is therefore not possible due to the overlying cribellum. The pores are visible through the outer layer, so the mean pore diameter and pore structure was found. The mean pore diameter of

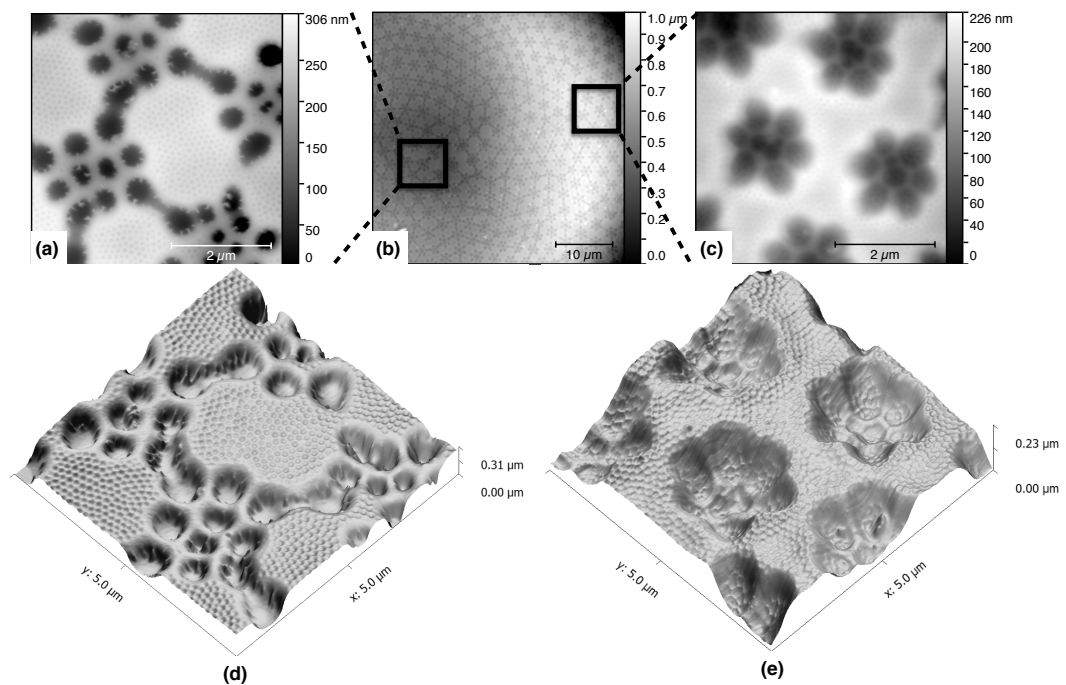


Figure 4.2: (b) Large scan size of cribrum with pores visible. The rectangles marks the area imaged in (a,c). Higher magnification image show the 2D and 3D structure at (a,d) the center and (c,e) towards the edge of the layer. A merged pore structure can be observed towards the edge compared with the center

the cribrum layer was determined to be $224 \pm 37\text{nm}$, measured on 5 different diatoms with 161 measurements in total. Overview of individual measurements can be found in [Appendix C Figure C.3](#) and [Table C.3](#). In center of the valve the pores are arranged in arrays of 7 pores with one center pore and 6 surrounding pores. Towards the edge of the valve the pores coalesces to a compact pore

structure, where the surrounding pores are packed closely to the central pore, see [Figure 4.2](#) for illustration of pore structure.

4.1.3 Cribellum

It was often observed that the outermost layer, cribellum, was partially destroyed by the cleaning process. It was therefore necessary to examine several diatoms before this layer was found intact. This layer is observed when the outer surface of the valve is pointing towards the AFM tip, and the imaged surface have a convex geometry. The pores in the cribellum layer was determined

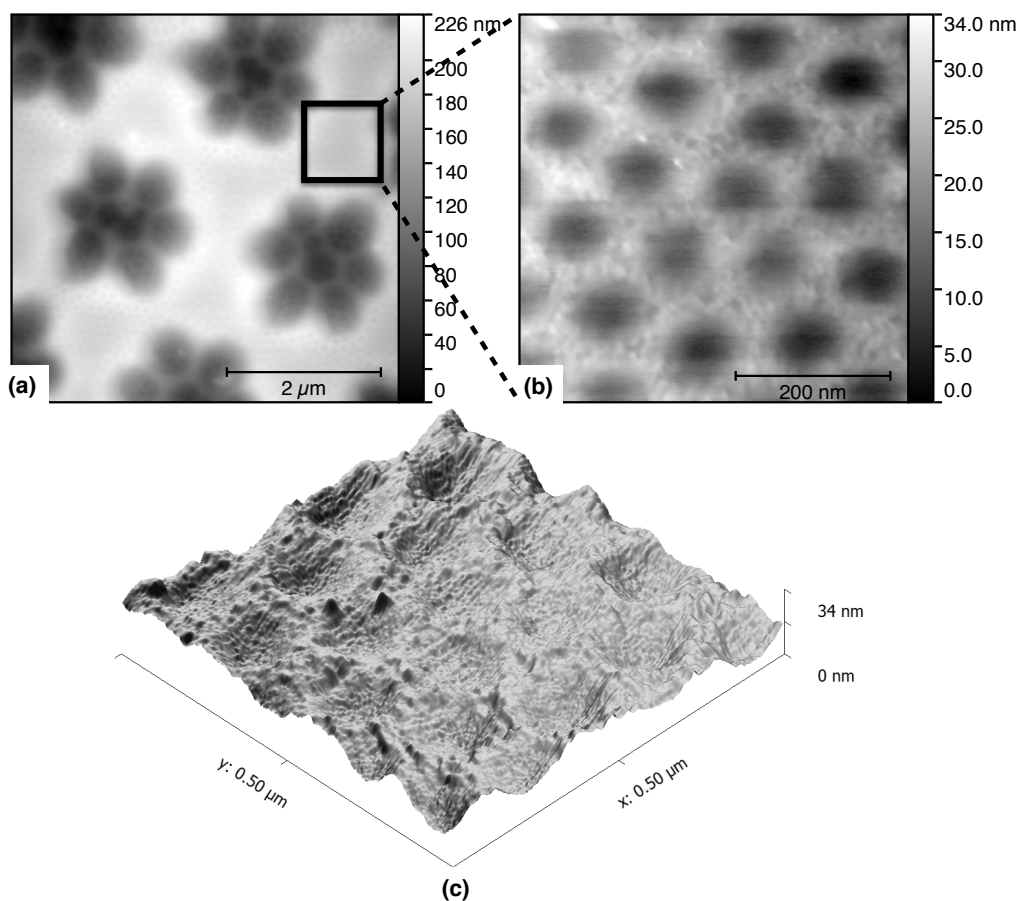


Figure 4.3: (b) Large scan with cribellum pores barely visible, dark spots are the underlying cribellum pores. The rectangle marks the area imaged in (b) and (c). Higher magnification image show the (b) 2D and (c) 3D structure of the cribellum layer with pores

to have mean pore diameter of 72 ± 11 nm, measured on 6 different diatoms

with a total of 71 measurements. See [Appendix C Figure C.2](#) and [Table C.2](#) for extended results. The pores are distributed evenly throughout the layer. In [Figure 4.3 \(b,c\)](#) the pore structure of the cribellum layer is visible and a granular surface structure can be observed. The particle size of the granular surface was found to be $22 \pm 5.6\text{nm}(n=93)$.

4.1.4 Cleaved Frustules

Cleaved frustules have been investigated in order to get a better understanding of the biosilica structure. Cleaved valves with both the foramen and cribellum layer pointing towards the AFM tip was imaged.

The cribellum and cribrum layer was imaged during the same scan, as illustrated in [Figure 4.4](#). From these images it is observed both horizontal and vertical stripes on the cleaved surface. First, this was thought to be an artifact due to the non horizontal surface scanned by AFM. Performing scans of fractured surfaces at different angles was performed to disprove this, which is discussed more thoroughly in [chapter 6](#). The stripes can indicate that the frustule is build up in a layered manner. Most of the cleaved surfaces illustrated this layered structure, however a granular structure between the layer was observed as in [Figure 4.4\(a,d\)](#) on one occasion. This was observed at high magnification and the area of granular surface was approximately 100-by-100 nm, between a layered structure.

A cleaved diatom valve with the foramen layer point towards the AFM tip was also imaged, as in [Figure 4.5](#). The fracture was observed when the valve was in close to horizontal position and it was later raised to a vertical position to obtain a high magnification image of the fracture surface. This revealed a highly layered structure as shown in [Figure 4.5\(b\)](#). It was not observed any indications of a granular structure on the cleaved surface. The observation reported above indicates that the different layers of the frustule have a similar microstructure built up by layers of biosilica stacked upon each other.

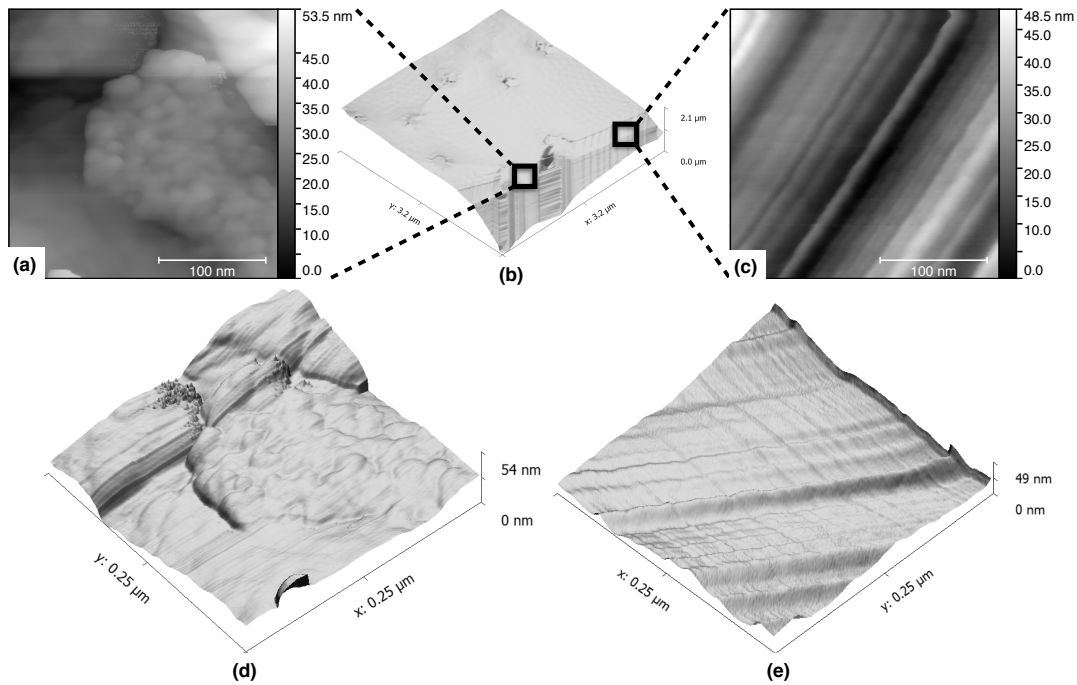


Figure 4.4: (b)Diatom valve, cleaved through the cribellum and cribrum layer. (a,d) High magnification 2D and 3D representation of cleaved surface with granular structure. (c,e) 2D and 3D figures of a cleaved surface, where layered structure is observed.

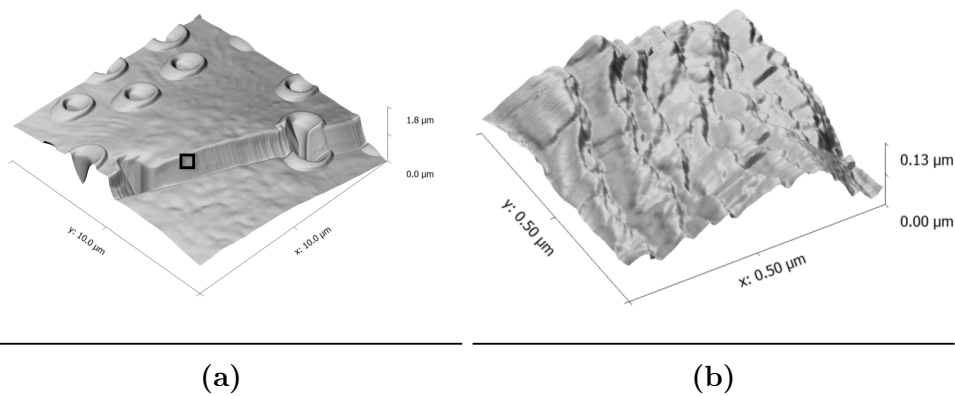


Figure 4.5: (a) Foramen cleaved through the central nodule, where the black rectangle marks magnified area imaged in (b).

4.2 Peak Force Quantitative Nanomechanical Mapping

Quantitative nanomechanical mapping have been performed in order to determine Young's modulus of the *Coscinodiscus sp.* diatom frustule. Both the

cribellum and foramen side of the valve have been examined by this method. Each layer have been mapped radially out from the central nodule by scanning three regions towards the edge of the valve, as marked in [Figure 4.6\(a\)](#). The purpose of this was to look for changes in Young's modulus systematically on the valve. The scanning size was $5\mu\text{m}$, except at the foramen central nodule where a scan size of $10\mu\text{m}$ was used to cover the whole pore-less area.

4.2.1 Foramen

Two foramen layers was imaged successfully with Peak Force QNM, [Figure 4.6](#) illustrates images from one of these layers. The images was obtained with a resolution of 256 samples per line, resulting in a total of 65536 individual measurements of Young's modulus per scan. An averaged Young's Modulus was determined to be $27 \pm 4.2\text{GPa}$, for all six scans with a total of 393216 measurements. See [Appendix C, Table C.5](#), for extended results.

Variations in Young's modulus for the three regions investigated was calculated to be $29 \pm 4.4\text{GPa}$ ($n=131072$), $31 \pm 5.1\text{GPa}$ ($n=131072$) and $20 \pm 3.1\text{GPa}$ ($n=131072$) for the central nodule(CN), mid region(Mid) and edge(Edge) of the frustule, respectively.

The quantitative nanomechanical mapping of the foramen layer also revealed another characteristic property of the frustule, namely a reduced modulus of the "lip" surrounding the foramen pores compared to the constituent material, as illustrated in [Figure 4.7](#). Young's modulus at the lips was measured to be $11 \pm 4.5\text{GPa}$ ($n=13575$), while Young's modulus for the constituent was estimated to $23 \pm 9.3\text{GPa}$ ($n=46438$) for this particular scan.

4.2.2 Cribellum

The cribellum layer have been systematically investigated in order to determine Young's modulus of this part of the valve. The thin cribellum layer is imaged,

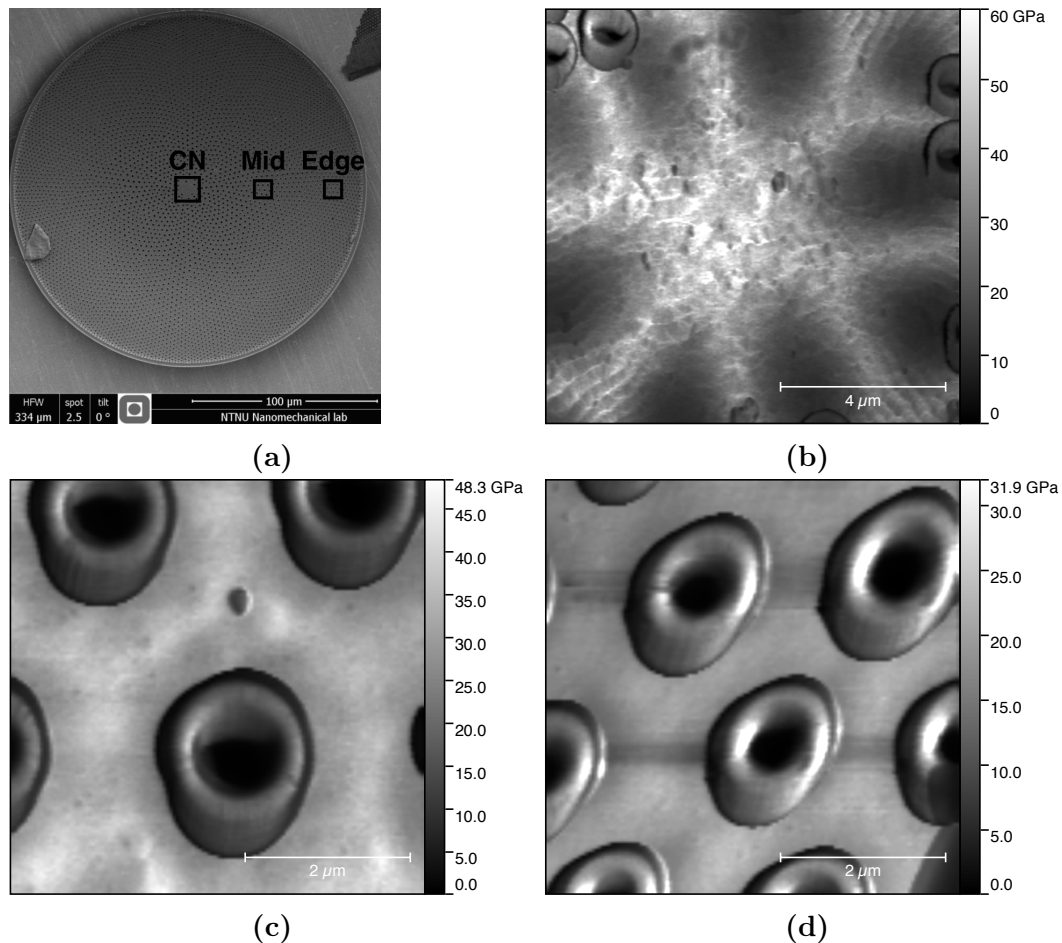


Figure 4.6: (a) Large SEM image of foramen with rectangles marking the three different regions radially towards the edge. Stiffness maps of the (b) central nodule, (c) mid region and (d) edge shows the local variation of Young's modulus.

but the underlying cribrum layer contribute with stiffness, so the measurements can be regarded as measurements of the combined elastic modulus of the two layers. Three regions radially from the center of the frustule have been imaged, similar to the measurements of foramen as marked [Figure 4.6\(a\)](#). The mean Young's modulus for all three regions measured on three different valves was calculated to be $25 \pm 3.6 \text{ GPa}$ ($n=589824$). Young's modulus for the central nodule, mid and edge region was calculated to be $23 \pm 2.3 \text{ GPa}$ ($n=196608$), $29 \pm 5.4 \text{ GPa}$ ($n=196608$) and $22 \pm 3.2 \text{ GPa}$ ($n=196608$), respectively. Stiffness maps are shown in [Figure 4.8](#). The underlying cribrum pores are visualized as a drop in modulus (dark area) in [Figure 4.8](#). Young's modulus is relatively uniform between the cribrum pores.

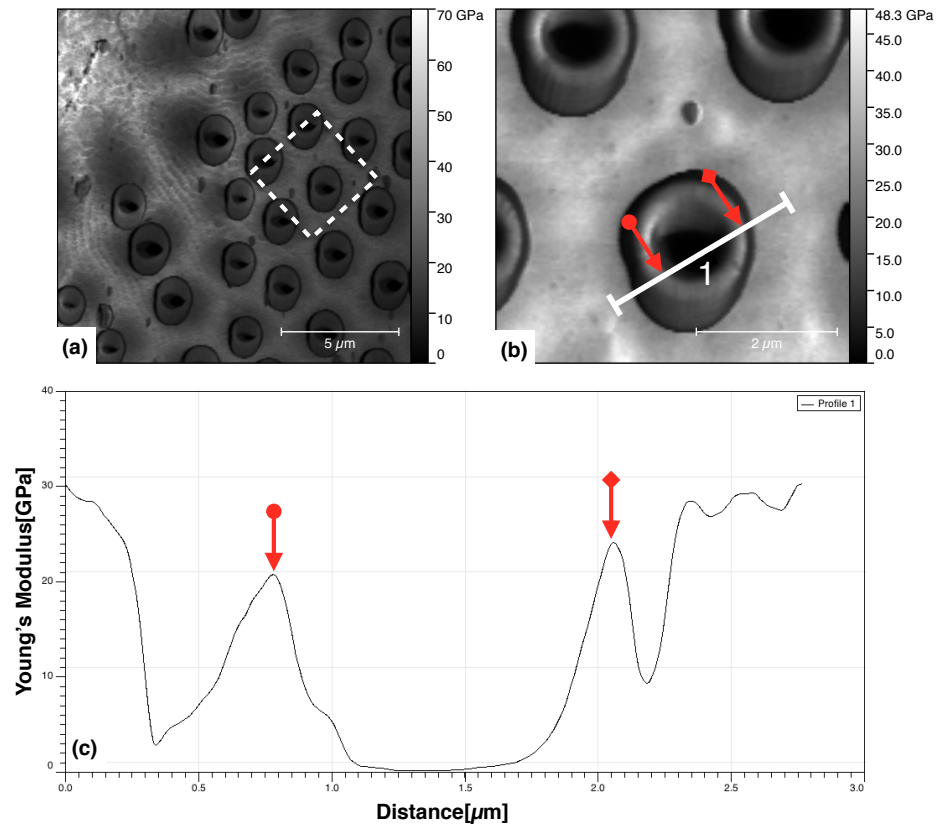


Figure 4.7: (a) Stiffness map of the foramen layer, where the white rectangle marks the magnified area in (b). (b) Stiffness map where the white line marks the modulus profile presented in (c). (c) Profile of Young's modulus, where the red arrows marks the measured Young's modulus on top of the "lip".

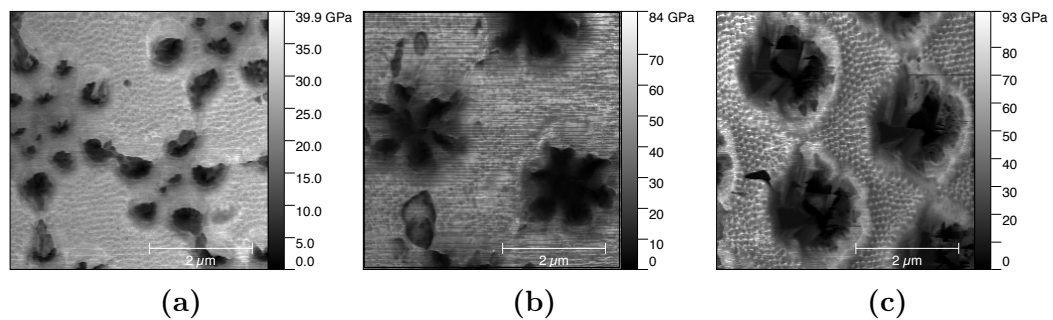


Figure 4.8: Stiffness maps of (a) the central nodule, (b) mid region and (c) edge shows the local variation of Young's modulus in the cribellum layer.

4.3 Summary of Results

The key takeaway from the foregoing sections is presented below to give the reader a short summary of the experimental findings in this thesis.

The pore structure of the diatom *Coscinodiscus sp.* was measured and is presented along with measured Young's modulus of the different layers in [Table 4.1](#). In addition, cleaved valves was investigated and a layered structure was found, with one occasion of granular appearance in-between the layers.

Table 4.1: Summary of pore size and Young's modulus measurements presented in the forgoing sections

Layer	Pore Diameter[nm]	Young's Modulus[GPa]			
		CN	Mid	Edge	Mean
Foramen	832±133	29±4.5	31±5.1	20±3.1	27±4.2
Cribrum	447±73	23±2.3	29±5.4	22±3.2	25±3.6
Cribellum	72±11	23±2.3	29±5.4	22±3.2	25±3.6

Chapter 5

Discussion

This chapter will discuss the results presented in the previous chapter and relate the findings to other reports in the literature. The discussion is presented in the same order as the results were presented.

5.1 Morphology of *Coscinodiscus sp.* Determined by AFM

Both the global porous structure of the frustule as well as the nanostructure of the biosilica has been investigated in order to determine the frustule morphology. A complex layered structure have been observed, where the pore arrangement of the different layers have been characterized. The results from the characterization will in later sections be compared to results reported by others. AFM is known to have good qualities in terms of resolution, but there are many pitfalls which can cause erroneous results. For this reason it is important to discuss any sources of error and if this can bias the results.

5.1.1 Foramen

Investigations of foramen demonstrated that this layer consists of relatively large pores arranged radially from the center of the layer. In center of the valve there is a pore-free region, called central nodule. In this region the first silica is deposited during valve formation. A granular structure of the biosilica was identified in this area, which can be a result of silica deposited as spheres or fused spheres. These observations are consistent with regard to the reports from Losic et al. [35] of the *Coscinodiscus sp.* Surface roughness of the central nodule was calculated to quantify how granular the region is compared to the surrounding material. This method will also include the natural curvature of the surface in the measurements, so strictly speaking it is not only the "granularity" but also the curvature of the surface that is included in these measurements.

Table 5.1: Comparison of measured pore diameter with similar measurements reported by Losic et al. [35]

Layer	Surface Characteristics	Surface Characteristics from Losic et al. [35]
	Pore Diameter[nm]	Pore Diameter[nm]
Foramen	832 ± 133	1152 ± 131
Cribrum	447 ± 73	192 ± 35
Cribellum	72 ± 12	45 ± 9

Measurements of the pore size is summarized in Table 5.1 and compared to a similar AFM study of the *Coscinodiscus sp.* performed by Losic et al. [35]. The slight difference in measured pore diameter can be due to difference in growing conditions, biological system, measuring techniques or calibration accuracy of the AFM. Growing conditions and biological system is not something that we had control over, as these diatoms was cached in the sea, pursuing this further is therefore difficult. The AFM was periodically calibrated and it is not likely that it would cause errors in the results. The most plausible cause is that the diatoms imaged by Losic et al. [35] is a different species within the *Coscinodiscus* genus and variation in the structure is expected. However, the the standard deviation is similar to what is reported by Losic et al. [35], which indicates that the variation in pore diameter is consistent across different species and biological systems.

5.1.2 Cribrum

The middle layer was imaged through the outermost layer, thus the images contains limited amount of information of the actual surface structure. The pore structure was visible and determination of the pore size was possible through the outer layer. The measured pore size in this layer was 133% higher than what Losic et al. [35] reports. The deviation is, as before, believed to be due to imaging a different species. Since the measurements was obtained through the cribellum layer there is a higher uncertainty related to the measurement technique compared to the other layers.

5.1.3 Cribellum

The outermost layer, cribellum, consists of many small pores. its function is believed to be of filtering purposes, allowing water to flow through the frustule but excluding foreign objects such as viruses. This indicates that the mechanical properties of this layer is of less importance. Through the investigations it was often observed that this layer had broken before imaging or that it broke during imaging due to the tip-sample interaction. This supports the previous argument; the outermost layer have pore mechanical performance.

The pore size calculated for this layer is 60% higher that what Losic et al. [35] reports. The explanation for the deviation is believed to be the same as before; a different species within the *Coscinodiscus* genus is reported by Losic et al. [35].

From high magnification images it could be observed a granular structure of the biosilica, and the particle size of each nodule was estimated. It is reasonable to assume that the nodules of the granular surface is a result of the silicification process within the SDV during valve formation. Losic et al. [35] also observed a granular surface on the cribellum layer and made the same conclusion. The size of the particles reported in this thesis is approximately 60% higher than what Losic et al. [35] reports. The measuring technique used by Losic et al.

[35] is not known and the deviation can be explained by uncertainties related to the measuring technique.

5.1.4 Cleaved Frustules

Cleaved frustules was imaged in order to get a better understanding of the biosilica's morphology. In order to do so the frustules had to be cleaved manually and positioned in a way that made them suitable for AFM imaging. The main challenge was to raise the cleaved valve close to a vertical position and fix it to the substrate. Once the valve was in position for imaging, the tip could be scanned over the fractured surface. Many scans only produced images with noise, due to a unstable sample, and was therefore discarded.

Sucesfull images of the fractured surface revealed a quite smooth, but layered structure of the fractured surface. On one occasion a sphere-like structure was observed in-between the layers. Interpreting these results in light of others' published data is essential to understand these observations. Observations of nanosized spheres was expected on the cleaved cross section, based on reports from others[9, 10]. However, we speculate that the method used for cleaving frustules can result in a fracture propagating along a weaker part of the biosilica. This is based on reports from Gordon et al. [16] and Kröger et al. [31], which indicates that the silica spheres are assembled to larger block-like structures causing a thickening of the frustule. The observations of a layered structure reported in this thesis can be due to the fracture running along these block-like structures. The sphere structure can be hidden from view due to presence of both a soluble and insoluble organic matrix as reported by Kröger et al. [31] and Scheffel et al. [47]. The amount of organic material associated with the insoluble matrix is of special interest as it is not known how it affects the nanostructure across different diatom species. This is supported by observations of a compacting of the silica structure observed by others[9, 48].

Layered structure of biosilica has not been observed in diatoms before, it is therefore necessary to consider if these results are reasonable. To assess this we can compare the diatoms to other similar biological materials. The deep sea sponge can be used as a comparative organism, as it shares many features with the diatoms. It is made out of biosilica and the smallest building blocks have been identified to be silica nanospheres[57]. The most characteristic feature of the sea sponge is the hierarchical structure and alternating layer of silica and organic material. We can speculate about this; is the layers observed in the diatoms something similar to the structure of the sea sponge? No hard conclusions can be made from the observations, but it is nevertheless an indulging thought that nature is consistent in how it builds its structures.

Based on own observations, and reports from others, we can summarize the above speculations: Biosilica is most likely to be built up by silica spheres together with both soluble and insoluble organic material. There are reasons to believe that the amount of organic material is varying between species and that the nanostructure can be "compacted" so that a homogenous structure is observed. Cleaved frustules could demonstrate a layered structure due to the fracture path running along a weaker part of the biosilica. This also highlights some of the challenge of research on diatoms and biosilica; can research on one diatom species be generalized to be valid for diatoms and biosilica as a whole?

5.2 Peak Force Quantitative Nanomechanical Mapping

By using Peak Force Quantitative Nanomechanical Mapping Young's modulus have been determined for three layers and regions of the frustule. The mean Young's modulus of all layers was calculated to be 26 ± 3.9 GPa. Others have reported Young's modulus of a variety of diatom species to vary between 21 MPa and 300 GPa[1, 45]. By assessing these reports it seems like a fair assumption that the mechanical properties of diatom frustules are species depend. To the

authors knowledge there have only been one report of mechanical properties of the *Coscinodiscus sp.*, published by Losic et al. [36], from another institution than NTNU. A modulus ranging from 1.7 to 15.61GPa was reported at various layers, obtained by AFM nanoindentation. Losic et al. [36] acknowledge that these measurements are associated with some uncertainty, due to large deformations in the frustule during testing.

Mapping of Young's modulus performed in this thesis is adding new knowledge of the mechanical behavior of biosilica in the diatom *Coscinodiscus sp.* The method used to obtain Young's modulus have higher spatial resolution than what have been reported earlier, and the measurements seems to be quantitative for all layers. However, there are still uncertainties related to the method used. The accuracy of Peak Force QNM is govern by the quality of the calibration and imaging procedure. As pointed out earlier, it is important to mach the deformation of the sample to the deformation measured during calibration. Scans where the average deformation of the frustule was deviating from the recorded calibration deformation was discarded. Another assumption necessary to calculate Young's modulus is Poisson's ratio of the sample, ν_s in Equation 2.10. It was assumed to be 0.3, in accordance to the manufacturer's(Bruker Inc.) recommendation for samples with modulus higher than 1GPa. The Poisson's ration is usually in the range from 0.2 to 0.5, leading to a 4 to 25% difference between the sample's and reduced modulus in Equation 2.10.

5.2.1 Foramen

Nanomechanical mapping of the foramen layer revealed a slightly decrease in measured mean Young's modulus on the edge compared to the center and mid region. The same trend was reported by Almqvist et al. [1] for another diatom species, which indicates that this is a trend among a variety of diatoms. Another interesting feature observed was a decrease in stiffness of approximately 50% in the material at the "lip" surrounding the foramen holes. This trend was seen on multiple scans and on different regions of the valve, which indicates that

the mechanical properties of the "lip" around the foramen holes differs from the constituent biosilica. A substantial decrease of Young's modulus at the outer edge of the "lips" was observed. This is believed to be an artifact of the AFM scanning procedure in which the close to vertical edge of the "lip" causes an unnatural drop in the measurements. This area was excluded from the calculations of the decrease in "lip" elastic modulus, so that it should not bias the results.

One can only speculate what the underlying reason for the change in mechanical properties are, but from an engineering standpoint, it is likely that the properties are a result of a continuous improvement process with regard to structural integrity. The reports of microrings indicates that the pore structure of the griddle bands are created by a template of organic material, this can also be the case for foramen pores[47]. This is only speculations, but such an organic template could lead to a decrease in Young's modulus.

5.2.2 Cribellum

The stiffness of the cribellum and cribrum layer was relatively homogenous and no clear trend could be found when measuring the change in modulus radially out from the center. As mentioned earlier, the cribellum and underlying cribrum layer was imaged simultaneously so the measurements are a combination of the two layers. The cribrum pores was visible, most likely because the weak cribellum layer had collapsed where it had no support from the underlying cribrum. This should not affect the results, since the overall deformation was averaged and equal to the deformation at calibration.

The mean modulus of the cribellum layer was measured to be slightly lower than the foramen layer, but within one standard deviation. This contradicts the reports of Losic et al. [36], where Young's modulus of cribellum and cribrum was measured to be substantially lower than on foramen. Losic et al. [36] used

nanindentation to determine Young's modulus, which causes large deformations in the material. For the thin cribellum layer this will certainly affect the results. Using Peak Force QNM to report Young's modulus seems like a better option than nanindentation to determine the real mechanical properties of the biosilica.

Chapter 6

Conclusion and Further Work

6.1 Conclusion

Atomic force microscopy have been used in order to determine the morphology and mechanical properties of the *Coscinodiscus sp.* diatom frustule. It have been demonstrated that AFM is a good tool for characterizing surface structures, where three dimensional images can be created and accurate measurements of surface characteristics have been presented.

Through the AFM studies it have been shown that the frustule is a complex structure. The pore arrangement and size in the different layers have been determined and reported. Determining the nanostructure of biosilica by exploiting the beneficial properties AFM offers in terms of resolution has been one of the focus areas. A layered structure could be observed on cleaved diatom frustules. Observations of a granular surface structure on the cribellum layer and one occasion of a granular appearance on a cleaved frustule is the only indication found in this study of sphere-like structure. From these observations and with the knowledge of diatoms reported by others, some speculations about the observed structure have been made, but without drawing any hard conclusions. The layered structure could be a results of the valve formation, where larger block-like structures consisting of close packed silica spheres are assembled into

a even larger structure. In-between the silica spheres a matrix of organic material, both soluble and insoluble, could compact the biosilica so that it looks homogenous. This speculations are draw based on own results in addition to relevant literature. More experiments must be performed in order to confirm this theory.

The mechanical properties of the diatom frustule have been determined by using Peak Force QNM. This method has provided a quantitative technique with high spatial resolution to map Young's modulus of the surface. Measurements performed radially out from the center of the foramen layer have demonstrated a slightly decrease in modulus at the edge, confirming earlier reports. Another interesting feature observed was a decrease in modulus at the "lip" structure around the foramen pores. An implication of a local changes in material properties is a corresponding change in nanostructure and/or chemical composition. This indicates that the biosilica is indeed a composite material, where the material properties changes at certain locations.

The ultimate goal of investigating the diatom frustule is to get a better understanding of the biosilica, so that humans can copy a material that nature have used millions of years to perfect. Through the presented results along with relevant literature I hope it have become clear that biosilica is a material which is tailored at the nanoscale to achieve mechanical properties and structural complexity beyond what human engineering can achieve today.

6.2 Further Work

There are many unanswered questions regarding the morphology and mechanical properties of diatom frustules. By considering the results presented in this thesis along with others published work, a recommendation of further work can be made. These recommendations are based on filling in holes in the knowledge regarding diatom frustules.

- **Develop a precise method for AFM imaging of cleaved diatoms:** Developing a more precise method for cleaving and subsequently imaging diatoms by AFM is of great interest. In this way a systematic investigation of cleaved frustules can be performed. In order to implement this, it is imperative that a more exact method for cleaving diatoms and fixing them against substrate is developed. Once this is found, cleaving frustules at different locations can be done to examine the nanostructure in a systematic manner. If the frustules were fixed better to the substrate it could also be interesting to perform Peak Force QNM on cleaved surfaces. This should find changes in material properties and maybe a determination of how organic material is distributed in the frustule is possible. Etching of the cleaved surface could also be performed to see if this would reveal a more complex nanostructure.
- **Study of living diatoms:** Examining living diatoms were one of the objectives when this thesis work was started. This could not be performed due to the lack of available living diatoms, but it is still an interesting topic which can be pursued further. Performing Peak Force QNM on diatoms in fluid could be performed to determine Young's modulus of living diatoms, and compared to the results reported in this thesis.
- **Determination of other characteristic material properties of biosilica:** Young's modulus of diatom frustules have been determined in this thesis, but there are other material parameters such as fracture strength and toughness that would be of interest. There have been efforts by others to determine these material properties by producing micrometer sized beams that can be tested. As biosilica have proven to be a challenging material to work with only a few tests have been successful, and more test data is required to ensure statistically valid data.
- **Testing of the AFM setup in Nanomechanical lab:** Only initial testing of the AFM setup in Nanomechanical lab has been performed. The

performance seems to be lower than what can be expected of such equipment, but more testing is needed in order to determine the performance of the system. Some thoughts about this can be found in [Appendix B](#)

Appendix A

Email correspondance

A.1 Hysitron email correspondance

Email correspondence between me(author), Ronnie Cooper as Hysitron Representative and Prof. Afrooz Barnoush at NTNU is given below. The support from Hysitron was crucial to make the installation of the AFM system flawless, and the planning of this work is reproduced below. The email is color-coded where mails sent from me, Ronnie Cooper and Afrooz Barnoush is marked in red, blue and gray fonts, respectively.

From: Torstein Svendsgaard [mailto:svendsgaard@icloud.com]

Sent: Tuesday, February 24, 2015 1:31 AM

To: Hysitron Customer Service

Subject: Hysitron TI950

Hi, I'm about to mount an AFM inside the TriboIndenter TI950 chamber. I'm therefor interested in getting some feedback on how this can be done, with as little risk as possible for damaging the equipment. the plan so far is to;

- Demount the indenter and microscope from the plate which they are mounted on.

- Demount the plate
- Install the new plate, with the AFM mounted
- Reinstall the indenter and microscope

I have attached two pictures. One of the existing setup, the other of the new plate with the AFM installed. What do you think about this plan?

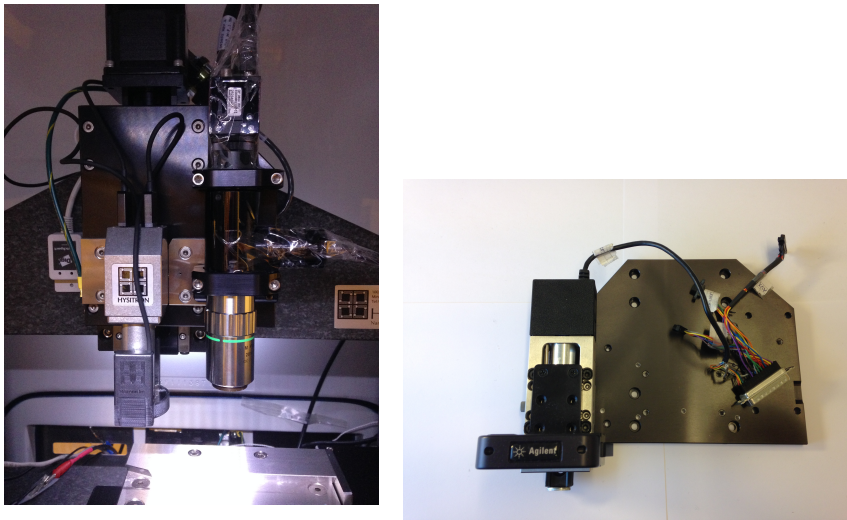


Figure A.1: Attached images

Torstein V. Svendsgaard

From: Hysitron Customer Service

Sent: Tuesday, February 24, 2015 8:21 AM

To: Ronnie Cooper

Subject: FW: Hysitron TI950

Torstein, I would first like to confirm that you are working on the TI 950 at NTNU in Trondheim.

Hysitron does not integrate with the Agilent AFM system so I can't give you very specific answers and will only be able to generalize based on the images that you have sent.

The major concern I have is with the height that you have chosen to mount the AFM head. The height of the AFM head (where you currently picture it) is much higher than the height of the tip and the optical focus. This will cause you many problems as you try to approach and test on any sample surface (you will contact with a different component prior to making contact with the desired head). I would suggest you try to set the tip height and AFM tip within a few millimeters of each other in the Z axis direction. Even with the heights very similar you will want to test with only one sample on the stage to avoid contact with a different component during the approach.

After you get the hardware installed you will need to find a way to integrate with the Z axis stages in order to move with the AFM head in feedback (and to stop when contact is made) so you may need to develop some scripting to work through the ESP 301 stage control (unless you have some other plans for that). This could cause problems as TriboScan will likely not allow a different software to "take over" the ESP 301 and seamlessly pass the control back to TriboScan when completed.

Regards, Ronnie Cooper

From: Torstein Svendsgaard [mailto:svendsgaard@icloud.com]
Sent: Thursday, February 26, 2015 2:58 AM
To: Ronnie Cooper
Subject: Re: Hysitron TI950

That is correct, TI 950 NTNU, Trondheim.

The AFM head is actually not mounted in the picture. The head will be clamped onto the «grip» which is on the picture. The whole AFM is mounted onto a dovetail rail system, so it can be adjusted up and down to wanted height(see picture).

For the z-axis motion the plan is to bring the sample into close proximity using the ESP 301 controller. Then switch to the Agilent software. The scanner is mounted on a miniature stage. We can than bring the AFM tip in contact with the sample only through the Agilent software and stage which the AFM is mounted on.

Do you think this will work? If so, how would you proceed installing it(how to demount the existing equipment and install it on the new plate)

Torstein V. Svendsgaard

Fra: Ronnie Cooper <rcooper@hysitron.com<mailto:rcooper@hysitron.com>>

Til: Torstein Svendsgaard <svendsgaard@icloud.com<mailto:svendsgaard@icloud.com>>

Emne: RE: Hysitron TI950

Dato: 26. februar 2015 kl. 16.46.04 CET

Torstein, It's difficult to say if it will work. Hysitron spends a great deal of time and resources on designing and testing products so with just an image and an idea it will be difficult to give a yes or no answer. In theory it would work but there are so many small unforeseeable quirks that could happen (some of which could cause serious damage to the transducer, scanner, or tip) that I'm going to need to give an official suggestion that you not do this. Assuming you've already considered the risks and are prepared to continue some things you will need to consider:

- Weight and resonance changes of system due to additional components.
- Height of AFM components in relation to indentation tip and optical components.
- Vibration/changing force causing system emergency stops with AFM moving but indentation tip not contacting.
- Stability of the linked together system Z axis and AFM Z axis.
- Possible damage to AFM if the system axes are purposely or accidentally adjusted while the AFM is functioning (no interaction between AFM and Hysitron software).

Regards, Ronnie Cooper

From: Torstein Svendsgaard [mailto:svendsgaard@icloud.com]

Sent: Monday, March 2, 2015 9:42 AM

To: Afrooz Barnoush

Subject: Fwd: AFM-Hysitron TI950

Hi, I have been emailing with Hysitron regarding the installation of the AFM. They are not too positive about it, see below correspondence! What do you think, should we proceed?

Torstein V. Svendsgaard

From: Afrooz Barnoush [mailto:afrooz.barnoush@ntnu.no]

Sent: Monday, March 02, 2015 5:23 AM

To: Ronnie Cooper; Lance Kuhn; Michael Fitzl; Michael G. Berg

Cc: Torstein Svendsgaard

Subject: RE: AFM-Hysitron TI950

Dear Ronnie, Thank you very much for the response. As you may know I used to have a TI system with an AFM head side by side. And it is used to be a standard system from Hysitron. So I can assume from a technical point of view the "Weight and resonance changes of system due to additional components" should not be of any concern as far as the weight of our AFM system is comparable with the AFM system you used to deliver with the TI. This is the most important thing for since I want to be able to perform the nanoDMA tests with system without a problem.

The rest of the points we should consider as you mentioned are listed below and I included our solutions to them and I would like to know your recommendation. Please don't forget that as we decided to purchase the TI950 system we told Hysitron that we want to attach another AFM into it and Hysitron promised to help us as far as possible so we can get it worked.

- Height of AFM components in relation to indentation tip and optical components.
 - We consider it and we will have the system installed in a way that no harm happens to Transducer and optical system.
- Vibration/changing force causing system emergency stops with AFM moving but indentation tip not contacting.
 - What was your solution to this problem in the systems with AFM head?
- Stability of the linked together system Z axis and AFM Z axis.
 - What do you mean by this point?

- Possible damage to AFM if the system axes are purposely or accidentally adjusted while the AFM is functioning (no interaction between AFM and Hysitron software).
 - If we put the Triboscanner software into pause mode during the usage of AFM can we expect something wrong happening. Is there any possibility to disable the z axis only.

I hope you can help us on this based on your experience with the systems with AFM.

Best regards, Afrooz

From: Ronnie Cooper [mailto:rcooper@hysitron.com]

Sent: Monday, March 2, 2015 6:19 PM

To: Afrooz Barnoush; Lance Kuhn; Michael Fitzl; Michael G. Berg

Cc: Torstein Svendsgaard

Subject: RE: AFM-Hysitron TI950

Dr. Barnoush,

You are correct, the weight of the AFM system should be ok and within the range that will not affect the vibration isolation system.

In regard to the points you asked about:

- Anytime you add a mass to the Z axis of the system (especially a cantilevered mass) you can encounter resonances and vibrations that are unexpected which may cause data collection issues or cause emergency stops/false engages on the transducer (if the mass resonates as the stages are raised and lowered). You will need to experiment with different masses/locations if you encounter this issue as this is often something that is considered when designing attachments at Hysitron and is evaluated during system testing.
- Stability of the linked Z axes. I was indicating that now instead of needing to track the position of one Z axis you have two linked together Z axes (one for the Hysitron system and one for the AFM). The accuracy of the two stages

independent is one value but if you try to position based on both stage movements you're going to have increased error and possibility for tip crashes/sample detection error.

- The Z axis of the system is disabled (no power or current to the motors) any time the stages are not in motion so you probably do not need to do anything to the Hysitron components as you use the AFM. Pausing and resuming the Hysitron system would be ok as long as you do not turn off power to the stage control or performech and you do not change the positions of the Hysitron stages. Keep in mind, if you pause the software all emergency stop and limit checking routines will be disabled so this may be desirable or detrimental depending on what action you are trying to perform with the AFM.

Regards, Ronnie Cooper

Hysitron 9625 West 76th Street Eden Prairie, MN 55344

From: Afrooz Barnoush [mailto:afrooz.barnoush@ntnu.no]

Sent: Monday, March 02, 2015 11:34 AM

To: Ronnie Cooper; Lance Kuhn; Michael Fitzl; Michael G. Berg

Cc: Torstein Svendsgaard

Subject: RE: AFM-Hysitron TI950

Dear Ronnie, Thank you very much for your valuable tips. I think together with your support we will be able to run our AFM very soon.

For now we need urgently the description of the procedure to dismantle the Optical microscope and Nanoindentation head from the supporting plate and dismantling of the supporting plate and then installation of the new support plate and head and optical microscope on it.

Is there anything to be take care or simply open up the screws and dismantle everything and then install everything back on the new plate. Can we do something wrong or since the screw holes on the new larger supporting plate are all made by Hysitron there is no chance of ruining something.

I really appreciate your support.

Best regards, Afrooz

From: Ronnie Cooper [mailto:rcooper@hysitron.com]
Sent: Monday, March 2, 2015 6:39 PM
To: Afrooz Barnoush; Lance Kuhn; Michael Fitzl; Michael G. Berg
Cc: Torstein Svendsgaard
Subject: RE: AFM-Hysitron TI950

Dr. Barnoush, We don't have a document for removing the optics and Z axis bracket as this process is typically only performed by a Hysitron service person. However, it's pretty easy to remove it and reinstall it as long as you take note of which screws are used in the different holes and take care of the fragile parts (scanner, transducer, objective lens, etc?).

Regards, Ronnie Cooper

From: Afrooz Barnoush [mailto:afrooz.barnoush@ntnu.no]
Sent: Monday, March 02, 2015 11:46 AM
To: Ronnie Cooper; Lance Kuhn; Michael Fitzl; Michael G. Berg
Cc: Torstein Svendsgaard
Subject: RE: AFM-Hysitron TI950

Great Ronnie, So if we take care of simple things we cannot do anything wrong.

Cheers, Afrooz

From: Ronnie Cooper [mailto:rcooper@hysitron.com]
Sent: Friday, March 20, 2015 8:00 PM
To: Afrooz Barnoush; Lance Kuhn; Michael G. Berg
Cc: Torstein Svendsgaard
Subject: RE: AFM-Hysitron TI950

Dr. Barnoush, I just wanted to let you know that I will be in Trondheim from April 20-22 for the upgrade of the TI 900 system. This upgrade is only scheduled to take two days so there will be additional time during the visit to work with your users or systems if they're available and have any questions or problems. Thanks,

Regards, Ronnie Cooper

From: Afrooz Barnoush [mailto:afrooz.barnoush@ntnu.no]
Sent: Wednesday, March 30, 2015 05:20 PM
To: Ronnie Cooper; Lance Kuhn; Michael Fitzl; Michael G. Berg
Cc: Torstein Svendsgaard
Subject: RE: AFM-Hysitron TI950

Dear Ronnie,

It is a great news we are looking forward to see you here in Trondheim. We have several issues that we would like to discuss with you and I think we have to use this time in most efficient possible way. So if you have an agenda please share it with me so I can arrange users with their problems accordingly.

Cheers, Afrooz

Fra: Ronnie Cooper <rcooper@hysitron.com>
Til: Afrooz Barnoush <afrooz.barnoush@ntnu.no>
Emne: Re: AFM-Hysitron TI950
Dato: 31. mars 2015 kl. 01.42.11 CEST

Dr. Barnoush, We don't have a solid schedule with the upgrade of the TI 900 but I expect the most open time will be on the third day (Wednesday).

Regards, Ronnie Cooper

Fra: Torstein Svendsgaard <tvs_90@hotmail.com>
Til: Ronnie Cooper <rcooper@hysitron.com>
Emne: AFM-Hysitron TI950
Dato: 16. april 2015 kl. 07.09.28 CEST

Mr. Cooper, As you are aware we are preparing to install an AFM inside the Hysitron TI950 TriboIndenter at NTNU. We are planning to perform this work at the dates you are in Trondheim, and hope for your support if any questions should arise during this process. I have made a plan on how this work can be executed in an efficient way, see below for a step-by-step plan. I would very much like yours comments on this, with special regard to safely dismantling without damaging any of the Hysitron equipment.

1. Power down all equipment(should this include the vibration stabilization unite?)
2. Demount top body of TriboIndenter
3. Disconnect transducer from TriboScanner(Hysitron manual - 1.7.2 INSTALLING THE TRANSDUCER)
4. Disconnect 2x wires on TriboScanner
5. Demount TriboScanner by unscrewing - 4x 3/32 " hex screw
6. Disconnect wires on optical microscope 2 wires
7. Demount optical microscope by unscrewing 4x 5/32 " hex screws
8. Demount mounting brackets for optical microscope - 4x hex screws(dimension unknown)
9. Demount optics and Z axis bracket - 6x hex screws 3/32
10. Install new bracket - 6x hex screws 3/32 "
11. Revers step 1. to 8 to mount new and larger plate and installing optical microscope and TriboScanner.
12. Mount AFM scanner holder
13. Mount scanner

Cabling for AFM is done one beforehand - 2x cables into the TriboIndenter.

Regards Torstein V. Svendsgaard

Fra: Ronnie Cooper <rcooper@hysitron.com>

Til: Torstein Svendsgaard <tvs_90@hotmail.com>

Kopi: "afrooz.barnoush@ntnu.no" <afrooz.barnoush@ntnu.no>

Emne: RE: AFM-Hysitron TI950

Dato: 16. april 2015 kl. 15.39.28 CEST

Torstein, Yes, I will be at NTNU on Monday-Wednesday next week. The primary goal is to complete the upgrade and training on the TI 900 TriboIndenter system but

we have scheduled about 1 day of additional on-site time. We can discuss your items during my visit.

Regards, Ronnie Cooper

A.2 Agilent email correspondance

Correspondence between me(author) and Agilent Support, as a part of the AFM installation planning, is given below. Red text is sent from me(author) and blue text is replies from Agilent support represented by Ashley Kibel.

From: Torstein Svendsgaard [mailto:tv_s_90@hotmail.com]
Sent: Thursday, January 27, 2015 6:34 AM
To: KIBEL,ASHLEY (K-Chandler,ex1)
Subject: Request for 5420 Support

Hi, I'm looking for the wiring schematics for the Agilent 5420 SPM 44 pin connector which is supposed to go from the back of the SPM to the head electronic box. We're doing some modification to the setup to install it into a nanoindenter. During this modification one of the wires going into the 44 pin have fallen off. I can't find the schematics for the wiring of the 44pin online. Can you help me with this?

Torstein Svendsgaard

Fra: <ashley_kibel@keysight.com>
Til: <svendsga@stud.ntnu.no>
Kopi: <afm-support@keysight.com>
Emne: Request for 5420 Support
Dato: 28. januar 2015 kl. 17.55.06 CET

Hi Torstein,

Our Parts center sent us your below request for support for your 5420. Our support organization does not typically make pin wiring and other schematics open to customers without documented non-disclosure agreements. That said, we can help you

determine what signal is on that pin and assist you with a repair if necessary. If you can send a picture of the connector with the broken pin, we could start from there.

From: Torstein Svendsgaard [mailto:tv_s_90@hotmail.com]

Sent: Thursday, January 29, 2015 5:54 AM

To: KIBEL,ASHLEY (K-Chandler,ex1)

Subject: RE: Request for 5420 Support

Hi, please see the attached photos for which wire that has broken. It is the black wire circled in the photo. I need to know how to connect it correctly into the backside of the 44pin.

Thanks, Torstein Svendsgaard

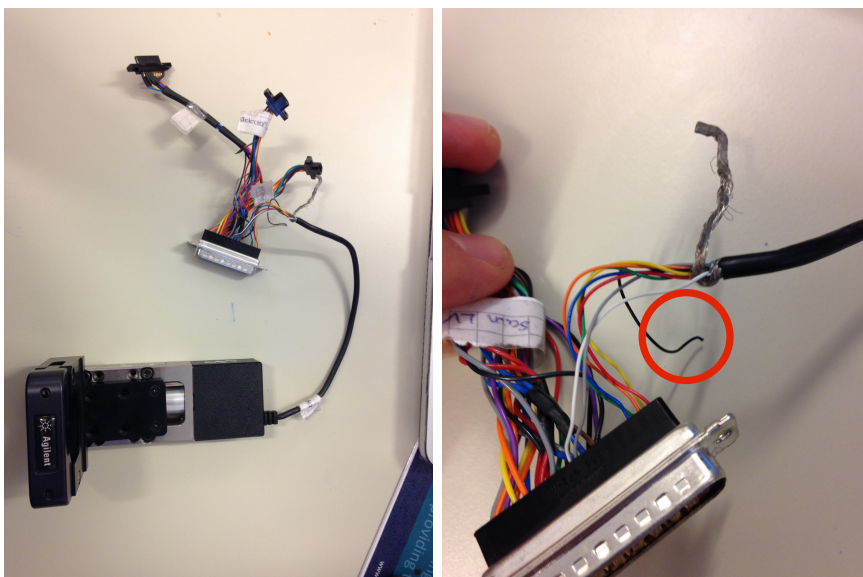


Figure A.2: Attached images

Fra: <ashley_kibel@keysight.com>

Til: <svendsga@stud.ntnu.no>

Kopi: <afm-support@keysight.com>

Emne: Request for 5420 Support

Dato: 29. januar 2015 kl. 22.51.14 CET

Hello Torstein,

That wire goes to pin 7 on the DB44 cable. It is a ground wire for the motor limit switches.

Best Regards, Ashley

From: Torstein Svendsgaard [mailto:tv_s_90@hotmail.com]
Sent: Wednesday, February 11, 2015 3:10 AM
To: KIBEL,ASHLEY (K-Chandler,ex1)
Subject: RE: Request for 5420 Support

Hi again,

How would you recommend to repair/install the wire into the sock again?

Regards, Torstein V. Svendsgaard

Fra: <ashley_kibel@keysight.com>
Til: <svendsga@stud.ntnu.no>
Kopi: <afm-support@keysight.com>
Emne: Request for 5420 Support
Dato: 11. februar 2015 kl. 17.22.56 CET

Hello Torstein,

You will need to make contact with the pin in the connector. Probably the easiest way would be to push the pin through from the connector side of the cable through to the back and out of the connector completely with a pair of sharp pliers (so that you don't damage any of the other pins). You can then solder that wire on to that pin and push the pin back through from the rear of the connector. There is some risk of damaging other pins, so just be as careful as possible.

Best Regards, Ashley

From: Torstein Svendsgaard [mailto:tv_s_90@hotmail.com]
Sent: Wednesday, March 04, 2015 1:12 AM
To: KIBEL,ASHLEY (K-Chandler,ex1)
Subject: RE: Request for 5420 Support

Hi, I'm in the process of setting the mounting the AFM up again, so it can be installed inside a nanoindenter chamber. Unfortunately I didn't demount the AFM, and I have therefore only limited information on how to do this. In one of the attached picture I have circled a wire. I'm guessing this should be connected to ground, is this correct?

I'm also interested in hearing what you believe about this set-up and if you could suggest a procedure to get the AFM up and running?

Regards, Torstein V. Svendsgaard

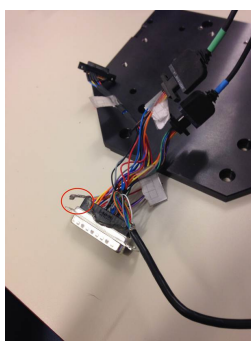


Figure A.3: Attached image

Fra: <ashley_kibel@keysight.com>

Til: <svendsga@stud.ntnu.no>

Emne: Request for 5420 Support

Dato: 6. mars 2015 kl. 00.40.00 CET

Hi Torstein,

According to our repair tech, it's the ground shield. Basically it gets wrapped around the hex screw threads and placed between the connector shell and housing.

I'm afraid that I can't comment too much on your setup as it's an application with which I'm fairly unfamiliar. That said, I would probably just start running the system using PicoView on a calibration grating and see how it images and approaches and go from there.

Best Regards, Ashley

From: Torstein Svendsgaard [mailto:tv_s_90@hotmail.com]
Sent: Monday, March 16, 2015 8:13 AM
To: KIBEL,ASHLEY (K-Chandler,ex1)
Subject: RE: Request for 5420 Support

Hi again, I would just like to confirm that I have connected the cables correctly before starting up the system(photos attached). The circled cables was not marked during dismantling and therefor I would like to confirm that the «red» cable from the scanner goes to the 9-pin and that the «blue» cable goes to the 44pin.

Regards, Torstein V. Svendsgaard

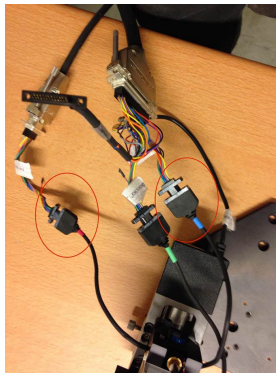


Figure A.4: Attached image

Fra: <ashley_kibel@keysight.com>
Til: <svendsga@stud.ntnu.no>
Emne: Request for 5420 Support
Dato: 16. mars 2015 kl. 18.40.24 CET

Hi Torstein,

Blue goes to the DB44 (low voltage) and red goes to the DB9 (high voltage). Looks like it is plugged in correctly in your picture below.

Best Regards, Ashley

Appendix B

Agilent 5420 AFM operating procedure

B.1 Procedure for AFM imaging and calibration

B.1.1 AFM-to-optic calibration

1. Start the calibration by moving the stage so that the aluminum sample is focused in optical camera. Define the sample boundaries in the Hysitron software. Locate the center-indent in the *H-pattern*. Record x- and y-coordinates at this point.
2. Move the stage so that AFM probe is above the aluminum sample, try to position the sample so that the AFM tip will image one of the larger indents. Approach the AFM probe, and start to image the sample with as large scan size as possible. Locate the larger indents and withdraw the tip.
3. Move the tip towards the *H-pattern* by adjusting the stage position. When the *H-pattern* is found and the center-indent is in center of the AFM image, record the x- and y-coordinates of the stage in the Hysitron software.
4. Subtract the two set of coordinates from each other to obtain the distance from the optical camera to the AFM probe. The distance should be recorded so that other users can use the AFM without doing the calibration again.

B.1.2 Imaging using the Agilent 5420 AFM

1. Place the sample that shall be imaged on the stage, and move the stage so that the sample is focused in the optical camera. Locate the area of interest and record the x- and y-coordinates.
2. Add the delta x and y coordinates from the calibration to the recorded coordinates, this is the target coordinates to image using the AFM.
3. Move the stage to the calculated coordinates, and approach the tip to the sample manually by pressing and holding down the *close* switch on the head electronic box. Stop the manual approach about 1-0,5 mm above the sample.
4. Press the *approach* button in the Agilent software, the tip will be lowered automatically towards the sample until the set point is reached. The user can choose scanning parameters such as image size, scan rate, offset and set point. An image can now be obtained, by pressing *scan up* or *scan down* in the Agilent software.

B.1.3 Ending an AFM scan

When the user is finished with the AFM, the tip has to be withdrawn from the sample. This is done by pressing the button *withdraw* in the Agilent software, and subsequently pressing down and holding in the *open* switch on the Head Electronic Box to lift the probe manually. The probe should be lifted to highest position possible to prevent unwanted damage when not using the AFM. The system should be powered down when it is not in use, and the cables to the scanner and detector shall be disconnected. This can prevent damage to the scanner in case of lightning or abnormalities in the power supply .

B.2 Performance of Agilent 5420 AFM

Through the work in this thesis only limited testing of the AFM setup has been done, because most of the necessary results were already obtained when the AFM was ready

for use. Initial testing however indicates a lower performance than what the original system is supposed to deliver. This is manifested in form of noise on images obtained with a small scanning size(sub micron). Noise in AFM images are often a result of vibrations in the building. The possible source of the vibrations are hard to determine, but some thoughts on this is presented.

1. A machine shop is located right next to the Nanomechanical lab which have rotating equipment that can induce vibrations
2. A heavily trafficked road is going just outside of the building where the nanomechanical labs is located
3. Building vibrations is known to disturb other equipment at nanomechanical so there is reason to believe that the same vibrations will affect the AFM
4. New mounting mechanism in the Hysitron chamber is less stable than than the original set up.

In benefit of having hindsight there are a couple of things that could have been done differently with regard to installing the AFM:(1)Testing the equipment in original state before dismantling. By doing this it had been possible determine if the location is suitable for mounting an AFM in the first place. (2)Planning and performing the work in one go. The work by installing the AFM was started by others, and it took three years from purchase to finished installation. Better control of the work and better preservation of the equipment would have been obtained by doing this.

Appendix C

Extended Results

This appendix present extended results.

C.1 Morphology of *Coscinodiscus sp.* Determined by AFM

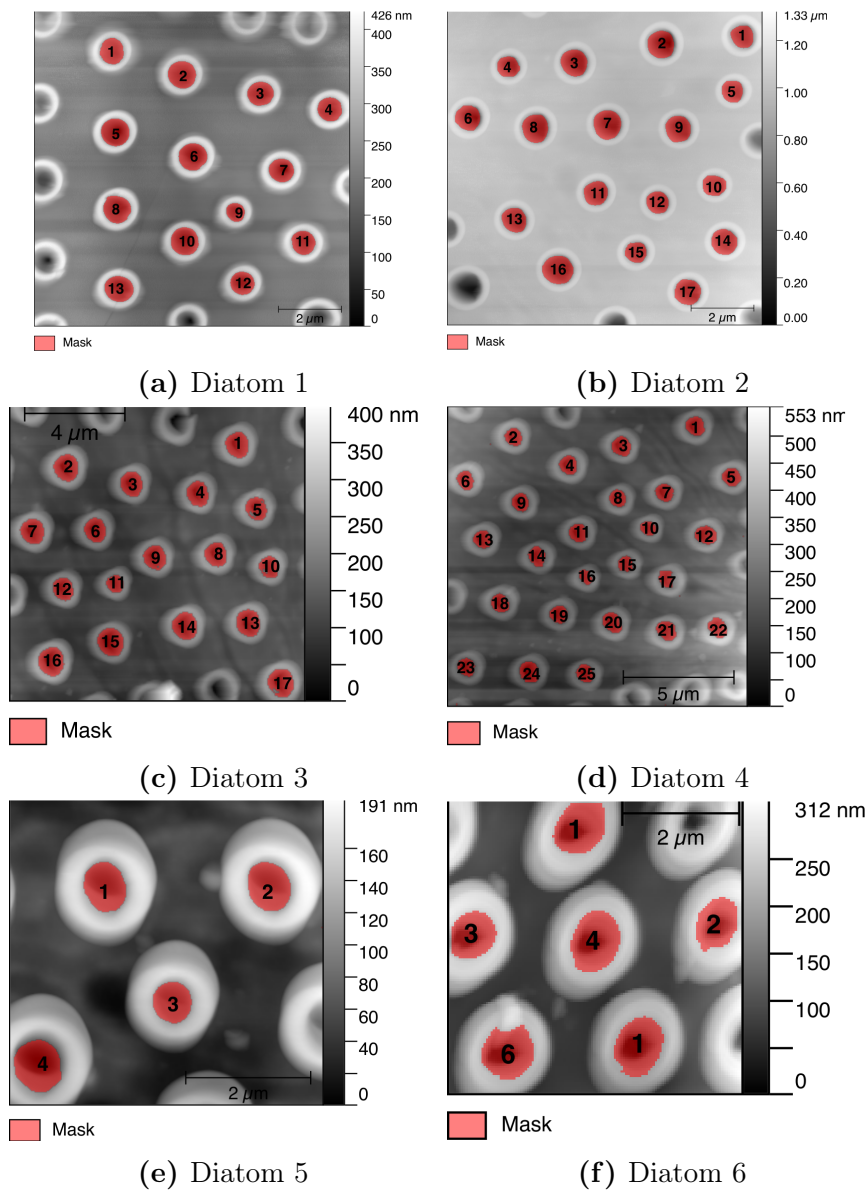


Figure C.1: Measurement of pore diameter in the foramen layer. Diatom number corresponds to measurements under *diatom* in [Table C.1](#), and labeled pores corresponds to pore # in [Table C.1](#)

Table C.1: Measurements of individual pore diameter on the foramen layer, for six different diatoms. *Diatom* marks measurement performed on different diatoms. *Pore #* is related to a *Diameter* measurement of a single pore, as marked in [Figure C.1](#). SD is standard deviation of the measurement.

Diatom	Pore #	Diameter[nm]	Diatom	Pore #	Diameter[nm]
1	1	796.20	4	1	872.13
	2	883.40		2	796.14
	3	800.40		3	887.04
	4	771.60		4	841.52
	5	893.40		5	841.52
	6	883.80		6	809.75
	7	773.60		7	820.48
	8	878.20		8	779.50
	9	593.40		9	804.34
	10	892.00		10	690.27
	11	759.60		11	833.69
	12	752.20		12	916.13
	13	871.80		13	815.13
	Mean	811.51		14	831.06
SD	86.04	15		702.82	
2	1	726.20		16	609.56
	2	875.40		17	721.24
	3	856.20		18	831.06
	4	692.40		19	815.13
	5	700.80		20	889.50
	6	804.00		21	869.62
	7	913.00		22	894.40
	8	874.40		23	809.75
	9	833.20		24	923.26
	10	715.40		25	809.75
	11	776.00	Mean	816.59	
	12	715.40	SD	73.15	
	13	788.40	5	1	733.26
	14	826.00		2	741.50
15	676.80	3		642.53	
16	949.80	4		794.92	
17	835.20	Mean	728.05		
Mean	797.56	SD	63.23		
SD	82.76	6	1	888.13	
3	1		985.11	2	794.62
	2		1032.76	3	798.27
	3		951.24	4	940.20
	4		946.64	5	909.75
	5		877.13	6	896.84
	6	925.62	Mean	871.30	
	7	985.11	SD	60.62	
	8	927.98	Average Diameter	841.21	
	9	942.01		Average SD	103.32
	10	825.79		Total pores	82
	11	699.71			
	12	872.13			
	13	1028.52			
	14	1053.72			
15	1094.41				
16	1092.42				
17	1076.29				
Mean	959.80				
SD	103.77				

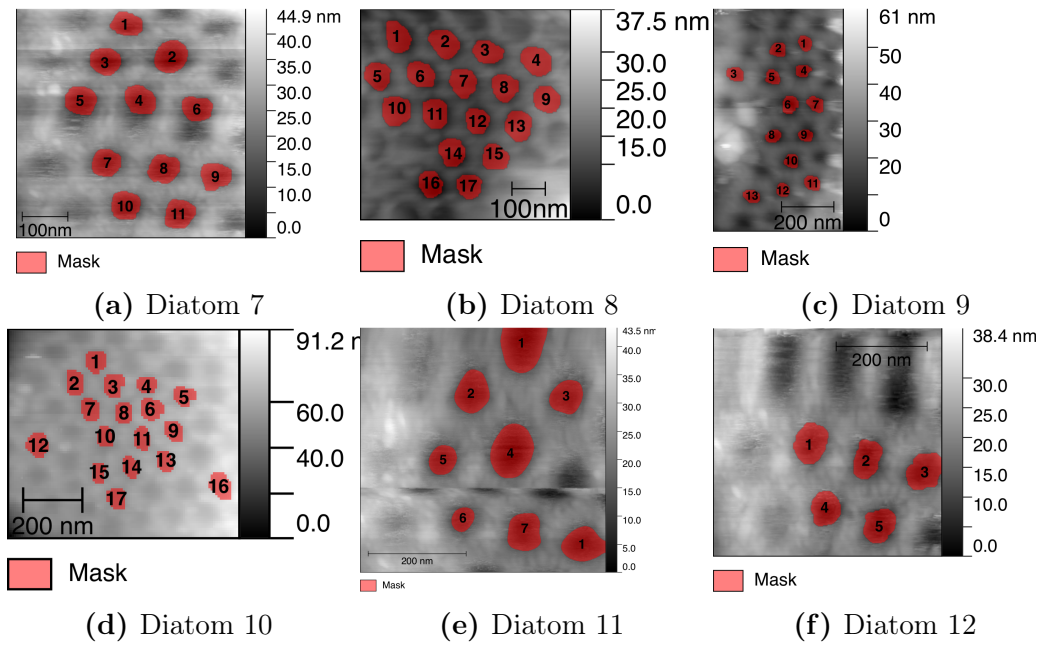


Figure C.2: Measurement of pore diameter in the cribellum layer. Diatom number corresponds to measurements under *diatom* in Table C.2, and labeled pores corresponds to pore # in Table C.2

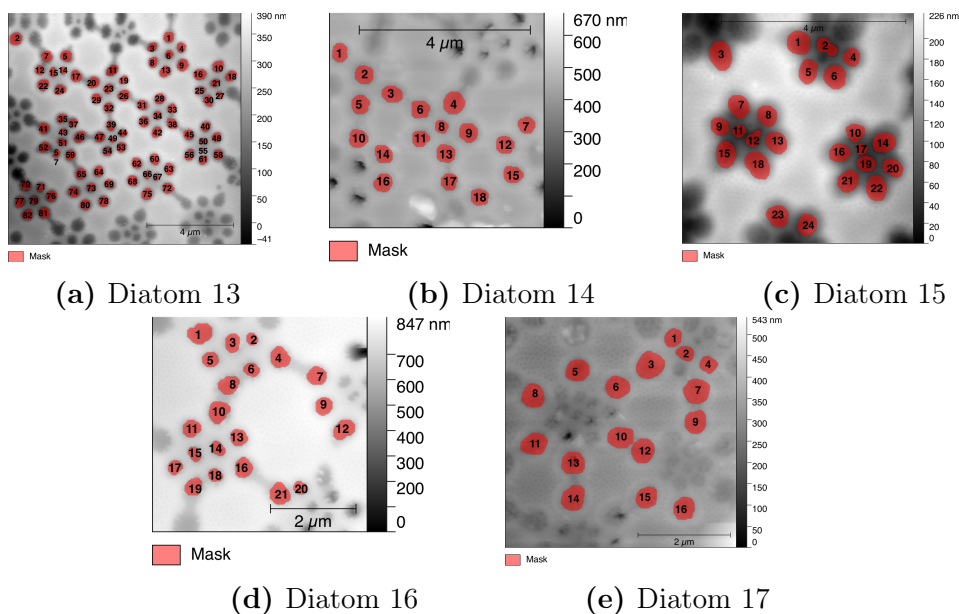


Figure C.3: Measurement of pore diameter in the cribrum layer. Diatom number corresponds to measurements recorded for one diatom specified in Table C.3, and labeled pores corresponds to pore # in Table C.3

Table C.2: Measurements of individual pore diameter on the cribellum layer, for six different diatoms. *Diatom* marks measurement performed on different diatoms. *Pore #* is related to a *Diameter* measurement of a single pore, as marked in [Figure C.2](#). SD is standard deviation of the measurement.

Diatom	Pore #	Diameter[nm]	Diatom	Pore #	Diameter[nm]
7	1	61.24	10	1	76.34
	2	73.20		2	74.28
	3	65.04		3	76.34
	4	67.28		4	65.96
	5	67.74		5	72.70
	6	62.22		6	78.36
	7	63.72		7	73.76
	8	67.32		8	67.72
	9	64.70		9	69.98
	10	65.46		10	65.38
	11	66.88		11	69.98
	Mean	65.89		12	80.32
	SD	3.22		13	64.78
8	1	86.94		14	65.38
	2	89.58		15	60.44
	3	81.40		16	84.56
	4	91.62		17	69.42
	5	83.64		Mean	70.98
	6	82.58		SD	6.86
	7	86.38	11	1	95.82
	8	83.28		2	77.92
	9	82.94		3	68.74
	10	91.82		4	98.16
	11	86.60		5	59.18
	12	77.36		6	48.14
	13	88.70		7	75.46
	14	84.44		8	78.02
	15	81.64		Mean	75.18
	16	77.86		SD	16.90
	17	76.98	12	1	82.32
	Mean	84.34		2	73.20
	SD	4.60		3	80.86
9	1	57.80		4	72.12
	2	60.76		5	74.08
	3	62.64		Mean	76.52
	4	55.06		SD	4.71
	5	58.80	Average Diameter		72.21
	6	67.56	Average SD		11.17
	7	63.72	Total Pores		71
	8	56.78			
	9	53.44			
	10	56.28			
	11	62.02			
	12	54.34			
	13	59.14			
	Mean	59.10			
	SD	4.11			

Table C.3: Measurements of individual pore diameter on the cribrum layer, for five different diatoms. *Diatom* marks measurement performed on different diatoms. *Pore #* is related to a *Diameter* measurement of a single pore, as marked in [Figure C.3](#). SD is standard deviation of the measurement.

Diatom	Pore #	Diameter[nm]	Diatom	Pore #	Diameter[nm]
13	1	498.00	13	54	427.40
	2	589.00		55	226.60
	3	433.80		56	485.00
	4	450.20		57	347.40
	5	545.60		58	452.20
	6	392.00		59	472.00
	7	530.60		60	494.00
	8	462.00		61	410.00
	9	546.60		62	498.60
	10	535.40		63	508.60
	11	521.00		64	471.60
	12	437.00		65	506.80
	13	512.40		66	345.00
	14	302.60		67	293.20
	15	374.40		68	503.60
	16	554.80		69	447.20
	17	528.40		70	441.60
	18	493.00		71	381.00
	19	398.20		72	516.80
	20	532.60		73	406.00
	21	383.20		74	503.60
	22	532.60		75	514.00
	23	448.40		76	502.00
	24	508.60		77	456.40
	25	423.40		78	489.00
	26	540.00		79	359.20
	27	336.80		80	484.40
	28	500.80		81	506.80
	29	469.80		82	480.80
	30	493.00		Mean	452.58
	31	489.60		SD	72.23
	32	468.60			
	33	422.20			
	34	370.00			
	35	432.60			
	36	484.40			
	37	405.20			
	38	500.80			
	39	455.20			
	40	456.40			
	41	489.60			
	42	487.80			
	43	314.40			
	44	373.60			
	45	486.60			
	46	496.80			
	47	472.60			
	48	434.60			
	49	264.20			
	50	301.80			
	51	380.40			
	52	479.80			
	53	439.60			

14	1	410.60	16	1	529.40
	2	445.20		2	284.80
	3	445.20		3	399.80
	4	522.00		4	477.80
	5	443.60		5	379.20
	6	441.80		6	351.20
	7	401.00		7	450.00
	8	316.40		8	461.80
	9	450.00		9	415.80
	10	444.00		10	501.60
	11	596.60		11	417.00
	12	430.20		12	480.80
	13	445.20		13	401.60
	14	429.00		14	333.60
	15	431.80		15	317.80
	16	436.40		16	441.40
	17	398.60		17	340.80
	18	415.80		18	325.40
	Mean	439.08	19	415.80	
	SD	55.15	20	320.80	
15	1	524.60	21	493.20	
	2	389.40	Mean	406.65	
	3	565.00	SD	68.60	
	4	382.60	17	1	394.60
	5	466.60		2	352.80
	6	507.40		3	599.80
	7	484.20		4	371.80
	8	450.40		5	501.40
	9	401.20		6	511.60
	10	399.80		7	563.80
	11	284.20		8	510.20
	12	321.20		9	498.40
	13	473.80		10	525.60
	14	475.40		11	531.40
	15	502.40		12	527.20
	16	437.60		13	513.00
	17	243.20		14	535.60
	18	559.00		15	475.40
19	374.40	16		488.00	
20	420.20	Mean	493.79		
21	472.00	SD	64.92		
22	504.20				
23	482.60				
24	458.60				
	Mean	440.83	Average Diameter	447.42	
	SD	80.39	Average SD	73.44	
			Total pores	161	

C.2 Peak Force Quantitative Nanomechanical Mapping

Table C.4: Cribellum Young's modulus measurements at three different regions, as marked in [Figure 4.6a](#). Measurements was taken on three different diatoms, marked diatom 18 to 20. SD is standard deviation

Diatom	Region	Mean Stiffness[GPa]	SD[GPa]
18	Central nodule	20.36	1.82
	Intermediate	29.07	6.16
	Edge	33.58	4.23
	Mean	27.67	4.07
19	Central nodule	22.88	1.79
	Intermediate	29.49	4.46
	Edge	14.37	2.61
	Mean	22.25	2.95
20	Central nodule	24.57	3.24
	Intermediate	28.21	5.47
	Edge	18.38	2.83
	Mean	23.69	3.85
18-20	Mean CN	22.60	2.29
	Mean Intermediate	28.92	5.36
	Mean Edge	22.08	3.22
	Total Mean	24.53	3.62

Table C.5: Foramen Young's modulus measurements at three different regions, as marked in [Figure 4.6a](#). Measurements was taken on two different diatoms, marked diatom 21 and 22. SD is standard deviation

Diatom	Region	Mean Stiffness[GPa]	SD[GPa]
21	Central nodule	27.41	5.07
	Intermediate	33.82	4.01
	Edge	24.38	4.36
	Mean	28.54	4.48
22	Central nodule	29.82	3.83
	Intermediate	27.64	6.17
	Edge	16.20	1.86
	Mean	24.56	3.95
21-22	Mean CN	28.62	4.45
	Mean Intermediate	30.73	5.09
	Mean Edge	20.29	3.11
	Total Mean	26.55	4.22

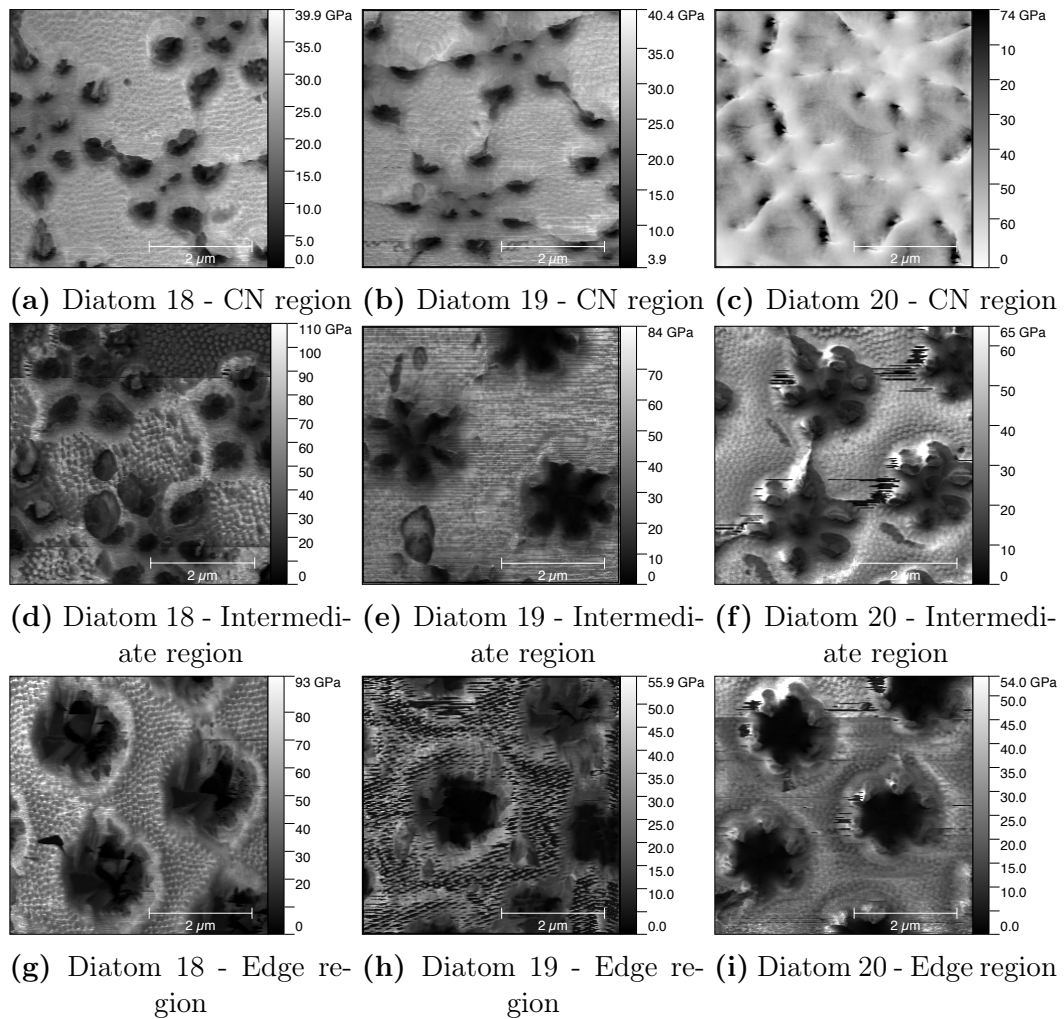


Figure C.4: Measurement of pore diameter in the cribrum layer. Diatom number corresponds to measurements recorded for one diatom specified in [Table C.3](#), and labeled pores corresponds to pore # in [Table C.4](#)

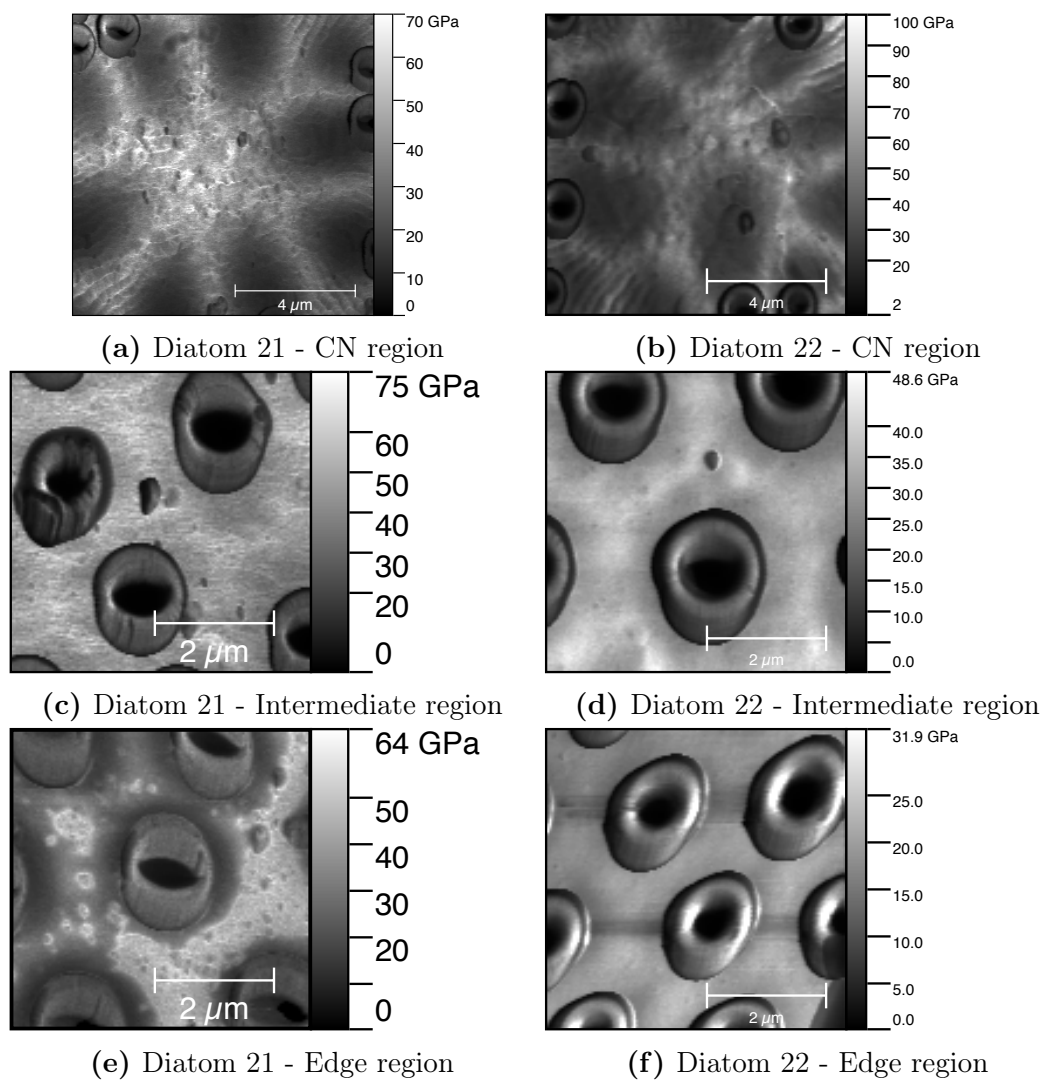


Figure C.5: Measurement of pore diameter in the foramen layer. Diatom number corresponds to measurements recorded for one diatom specified in [Table C.5](#), and labeled pores corresponds to pore # in [Table C.5](#)

Appendix D

Cleaning Procedure

FRUSTULEVASKING - SDS/EDTA

1. Sentrifugere ned kultur(5 min, 4500 rpm)
2. Vaske i MQ-vann(10mL), sentrifugere(5 min, 4500 rpm) - **3x**
3.
 - Vortex 1 min, reaksjonstid 20 min - **3x**
 - Sentrifugere(5 min, 4500) - **3x**
4. Vaske i MQ-vann(10mL), sentrifugere(5 min, 4500rpm) - **3x**
5. Tørking i ca 2 timer, eller til pellet er tørr
6. Resuspendere i metanol, sentrifugere (5 min, 4500 rpm), pass på; frustulene kommer lett i suspensjon - **3x**
7. Overføre til mindre sentrifugerør og lagre i metanol (1,5 mL) i fryser

Appendix E

Formal Requierments

A risk assessment of experimental activities and A3 sheet illustrating the work performed in this thesis is attached in this appendix. This is a formal requirement form the Department of Engineering Design and Materials.

NTNU	Risikovurdering	Understøttende	Navn	Dato
HMS		HMS	HMS/0001	22.03.2011
		Godekjenner	Emne	
		Risikovurdering		01.12.2006

Emne: **Dato: 16.09.14**

Delikater ved kartleggingen (nr/funksjon): **Torslein Svendsgaard**

Risikovurderingen gjelder hovedaktivitet: **Mastetoppgrave Torslein Svendsgaard- Nannabice**

Siganturen: **Ansvarlig veileder: Student**

Artikkel fra kartleggings-skjemaet	Mulig uansett hendelse	Vurdering av samvinn-lighet (1-5)	Vurdering av konsekvens: Helse (A-E)	Ytre miljø (A-E)	Økonomi (A-E)	Risiko-Verdi (min-max)	Kommentar/forutsetning
1	Etasjering av kjemikalier	1	B	B	A	B1	Ungt utnyttet bruk av kjemikalier og bruk av PPE eller prosedyrer for NTNU Nannabice
1	Etasjering av nanopartikler	2	B	A	A	B2	Bruke korrekt vernetøy og kjemikalier og bruke korrekt prosedyrer for NTNU Nannabice
2	Etasjering av kontaminert ved bruk av SEM	1	B	A	A	B1	Ungt utnyttet bruk av kjemikalier og bruk av PPE eller prosedyrer for NTNU Nannabice
3	Møteoppgave	2	B	B	A	B1	Ungt utnyttet bruk av kjemikalier og bruk av PPE eller prosedyrer for NTNU Nannabice

NTNU	Kartlegging av risikofylt aktivitet	Understøttende	Navn	Dato
HMS		HMS	HMS/0001	22.03.2011
		Godekjenner	Emne	
		Risikovurdering		01.12.2006

Emne: **Dato: 06.02.16**

Delikater ved kartleggingen (nr/funksjon): **Torslein Svendsgaard**

Risikovurderingen gjelder hovedaktivitet: **Mastetoppgrave Torslein Svendsgaard**

Siganturen: **Ansvarlig veileder: Student**

ID nr.	Artikkelprosess	Ansvarlig	Estimerende dokumentasjon	Estimerende sikkerhetsplan	Low/forhørt o.l.	kommentar
1	Løberbed Nannabice			Gjennomført i bakrus med PPE og PPE		
2	Løberbed Nannabice lab			Oppfølging av PPE-ken brukes		
3	Løberbed metallurgisk lab			HMS-kurs		

NTNU	Risikoprøve	Understøttende	Navn	Dato
HMS		HMS	HMS/0001	08.03.2010
		Godekjenner	Emne	
		Risikovurdering		09.02.2010

MARISE FOR RISIKOVURDERINGER ved NTNU

Kategori	E1	E2	E3	E4	E5
K Svært alvorlig	E1	E2	E3	E4	E5
O Alvorlig	D1	D2	D3	D4	D5
N Moderat	C1	C2	C3	C4	C5
M Liten	B1	B2	B3	B4	B5
N Svært liten	A1	A2	A3	A4	A5
S Svært liten	I1	I2	I3	I4	I5

SANNSYNLIGHET

Liten Middels Stor Svært stor

Prinsipp over aksjonstakelse: Følgende av fagene som er brukt i risikoprøven.

NTNU	Risikovurdering	Understøttende	Navn	Dato
HMS		HMS	HMS/0001	22.03.2011
		Godekjenner	Emne	
		Risikovurdering		01.12.2006

Samsvinnighet vurderes etter følgende kriterier:

1 gang pr år eller oftere	1 gang pr 10 år eller sjeldnere	1 gang pr år eller sjeldnere	1 gang pr måned eller sjeldnere	Sjeldnere	Svært sjeldnere
---------------------------	---------------------------------	------------------------------	---------------------------------	-----------	-----------------

Konsekvens vurderes etter følgende kriterier:

Omfang	Personer	Ytre miljø	Økonomisk	Øndomme
E Svært alvorlig	Død	Svært alvorlig og store reversible skader	Dødt eller alvorligsskadd	Trossviktige og/eller alvorlig skadet
D Alvorlig	Alvorlig personskade	Lansert skade, langvarig	Dødt eller alvorligsskadd	Trossviktige og/eller alvorlig skadet
C Moderat	Alvorlig personskade	Midtlig skade og langvarig	Dødt eller alvorligsskadd	Trossviktige og/eller alvorlig skadet
B Liten	Skade som krever medisinsk behandling	Mindre skader og kortvarig	Dødt eller alvorligsskadd	Trossviktige og/eller alvorlig skadet
A Svært liten	Skade som krever førstehjelp	Utsyngende skade og kortvarig	Dødt eller alvorligsskadd	Trossviktige og/eller alvorlig skadet

Risikoprøve = Samsvinnighet i vurdering av den samlede risikoen for helse, miljø og økonomi ved bruk av de ulike fagene som er brukt i risikoprøven. Dette er en vurdering av den samlede risikoen for helse, miljø og økonomi ved bruk av de ulike fagene som er brukt i risikoprøven. Dette er en vurdering av den samlede risikoen for helse, miljø og økonomi ved bruk av de ulike fagene som er brukt i risikoprøven.

Master Thesis

IPM

Fall 2014

Diatoms Investigated by Atomic Force Microscopy

by

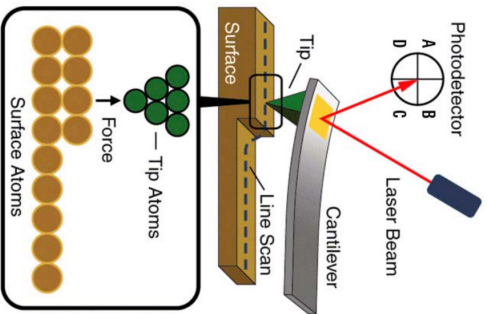
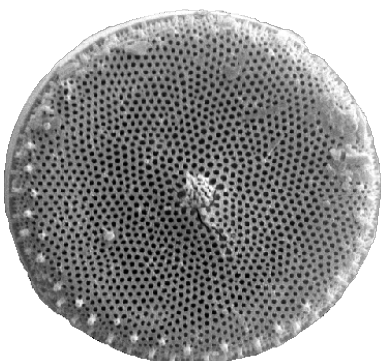
Torstein Svendsgaard



Supervisor: Prof. Dr. Christian Thaulow,
IPM, NTNU

Diatoms

The diatoms are a large group of unicellular algae that are present in almost every water habitat on earth. The silicious shell surrounding the diatom have been shown to have incredible material properties.

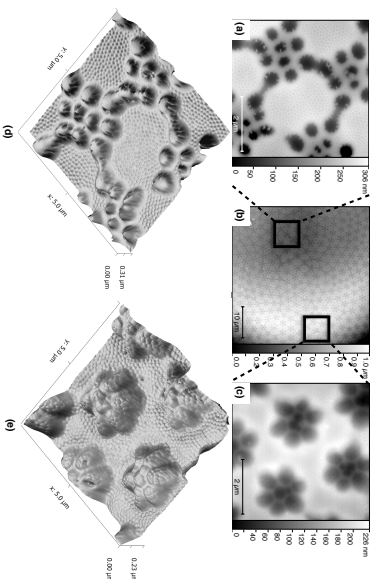


Diatom Morphology

The unexpected material behavior of the diatom shell can be explained by the presence of organic material, making the biosilica a composite material.

AFM

To investigate the morphology and material properties, an atomic force microscopy have be used. The objective was to get a better understanding of the biosilica.



Bibliography

- [1] N. Almqvist, Y. Delamo, B. Smith, N. Thomson, Å. Bartholdson, R. Lal, M. Brzezinski, and P. Hansma. Micromechanical and structural properties of a pennate diatom investigated by atomic force microscopy. *Journal of microscopy*, 202(3):518–532, 2001.
- [2] B. Bhushan. *Springer handbook of nanotechnology*. Springer Science & Business Media, 2010.
- [3] G. Binnig, H. Rohrer, C. Gerber, and E. Weibel. Surface studies by scanning tunneling microscopy. *Physical review letters*, 49(1):57, 1982.
- [4] G. Binnig, C. F. Quate, and C. Gerber. Atomic force microscope. *Physical review letters*, 56(9):930, 1986.
- [5] S. H. Bjørnøy. Nanomechanical testing of diatoms. Master’s thesis, NTNU, 2012.
- [6] J. Bradbury. Nature’s nanotechnologists: unveiling the secrets of diatoms. *PLoS biology*, 2(10):e306, 2004.
- [7] M. C. Two letters from a gentleman in the country, relating to mr leuwenhoeck’s letter in transaction, no. 283. communicated by mr c. *Philosophical Transactions*, 23(277-288):1494–1501, 1702.
- [8] B. Cappella and G. Dietler. Force-distance curves by atomic force microscopy. *Surface science reports*, 34(1):1–104, 1999.
- [9] M. L. Chiappino and B. Volcani. Studies on the biochemistry and fine structure of silicia shell formation in diatoms vii. sequential cell wall development in the pennatenavicularia pelliculosa. *Protoplasma*, 93(2-3):205–221, 1977.

- [10] S. A. Crawford, M. J. Higgins, P. Mulvaney, and R. Wetherbee. Nanostructure of the diatom frustule as revealed by atomic force and scanning electron microscopy. *Journal of Phycology*, 37(4):543–554, 2001.
- [11] B. V. Derjaguin, V. M. Muller, and Y. P. Toporov. Effect of contact deformations on the adhesion of particles. *Journal of Colloid and interface science*, 53(2):314–326, 1975.
- [12] M. E. Dokukin and I. Sokolov. Quantitative mapping of the elastic modulus of soft materials with harmonix and peakforce qnm afm modes. *Langmuir*, 28(46):16060–16071, 2012.
- [13] R. W. Drum and H. S. Pankratz. Post mitotic fine structure of gomphonema parvulum. *Journal of ultrastructure research*, 10(3):217–223, 1964.
- [14] R. Erlandsson, G. McClelland, C. Mate, and S. Chiang. Atomic force microscopy using optical interferometry. *Journal of Vacuum Science & Technology A*, 6(2):266–270, 1988.
- [15] R. Gordon and R. W. Drum. The chemical basis of diatom morphogenesis. *International review of cytology*, 150:243–372, 1994.
- [16] R. Gordon, D. Losic, M. A. Tiffany, S. S. Nagy, and F. A. Sterrenburg. The glass menagerie: diatoms for novel applications in nanotechnology. *Trends in biotechnology*, 27(2):116–127, 2009.
- [17] D. Hall. Review nonlinearity in piezoelectric ceramics. *Journal of materials science*, 36(19):4575–4601, 2001.
- [18] H. Hamaker. The london—van der waals attraction between spherical particles. *physica*, 4(10):1058–1072, 1937.
- [19] C. E. Hamm, R. Merkel, O. Springer, P. Jurkojc, C. Maier, K. Prechtel, and V. Smetacek. Architecture and material properties of diatom shells provide effective mechanical protection. *Nature*, 421(6925):841–843, 2003.
- [20] S. Hazelaar, H. J. Van Der Strate, W. W. Gieskes, and E. G. Vrieling. Monitoring rapid valve formation in the pennate diatom navicula salinarum (bacillariophyceae) 1. *Journal of phycology*, 41(2):354–358, 2005.

- [21] <http://imgkid.com/normal-force-definition.shtml>. <http://imgkid.com/normal-force-definition.shtml>, 2015. URL <http://imgkid.com/normal-force-definition.shtml>.
- [22] <http://nanoprobes.com/>. Non contact and tapping - fpn20, 2015. URL http://nanoprobes.aist-nt.com/index.php?main_page=product_info&products_id=190.
- [23] <http://www.bio.vu.nl/thb/deb/quest2007.html>. Theoretical biology vu univerty amsterdam, 2015. URL <http://www.bio.vu.nl/thb/deb/quest2007.html>.
- [24] <http://www.doitpoms.ac.uk/tlplib/afm/>. Tip surface interaction, August 2009.
- [25] <http://www.doitpoms.ac.uk/tlplib/afm/>. Modes of operation, 2015. URL http://www.doitpoms.ac.uk/tlplib/afm/modes_operation.php.
- [26] <http://www.keysight.com/>. Atomic force microscopy - what is it?, 2015. URL <http://www.keysight.com/main/editorial.jsp?ckey=1774141&id=1774141&nid=-33986.0&lc=spa&cc=VE>.
- [27] <http://www.nanoandmore.com/>. Nanoworld ag introduces ultra-short cantilevers for high-speed atomic force microscopy (hs-afm), 2014. URL <http://www.nanoandmore.com/USA/NanoWorld-AG-introduces-Ultra-Short-Cantilevers-for-High-Speed-Atomic-Force-Mic>
- [28] J. N. Israelachvili. *Intermolecular and surface forces: revised third edition*. Academic press, 2011.
- [29] E. Kreyszig. *Advanced engineering mathematics*. John Wiley & Sons, 2010.
- [30] N. Kroger, R. Deutzmann, and M. Sumper. Polycationic peptides from diatom biosilica that direct silica nanosphere formation. *Science*, 286(5442):1129–1132, November 1999.
- [31] N. Kröger, R. Deutzmann, C. Bergsdorf, and M. Sumper. Species-specific polyamines from diatoms control silica morphology. *Proceedings of the National Academy of Sciences*, 97(26):14133–14138, 2000.
- [32] J. E. Lennard-Jones. Cohesion. *Proceedings of the Physical Society*, 43(5):461, 1931.

- [33] L. Lenoci and P. J. Camp. Diatom structures templated by phase-separated fluids. *Langmuir*, 24(1):217–223, 2008.
- [34] D. Losic, G. Rosengarten, J. G. Mitchell, and N. H. Voelcker. Pore architecture of diatom frustules: potential nanostructured membranes for molecular and particle separations. *Journal of nanoscience and nanotechnology*, 6(4):982–989, 2006.
- [35] D. Losic, R. J. Pillar, T. Dilger, J. G. Mitchell, and N. H. Voelcker. Atomic force microscopy (afm) characterisation of the porous silica nanostructure of two centric diatoms. *Journal of Porous Materials*, 14(1):61–69, 2007.
- [36] D. Losic, K. Short, J. G. Mitchell, R. Lal, and N. H. Voelcker. Afm nanoindentations of diatom biosilica surfaces. *Langmuir*, 23(9):5014–5021, 2007.
- [37] D. G. Mann. The species concept in diatoms. *Phycologia*, 38(6):437–495, 1999.
- [38] A. . U. Manual. Agilent 5420 user manual, 2015. URL http://nano.em.keysight.com/PDFs/5420_User_Guide_Revision_D.pdf.
- [39] A. D. McNaught and A. Wilkinson. Iupac compendium of chemical terminology, 2000.
- [40] E. MEYER. Atomic force microscopy. *Progress in Surface Science*, 41(1):3–49, September 1992.
- [41] M. A. Meyers, P.-Y. Chen, A. Y.-M. Lin, and Y. Seki. Biological materials: structure and mechanical properties. *Progress in Materials Science*, 53(1):1–206, 2008.
- [42] M. Morland. Diatoms in new design. Master’s thesis, NTNU, 2014.
- [43] F. Noll, M. Sumper, and N. Hampp. Nanostructure of diatom silica surfaces and of biomimetic analogues. *Nano Letters*, 2(2):91–95, 2002.
- [44] B. Pittenger, N. Erina, and C. Su. Quantitative mechanical property mapping at the nanoscale with peakforce qnm. *Application Note Veeco Instruments Inc*, 2010.
- [45] G. Pletikapić, A. Berquand, T. M. Radić, and V. Svetličić. Quantitative nanomechanical mapping of marine diatom in seawater using peak force tapping atomic force microscopy1. *Journal of phycology*, 48(1):174–185, 2012.

- [46] F. E. Round, R. M. Crawford, and D. G. Mann. *The diatoms: biology & morphology of the genera*. Cambridge University Press, 1990.
- [47] A. Scheffel, N. Poulsen, S. Shian, and N. Kröger. Nanopatterned protein microrings from a diatom that direct silica morphogenesis. *Proceedings of the National Academy of Sciences*, 108(8):3175–3180, 2011.
- [48] A.-M. M. Schmid and D. Schulz. Wall morphogenesis in diatoms: deposition of silica by cytoplasmic vesicles. *Protoplasma*, 100(3-4):267–288, 1979.
- [49] Y. Seo and W. Jhe. Atomic force microscopy and spectroscopy. *Reports on Progress in Physics*, 71(1):016101, 2008.
- [50] M. Sumper and E. Brunner. Learning from diatoms: nature’s tools for the production of nanostructured silica. *Advanced Functional Materials*, 16(1):17–26, 2006.
- [51] M. Sumper and E. Brunner. Silica biomineralisation in diatoms: the model organism *thalassiosira pseudonana*. *ChemBioChem*, 9(8):1187–1194, 2008.
- [52] M. Sumper and G. Lehmann. Silica pattern formation in diatoms: Species-specific polyamine biosynthesis. *ChemBioChem*, 7(9):1419–1427, 2006.
- [53] C. S. The Faculty of Mathematics and N. S. at RWTH Aachen University. Atomic force microscopy - an advanced physics lab experiment, April 2014. URL http://institut2a.physik.rwth-aachen.de/de/teaching/praktikum/Anleitungen/Versuch_AFM_v4_engl.pdf.
- [54] M. A. Tiffany. Valve development in *aulacodiscus*. *Diatom research*, 23(1):185–212, 2008.
- [55] M. J. Vebner. Nanomechanical testing of diatoms. Master’s thesis, NTNU, 2013.
- [56] S. Wenzl, R. Hett, P. Richthammer, and M. Sumper. Silacidins: highly acidic phosphopeptides from diatom shells assist in silica precipitation in vitro. *Angewandte Chemie*, 120(9):1753–1756, 2008.
- [57] A. Woesz, J. C. Weaver, M. Kazanci, Y. Dauphin, J. Aizenberg, D. E. Morse, and P. Fratzl. Micromechanical properties of biological silica in skeletons of deep-sea sponges. *Journal of Materials Research*, 21(08):2068–2078, 2006.

-
- [58] T. Young, M. Monclus, T. Burnett, W. Broughton, S. Ogin, and P. Smith. The use of the peakforce-tm quantitative nanomechanical mapping afm-based method for high-resolution young's modulus measurement of polymers. *Measurement Science and Technology*, 22(12):125703, 2011.